THE UNIVERSITY *of* EDINBURGH

Genetic factors influencing the peripheral nervous system in health and disease

Laura Helen Comley

A thesis submitted for the degree of PhD at the University of Edinburgh

2011

Declaration

I declare that the work described in this thesis and its composition are entirely my own.

…….

Laura H. Comley

Acknowledgements

I would firstly like to thank my supervisor Tom Gillingwater for all the support, advice and motivation he has given me over the past four years. I have thoroughly enjoyed my PhD, and a huge part of that has been due to his continual encouragement.

I would also like to thank my second supervisors Simon Parson and Karen Horsburgh for all their help and advice, and the rest of the Gillingwater lab for making it such a good lab to be part of. Special thanks to Tom Wishart for all the molecular biology help, to Lyndsay Murray for all her support in the lab and for jolly gourd times out with, and to Derek Thomson for lessons on the monarchy of Russia, electrophysiology and the Charge of the Light Brigade.

I would also like to thank the BBSRC for the studentship that enabled me to spend four years doing something I found so interesting and rewarding.

Thank you to my parents for being so supportive and enthusiastic about my studies, and for listening to me chatter on any time of the day or night. Extra thanks to Nosh for all the tea and goulashties.

I would have had an interesting but far less entertaining time without my A-team. Thank you chums, for road-trips and tea parties and endless whimsy and nonsense. Special thanks to the Kezia and EM for good food and awful

entertainment every Monday night; Kathleen for her outstanding grammar and being my person; Yvonne and Chantal for their never-ending support and persuading me out to Ecco Vino when I needed it; Morven and Mal for eight years of Bogwarts, Dawson and crafts; Rich for appearing whilst I was at my most stressed and crazy-haired, and still deciding to stick around; and to JH and her team of P4/5 minions for inspirational drawings and timetables, and for always being there radiating calmness.

Finally, I'd like to thank the Lothian bus driver who drove out to the Royal Infirmary of Edinburgh to return the crucial YFP slides that I left under my seat on the number 8 bus. Without him my YFP chapter would be a figure and a conclusion less than it is today.

Abstract

Lower motor neurons of the peripheral nervous system are responsible for innervating skeletal muscle and controlling all voluntary movements of the body. Degeneration of motor neurons underlies conditions such as amyotrophic lateral sclerosis and spinal muscular atrophy. The identification of genetic factors that influence the form and function of the peripheral nervous system in vivo will be important for our understanding of the neuromuscular system in health and disease. Here, I have studied the effects of three different genes and their respective protein products on the peripheral nervous system: yellow fluorescent protein (YFP), apolipoprotein E (apoE) and Ercc1 (excision repair cross-complementing group 1). YFP has been used as a reporter protein in many fields of research, including as a powerful tool for visualising neurons in mice. It is used under the assumption that it is biologically inert. However, my findings have revealed that YFP expressed in neurons in mice is not inert: it induces a cell stress response at both the RNA and the protein level and alters the time course of dying-back neuropathy. ApoE is a lipid transport protein with three distinct isoforms in humans (apoE2, apoE3 and apoE4), which are known to differentially affect risk and outcome in a number of central nervous system disorders. However, the effects of different apoE isoforms on the peripheral nervous system have yet to be established. I have shown that apoE4 delays peripheral nerve regeneration and subsequent neuromuscular junction reinnervation compared to apoE3, in the absence of any effects on normal form or function, degeneration or developmental plasticity. Ercc1 protein is involved in several DNA repair systems. Ercc1$^{\Delta/-}$ mice have reduced levels of functional Ercc1 protein, which leads to a reduced life span and motor abnormalities, potentially due to a build of up DNA damage. Here I have shown that Ercc1$^{\Delta/-}$ mice also have increased abnormalities at the neuromuscular junction (an early pathological target in neurodegeneration) with age. These findings contribute significantly to our understanding of the influence of specific genes on the form and function of the peripheral nervous system in health and disease.

Table of contents

Declaration	**ii**
Acknowledgements	**iii**
Abstract	**v**
Table of contents	**vi**
List of abbreviations	**x**
Chapter 1 – Introduction	**1**
1.1 History of the nervous system	**1**
1.2 Structure of the PNS	**4**
1.2.1 Structure of the NMJ	6
1.3 Development of the PNS	**9**
1.3.1 Development of the NMJ	10
1.4 Injury in the PNS	**13**
1.4.1 Wallerian Degeneration	13
1.4.2 Dying-back neuropathy	15
1.4.3 Regeneration	16
1.5 Diseases of the PNS	**17**
1.5.1 ALS	18
1.5.2 SMA	18
1.5.3 NMJs as early pathological targets in MND	19
1.6 Factors affecting the PNS	**21**
1.6.1 YFP	21
1.6.2 ApoE	21
1.6.3 ERCC1	22
1.7 Aims	**23**
Chapter 2 – General Materials and Methods	**25**
2.1 Surgery	25

2.2 Quantitative fluorescent (Li-COR) western blots 25
2.3 Immunohistochemistry 26
2.4 Microscopy 27
2.5 Quantification of NMJs 28
2.6 Statistical analysis 29

Chapter 3 – Yellow fluorescent protein 31
3.1 Introduction 31
3.2 Materials and Methods 36
3.2.1 Mice 36
3.2.2 Cell stress array 37
3.2.3 Quantitative fluorescent (Li-COR) western blots 37
3.2.4 Spinal cord immunohistochemistry 37
3.2.5 NMJ immunohistochemistry 38
3.2.6 Surgery 38
3.2.7 Microscopy 42
3.2.8 Quantification of neuromuscular junctions 42
3.2.9 Statistical Analysis 42
3.3 Results 43
3.3.1 YFP expression activates cell stress responses in neurons in vivo 43
3.3.2 YFP expression in motor neurons subtly disrupts neuronal morphology 58
3.3.3 YFP expression in neurons alters responses to dying-back neuropathy but not Wallerian degeneration 64
3.4 Discussion 73

Chapter 4 – Apolipoprotein E 81
4.1 Introduction 81
4.2 Materials and methods 90
4.2.1 Mice 90
4.2.2 Quantitative fluorescent (Li-COR) western blots 91

4.2.3 Electron microscopy 92
4.2.4 Regenerating peripheral nerve quantification 92
4.2.5 Surgery 96
4.2.6 Immunohistochemistry 96

4.2.7 Microscopy 96
4.2.8 Quantification of neuromuscular junctions 96
4.2.9 Electrophysiology 96
4.2.10 Statistical analysis 97
4.2.11 Proteomics 97
4.3 Results **99**
4.3.1 ApoE genotype has no effect on normal form or function of the mouse PNS 99
4.3.2 ApoE4 expression at physiological levels has no effect on developmental plasticity at the neuromuscular junction 111
4.3.3 ApoE4 expression has no effect on Wallerian degeneration of axons or NMJs following peripheral nerve injury 115
4.3.4 ApoE4 significantly delays nerve regeneration and neuromuscular reinnervation following peripheral nerve injury 125
4.3.5 ApoE genotype modifies expression levels of proteins associated with cellular outgrowth and blood-nerve barrier integrity in peripheral nerve 138
3.4 Discussion **161**

Chapter 5 – ERCC1 **169**
5.1 Introduction **169**
5.2 Materials and methods **173**
5.2.1 Mice 173
5.2.2 NMJ Immunohistochemistry 173
5.2.3 Microscopy 173
5.2.4 Quantification of NMJs 173

5.2.5 Statistical analysis 174
5.3 Results **175**
5.3.1 NMJ pathology in Ercc1$^{\Delta/-}$ mice 175
5.4 Discussion **185**

Chapter 6 – General Discussion **189**
6.1 Overview of results 189
6.2 Experimental manipulation of the PNS 190
6.3 Clinical Implications 191
6.4 Conclusions 192

7 – References **195**

8 – Appendices **231**
Appendix 8.1 – iTRAQ proteomics methodology 231
Appendix 8.2 – Publications 235
Appendix 8.3 – Selected conference abstracts 237

Table of abbreviations

µm	Micrometre
ALS	Amyotrophic lateral sclerosis
ANS	Autonomic nervous system
ApoE	Apolipoprotein E
BSA	Bovine serum albumin
BER	Base excision repair
BTX	Bungarotoxin
CNS	Central nervous system
ERCC1	Excision repair cross-complementing group 1
EPP	Endplate potential
FDB	Flexor digitorum brevis
FITC	Fluorescein isothiocyanate
GFP	Green fluorescent protein
LAL	Levator auris longus
mEPP	Miniature endplate potential
mg	Milligram
mM	Millimolar
MMR	Mismatch repair
MND	Motor neuron disease
MuSK	Muscle-specific kinase
NER	Nucleotide excision repair

NMJ	Neuromuscular junction
P	Postnatal (i.e. P15 - postnatal day 15)
PCR	Polymerase chain reaction
PNS	Peripheral nervous system
SMA	Spinal muscular atrophy
TA	Transversus abdominis
TRITC	Tetramethyl-rhodamine isothiocyanate
XP	Xeroderma pigmentosum
XPF	Xeroderma pigmentosum group F
YFP	Yellow fluorescent protein

Chapter 1 – Introduction

"To move things is all that mankind can do. For such, the sole executant is muscle – whether in whispering a syllable or felling a forest."

C. S. Sherrington, English neurophysiologist (1857-1952)

Every movement within the body is produced by patterns of muscle contraction, controlled by motor neurons from the brain and spinal cord. Understanding how this system works is therefore essential to understand both normal behaviour, and how it functions in disease.

1.1 History of the nervous system

It was Luigi Galvani who first proposed the idea that neural communication is due to bioelectricity, or animal electricity as he described it, in 1791, following his experiments on the interactions between electricity and muscular motion in frogs legs (Galvani, 1791; Lopez-Munoz and Alamo, 2009). This represented the beginning of modern neuroscience – before this the prevailing idea of how the nervous system functioned was based on an idea proposed by the classical Greek philosophers and modified by Galen (131-200), that inhaled air was transformed into '*pneuma*' or '*spiritus animalis*', which flowed through hollow nerves causing movement and sensation (Lopez-Munoz and Alamo, 2009).

Further breakthroughs in neuroscience came with the invention of the achromatic lens in 1824, which improved microscopes and allowed anatomists to see new levels of detail. The improvements in microscopy lead to the first descriptions of the structure of neurons by Valentin, (Lopez-Munoz and Alamo, 2009; Valentin, 1836), and the idea that the nervous system could be composed of cells in the same way as other tissues in the body (Virchow, 1855), although the cells themselves remained unnamed until the end of the century, when the term 'neuron' was first used (Waldeyer, 1891).

Whilst microscopy had improved, staining techniques were still not sophisticated enough to determine the cellular structure of the brain. This was a cause of much debate in the second half of the nineteenth century, with two opposing schools of thought: the reticularist theory and the neuron doctrine. The reticularist theory of the connectivity of neurons was proposed by Gerlach (Gerlach, 1871) and strongly supported by Camillo Golgi. It stated that the nervous system was made up of a 'neural net' with fused axons, along which a nervous impulse was propagated. In contrast, proponents of the neuron doctrine, such as Santiago Ramon y Cajal, believed that the nervous system was anatomically composed of individual cells that communicated with one another through points of contact (De Carlos and Borrell, 2007). It was Cajal's use of a histological technique discovered by Golgi, 'la reazione nera' (Golgi, 1873; De Carlos and Borrell, 2007), that allowed him to stain entire neurons and clearly see free terminals rather than anastomoses, which finally convinced people that

the neuron doctrine was the correct theory (Cajal, 1888a; Cajal, 1888b; Cajal, 1889; De Carlos and Borrell, 2007).

Once it had been established that neurons did not fuse, the major question was how electrical impulses were passed between cells. Sir Charles S. Sherrington studied the physiology of the synapse in the first half of the twentieth century, providing evidence for an integrated nervous system and excitatory and inhibitory synapses (a term which he coined from the Greek for connection; Lopez-Munoz and Alamo, 2009; Sherrington, 1906). However, it was not possible to visualise the gap between neurons until the invention of the electron microscope in 1954.

In 1936 Dale and Loewi shared the Nobel Prize for their work on chemical neurotransmission. Dale used the peripheral nervous system (PNS) as a model to show that acetylcholine was functioning as a neurotransmitter, proving that synapses worked by chemical, and not electrical transmission (Dale and Feldberg, 1934; Tansey, 2006). With the advent of electrophysiology the PNS, and the neuromuscular junction (NMJ) in particular, became instrumental in discovering how synapses functioned. The NMJ was useful because it is large and easily accessible, and relatively simple compared to synapses of the central nervous system (CNS).

1.2 Structure of the PNS

The PNS is defined as all neurons lying out with the brain and spinal cord. This includes the autonomic nervous system, cranial nerves III to XII and the somatic nervous system, which innervates skeletal muscle causing movement.

Muscles can be broadly divided into smooth muscle and striated muscle (due to it's striped appearance under a microscope), which can be further subdivided into skeletal muscle and cardiac muscle. These groups of muscles differ in their functions and the parts of the nervous system that provide their innervation. Smooth muscle is innervated by the autonomic nervous system (ANS) and is found lining arteries and the digestive tract. Cardiac muscle is responsible for the heartbeat, and contracts rhythmically without the control of any innervation, although its rate can be changed by input from the ANS (Bear et al., 2001). The majority of muscle mass within the body is skeletal muscle, which is under the control of the somatic nervous system. This muscle is responsible for all voluntary movement: it moves bones, controls respiration and produces all facial expressions (Bear et al., 2001).

The neurons responsible for innervating all skeletal muscle are lower motor neurons, which Sherrington called "the final common pathway" for the control of movement. The cell bodies of these are found in the ventral horn of the spinal cord and the brainstem (for motor neurons controlling muscles of the head and neck), from where bundles of axons will originate and pass out of the spinal cord through notches in between the vertebrae in a ventral root or via the

cranial nerves (Purves et al., 2004). In the periphery ventral roots will join dorsal roots (containing sensory fibres) and form mixed spinal nerves (Bear et al., 2001). Lower motor neurons can be subdivided into two types: alpha motor neurons and gamma motor neurons. Gamma motor neurons adjust the level of tension in the intrafusal muscle fibres at either end of the muscle spindle, regulating the stretch reflex (Rossi-Durand, 2006). However, this thesis is primarily concerned with alpha motor neurons, which are directly responsible for the force of contraction produced by a muscle.

At their distal end lower motor neurons communicate directly with skeletal muscle; these specialised junctions are NMJs, and are discussed below. An alpha motor neuron and all the muscle fibres it innervates is known as a motor unit (Sanes and Lichtman, 1999). All the motor neurons innervating a single muscle make up a motor neuron pool (Bear et al., 2001).

An individual nerve is made up of many motor neuron axons bundled together, and contains several different cell types. The entire nerve is contained in a thick sheath of connective tissue, called the epineurium. The epineurium contains the blood vessels supplying the nerve, adipose tissue and bundles of axons held together in fascicles within a second connective tissue sheath – the perineurium (Sunderland, 1965). These two outer connective tissue layers were first described by Ranvier in 1878 (Ranvier, 1878; Stolinski, 1995). Within the fascicles a delicate layer of connective tissue called the endoneurium surrounds each individual axon. The endoneurium contains endoneurial fluid, analogous to

cerebrospinal fluid in the CNS, and functions as the blood-nerve barrier (BNB), tightly regulating the endoneurial microenvironment (Weerasuriya and Mizisin, 2011).

Peripheral nerves also contain two types of Schwann cells: myelinating and non-myelinating (ensheathing) Schwann cells. Myelinating Schwann cells form a layered myelin sheath around large calibre peripheral axons (Gaudet et al., 2011). The sheath is interrupted by short lengths of exposed axonal membrane between Schwann cells, known as nodes of Ranvier. These allow for fast saltatory conduction (from the Latin for 'to leap') of an action potential along a myelinated axon (Bear et al., 2001). Non-myelinating Schwann cells form a loose sheath around multiple small diameter axons, separating and surrounding them, and grouping them into what is known as a Remak bundle (Griffin and Thompson, 2008).

1.2.1 Structure of the NMJ

The NMJ was first described in 1862 by Wilhelm Friedrich Kühne. He described how nerve cells in a frog terminated on muscle, and coined the phrase 'neuromuscular junction' (Kühne, 1862; Lopez-Munoz and Alamo, 2009).

The NMJ is generally thought to be made up of three main cell types: the motor neuron, the skeletal muscle fibre and perisynaptic terminal Schwann cells. However, more recently a fourth cell type, termed a kranocyte, has also been

identified at the NMJ (Court et al, 2008). Each of these cell types is highly specialised according to the function that it has to perform.

The nerve terminal of a motor neuron is specialised for neurotransmitter release. It contains large numbers of synaptic vesicles filled with the neurotransmitter acetylcholine, and mitochondria to provide the energy needed for neurotransmitter synthesis and release. Vesicles are found mainly in the part of the terminal nearest the muscle fibre, many are localized in active zones at the pre-synaptic membrane, ready to fuse and release acetylcholine into the synaptic cleft (Sanes and Lichtman, 1999).

Directly opposite the nerve terminal lies the motor endplate of a skeletal muscle fibre. This is specialised to respond rapidly and efficiently to neurotransmitter released by the overlying nerve terminal, and has an extremely high concentration of acetylcholine receptors (Salpeter and Loring 1985). The postsynaptic membrane is folded into 1μm deep folds, known as junctional folds. These junctional folds are directly opposite the active zones in the pre-synaptic terminal. Acetylcholine receptors are located at the top of the folds, and sodium channels are found at the bottom, an arrangement that leads to more efficient transmission (Wood and Slater 1997).

Distinct from the Schwann cells of the axonal compartment of a motor neuron, perisynaptic terminal Schwann cells form a cap over the motor terminal branches and the nerve terminal. These Schwann cells are necessary for

maintaining the pre-synaptic structure and function of NMJs (Reddy et al, 2003), and aid path finding of neurons following injury.

Kranocytes were first described in 2008 by Court and colleagues (Court et al, 2008). These cells lie out with the synaptic basal lamina and form caps over the NMJ during postnatal development, for which the name 'krano', from the Greek word for helmet, is derived. Following denervation or paralysis they proliferate and spread throughout the perijunctional region before either Schwann cells or regenerating axons begin to sprout, thereby taking the lead in forming bridges between NMJs, suggesting that they may play a role in repairing neuromuscular connections in regeneration (Court et al, 2008).

Finally, each muscle fibre is surrounded by a basal lamina, which also ensheaths the nerve terminal and terminal Schwann cells, although not kranocytes. The basal lamina passes between the pre-synaptic and post-synaptic membranes, through a gap known as the synaptic cleft (approximately 50nm wide) and extends down into the junctional folds of the post-synaptic membrane (Hughes et al., 2006). This synaptic portion of basal lamina is also specialised, containing a high concentration of acetylcholinesterase to break down acetylcholine released into the synaptic cleft but not activating a receptor (Krejci et al., 1997). It also contains the signalling molecules agrin and neuregulin (Sanes and Lichtman, 1999), necessary for the clustering of acetylcholine receptors at the motor endplate on the post-synaptic membrane (Reist et al., 1992; Sandrock et al., 1997).

1.3 Development of the PNS

In its earliest stage (three weeks post gestation), an embryo is a flat disc of cells, three cell layers thick. These layers are termed the endoderm, mesoderm and ectoderm, and it is from the ectoderm that the entire nervous system, including the PNS, is formed. The part of the ectoderm that gives rise to the nervous system is the neural plate, and in a process known as neurulation the two edges of the neural plate move together and fuse to form the neural tube. The central nervous system is entirely formed from the walls of the neural tube. The tube itself eventually becomes the ventricular system (for review see Bear et al, 2002).

As the two folds of the neural plate come together to from the neural tube some tissue is pinched off and ends up lying laterally to the tube. This is the neural crest, and is the source of all the cells of the PNS that have their cell bodies out with the CNS. At this stage of development the underlying mesoderm forms bulges on wither side of the neural tube, known as somites. These somites become the vertebrae of the spinal column and all related musculature, and it is from them that the term 'somatic nervous system' derives (for review see Bear et al, 2002).

The rostral end of the neural tube differentiates to form the brain, while the caudal end becomes the spinal cord. The neural tube narrows to become the spinal canal, and the tissue in the walls of the tube expands, eventually forming the dorsal horn and the ventral horn, where the cell bodies of lower motor

neurons are found after differentiation, projecting their axons out to the periphery (for review see Bear et al, 2002).

In order to reach their intended target muscles lower motor neurons have to extend processes over large distances and form contacts with the correct muscle. In order to achieve this a neurite extends a growing tip called a growth cone (for review see Mueller, 1999). Growth cones are adapted to identify pathways for the neurite to grow down. Their leading edges are extremely motile, with a sheet called a lamellipodium from which filopodia rapidly form and then retract, probing the surrounding environment. If the extracellular matrix contains appropriate proteins, such as laminins, the filopodia attach to the substrate and pull the growth cone forward. In this way, axons are guided along the substrate by permissive cues, and prevented from moving in other directions by repellent ones (Mueller, 1999; Purves et al., 2004).

1.3.1 Development of the NMJ

When the growth cone of a growing lower motor neuron comes into contract with its target muscle fibre a NMJ is formed. Initially, the neuron secretes agrin into the basal lamina, where it interacts with muscle-specific kinase (MuSK) on the membrane of the muscle cell (Liyanage et al., 2002). MuSK interacts with rapsyn, which acts to pull acetylcholine receptors together to form a motor endplate on the post-synaptic membrane (for review see Sanes and Lichtman, 1999).

Whilst the post-synaptic membrane is maturing the pre-synaptic nerve terminal also undergoes changes. Synaptic vesicles increase in number and become concentrated in newly formed active zones, and the synaptic area itself increases (Sanes and Lichtman, 1999; Takahashi et al., 1987). Specialisation of the motor nerve terminal only occurs when the nerve is in contact with a muscle fibre, leading to the theory that factors are secreted into the basal lamina by the muscle cell and act as retrograde signals causing the motor neuron to differentiate (Lupa et al., 1990). To date many factors have been identified and implicated in the formation of NMJs, but at present the precise mechanisms remain unknown. Factors implicated include fibroblast growth factors, laminin, collagen, glial cell line-derived neurotrophic factor (Gdnf). Proteins in the fibroblast growth factor family and collagen IV α2 are thought to be involved in the early stages of synaptic vesicle clustering, but are not necessary for the maturation of the nerve terminals. This instead depends on laminin β2 and other, synapse specific, isoforms of collagen IV (α3 and α6; Fox et al., 2007). Gdnf is expressed in muscle cells, but its receptors are expressed on motor neurons. It is critical for motor neuron survival, and activation of the receptors leads to maturation of the pre-synaptic terminal (Baudet et al., 2008), suggesting that Gdnf might be a muscle-derived factor regulating specialisation of the pre-synaptic nerve terminal (for review see Wu et al., 2010).

Initially each endplate is innervated by branches of several axons, and is said to be poly-innervated. During the first few weeks of post-natal development all

but one of these inputs withdraws and is lost in the process of synapse elimination, until all motor endplates are mono-innervated: one axon branch innervates one muscle fibre (Brown et al, 1976). Although branches of motor neurons are removed in synapse elimination, the number of motor axons innervating the muscle as a whole remains constant. Studies using XFP transgenic mice have shown that this process occurs asynchronously, and without any kind of spatial bias, suggesting that events occurring locally at each NMJ are responsible for the withdrawal of some inputs and the strengthening of others (Keller-Peck et al, 2001). However, the mechanisms regulating synapse elimination remain unclear, although activity appears to play a role, with active axons having a competitive advantage (Ribchester and Taxt, 1983; Balice-Gordon and Lichtman, 1994).

1.4 Injury in the PNS

Under normal circumstances, peripheral nerves and their target muscles maintain stable connections throughout life. However, injury or disease can disrupt these connections with catastrophic consequences.

Wallerian degeneration and dying-back neuropathy are distinct pathways known to be able to cause breakdown of axons and nerve terminals, and have distinct morphological characteristics (Murray et al., 2008b). Wallerian degeneration is associated with breakdown following traumatic nerve injury and with diseases such as Multiple Sclerosis, whereas motor neuron diseases such as amyotrophic lateral sclerosis (ALS) and spinal muscular atrophy (SMA) are associated with patterns of degeneration such as those seen in dying-back neuropathies (Murray et al., 2010).

1.4.1 Wallerian Degeneration

Wallerian degeneration was first described by the English physiologist Augustus Volney Waller in 1850 (Waller, 1850). He sectioned the hypoglossal and glossopharyngeal nerves in the tongues of frogs, and recorded that distal to the injury (where the connection to the cell body is broken) the axon disintegrated and all debris was cleared away within a few days of injury, whilst the proximal section remained intact for a much longer period of time (Waller, 1850).

The first step in Wallerian degeneration is fragmentation of the nerve terminals and distal axons (Vial, 1958). This occurs within 24-48 hours in rodents (Beirowski et al., 2005), but in humans may take several days to initiate (Chaudhry and Cornblath, 1992). In the PNS myelinating Schwann cells respond to injury by altering gene expression (Guertin et al., 2005), no longer producing myelin proteins (Trapp et al., 1988) and degrading their own myelin (Gaudet et al., 2011). The myelin sheath around fragmenting axons is drawn back from the nodes of Ranvier to form distinct compartments called 'ellipsoids', in which the remaining axonal fragments are completely broken down (for review see Gillingwater and Ribchester, 2001). These ellipsoids are then removed by phagocytosing Schwann cells and invading macrophages, which are attracted to the site of injury by cytokines and chemokines secreted by Schwann cells and injured axons (Gaudet et al., 2011).

At the same time, remaining Schwann cells proliferate and join together to form 'bands of Büngner', which secrete many growth factors and aid in guiding regenerating proximal nerve stumps back to he denervated site (see section 1.4.3 below; Gillingwater and Ribchester, 2001).

At the NMJ, Wallerian degeneration is associated with mitochondrial damage, a reduction in the density of synaptic vesicles (Winlow and Usherwood, 1975), and fragmentation of the nerve terminal, which becomes surrounded and eventually replaced by processes extended by terminal Schwann cells (Miledi and Slater, 1970).

1.4.2 Dying-back neuropathy

In contrast to the rapid fragmentation along the length of the distal nerve seen in Wallerian degeneration, dying-back neuropathies are characterised by a wave of asynchronous withdrawal, starting at the NMJ. From the distal end of a nerve the degeneration then progresses retrogradely. There is no fragmentation of the nerve; instead the NMJs and distal axon appear to be reabsorbed into the axon, which ends in a retraction bulb (for review see Gillingwater and Ribchester, 2003).

A mouse model of dying-back neuropathy with a mutation known *wasted* has been used in this thesis (see chapter 3). *Wasted* is an autosomal recessive mutation in which the gene encoding translation elongation factor eEF1A2 is deleted (Chambers et al., 1998). eEF1A2 is one of two variant forms of eEF1A (the other being eEF1A1), which play a key role in protein synthesis (Condeelis, 1995). At birth eEF1A1 is expressed ubiquitously, but its expression in nerve and muscle declines and is absent by P21 in mice (Pan et al., 2004). At this point eEF1A2 has normally replaced the role of eEF1A1, but is absent in *wasted* mice. Homozygous *wasted* mice therefore develop normally until P21, and then develop tremors, weight loss and an uncoordinated gait, which is followed by paralysis and death by P28 (Newbery et al., 2005). The pathology seen in these mice is due to dying-back neuropathy, leaving skeletal muscle denervated (Murray et al., 2008b).

1.4.3 Regeneration

Unlike the CNS, the PNS has the ability to regenerate following degeneration. Following the clearance of debris distal to the injury the proximal stump of a peripheral nerve is able to sprout axons with growth cones. These axons are guided back to the remaining endoneurial tube from the degenerated portion of the nerve by chemotactic factors released by Schwann cells. These Schwann cells form bands of Büngner along which the regenerating axons can grow to reach their target muscle (Belkas et al., 2004). In humans large nerves can regrow up to 5mm a day.

At the cell body proteins associated with regeneration, such as actin, tubulin and growth associated proteins, are up-regulated (Fawcett and Keynes, 1990). The patterns of up-regulation recapitulate those seen in the development of the PNS (Miller et al 1989).

Within a few hours of axotomy both myelinated and unmyelinated axons in the proximal stump begin to sprout. The mechanisms giving rise to regeneration at the axon tip are still unknown, but this rapid onset argues against control by the cell body, and rather for local control. Each axon can give rise to several new sprouts, which grow across the injury site until they make contact with the bands of Büngner, down which they can grow towards their target muscle. This process is considerably faster and more successful in crush injuries compared to transections, as the endoneurial tubes remain unbroken and there is no physical gap for the axons to cross (Fawcett and Keynes, 1990; Sunderland, 1978). Axons

therefore remain in their original 'parent' tubes and are guided back to their original target muscle fibre (Fawcett and Keynes, 1990).

Interactions between axons and Schwann cells are essential for successful regeneration, as demonstrated by studies in which Schwann cells are killed, through freezing or by cytotoxic agents, and axons fail to regenerate (for review see Fawcett and Keynes, 1990; Hall, 1986). Whether an axon becomes myelinated or unmyelinated is dependent on the axon itself, rather than the previous role of the surrounding Schwann cells. Previously myelinated axons are remyelinated, and previously unmyelinated axons remain unmyelinated (Weinberg and Spencer, 1975).

Once regenerating axons reach the NMJ the endplate is reinnervated by multiple inputs in way that replicates neonatal development. As in development excess inputs are pruned back until all motor endplates are mono-innervated (Barry and Ribchester, 1995).

1.5 Diseases of the PNS

Diseases affecting the motor neurons are broadly termed motor neuron disease (MND), although this term covers a number of different diseases. All are characterised by degeneration of motor neurons, atrophy of skeletal muscle and associated loss of movement. ALS and SMA are two of the most common forms of MND. In both these diseases NMJs appear to be an early pathological target (Murray et al., 2010)

1.5.1 ALS

The French neurologist Jean-Martin Charcot first described ALS in 1869 (Charcot and Joffroy, 1869). It is a late onset and progressive neurodegenerative disease, and the most common form of adult motor neuron disease with a prevalence of 1 in 50,000. It is characterised by loss of both upper and lower motor neurons resulting in muscle atrophy, weakness and spasticity. ALS is fatal, usually due to denervation of respiratory muscles and the diaphragm, which occurs within 5 years of disease onset in most cases (for review see Boillée et al, 2006; Rothstein, 2009).

Although 90-95% of cases of ALS are sporadic, the remaining 5-10% of cases are inherited (Cleveland and Rothstein, 2001). Through identification of genes involved in these familial cases, and the development of transgenic animal models, some light has been shed on the potential mechanisms underlying ALS. Approximately 20% of cases of familial ALS are caused by mutations in the Cu/Zn superoxide dismutase (SOD1) gene (Rosen et al, 1993).

1.5.2 SMA

SMA is a childhood form of motor neuron disease. SMA is the leading genetic cause of infant mortality and, after cystic fibrosis, the most common autosomal recessive illness in humans. It has an incidence of 1 in 6000 and a carrier frequency of 1 in 35 (Monani, 2005).

SMA is also a progressive neurodegenerative disease, but unlike ALS is characterised by lower motor neuron death with no upper motor neuron involvement. Symptoms include weakness and atrophy of voluntary muscles, which is often more severe in the legs than the arms (Wirth, 2000). Those affected may have difficulty feeding and have increased susceptibility to respiratory tract infections. Pneumonia is a common cause of death in SMA patients (Hardart et al. 2002).

95% of SMA patients have a deletion of the survival motor neuron 1 gene (SMN1), leading to a loss of function of SMN protein (Cifuentes-Diaz et al, 2001; Le et al. 2005; Monani, 2005). The remaining 5% have mutations within the same gene. In humans and higher primates a highly homologous gene termed centromeric SMN (SMN2) also produces SMN protein, but chiefly produces a transcript missing exon 7 (SMN Δ7) and only low levels of full length SMN. Therefore a greater copy number of SMN2 gives rise to a milder phenotype of the disease by producing higher levels of full length SMN protein (Monani, 2005).

1.5.3 NMJs as early pathological targets

NMJs and distal axonal compartments have been shown to be early pathological targets and to play a critical role in neuronal loss in many neurodegenerative diseases in both the PNS and CNS, including ALS and SMA (Wishart et al., 2006). Studies of NMJs from both ALS patients and animal models demonstrate

degeneration of NMJs before any changes are seen in the proximal axon or soma (Fischer et al., 2004).

It is not yet clear why NMJs are particularly vulnerable, but the theory of compartmentalised neurodegeneration proposes that synapses, axons and neuronal soma have distinct responses to degenerative stimuli (Gillingwater and Ribchester 2001). The molecular mechanisms behind NMJ breakdown remain unclear, however, a number of potential cellular pathways that could contribute to NMJ dysfunction have been identified (Murray et al., 2010). These include disruption of axonal transport and cytoskeletal architecture, oxidative stress and mitochondrial disruption, endoplasmic reticulum stress, RNA processing and growth factor signalling (for review see Murray et al., 2010).

Previous therapeutic strategies against neurodegenerative disease have targeted the neuronal cell body, but have failed to prevent degeneration of axons and synapses (Chiesa et al., 2005; Sagot et al., 1995). The body of evidence highlighting synapses as early pathological targets in a range of neurodegenerative conditions, along with increasing understanding of cellular pathways underlying synaptic loss, offers the potential to target therapeutic strategies to this particularly vulnerable region of the neuromuscular system, and to target neurodegenerative disorders in their early stages.

1.6 Factors influencing the PNS

Identification of genetic factors that influence the form and function of the PNS *in vivo* is important in aiding our understanding of the neuromuscular system in health and disease. For this reason I have studied the effect of three different genes on the PNS: yellow fluorescent protein (YFP), apolipoprotein E (APOE) and ERCC1 (excision repair cross-complementing group 1).

1.6.1 YFP

YFP is a widely used tool in many different biological systems. Its use as a reporter gene since its discovery in the 1960s by Shimomura and colleagues (Shimomura et al, 1962) has been instrumental in many breakthroughs. It is commonly used under the control of a thy-1 promoter to visualise the nervous system, under the assumption that it is biologically inert (Feng et al., 2000). However, cells expressing XFPs contain large amounts of a foreign protein, which has previously been shown to induce a cell stress response (Detrait et al., 2002; Liu et al., 1999). My first hypothesis, therefore, is that YFP is not an inert reporter protein, but has effects throughout the PNS.

1.6.2 ApoE

ApoE is a lipid transport protein with three naturally occurring isoforms in the human population, termed apoE2, apoE3 and apoE4 (Utermann et al, 1977). Previous work has shown that these isoforms differentially affect outcome in the CNS following traumatic brain injury, and the age of onset and progression in a number of CNS diseases, including Alzheimer's disease and Parkinson's disease

(Millar et al., 2003; Strittmatter et al., 1993; Zareparsi et al., 1997). Despite a number of studies on the effect of the isoforms on diseases of the PNS, results remain inconclusive (Geranmayeh et al., 2005). My second aim is therefore to determine whether or not the different isoforms of apoE differentially affect rates of degeneration and regeneration in the PNS.

1.6.3 ERCC1

Ercc1 is a DNA repair protein. It functions as part of a heterodimer with xeroderma pigmentosum group F (XPF), playing a role in the nucleotide excision repair pathway (NER), and in repairing some double strand breaks and interstrand crosslinks (Ahmad et al., 2008; Bergstralh and Sekelsky, 2008; Gregg et al., 2011). Deficient DNA repair mechanisms are linked to cancer and accelerated aging (de Boer and Hoeijmakers, 2000; Schumacher et al., 2008), and have also been implicated in neurodegeneration (Kraemer et al., 2007; Rass et al., 2007). As NMJs are primary pathological targets in many neurodegenerative diseases (Wishart et al., 2006) I have used mice deficient in Ercc1 in order to investigate the effect of reduced DNA repair on NMJ morphology.

1.7 Aims

Hypothesis I: *YFP is not an inert reporter protein, but has effects throughout the PNS.*

Aim I: Investigate the effect of YFP on the PNS.

i. Examine the levels of cell stress proteins in YFP spinal cord.
ii. Examine the effect of expression of YFP on the morphology of NMJs in healthy adult mice.
iii. Investigate the effect of YFP on the time course of Wallerian degeneration following nerve injury and in pathological dying-back neuropathy.

Hypothesis II: *ApoE isoforms differentially affect degenerative and regenerative events in the PNS.*

Aim II: Investigate the effect of the apoE3 and apoE4 transgenes on the PNS.

i. Examine the effect of expression of the apoE transgenes on the morphology of NMJs and peripheral nerve in healthy adult mice.
ii. Compare the rate of Wallerian degeneration in mice expressing apoE3 or apoE4 after a nerve crush injury.
iii. Compare the rate of subsequent regeneration and neuromuscular reinnervation in mice expressing apoE3 or apoE4.

Hypothesis III: *Loss of Ercc1 leads to pathological changes at the NMJ.*

Aim III: Investigate the effect of the loss of Ercc1 at the NMJ.

i. Examine the effect of loss of Ercc1 on the morphology of the NMJ.

ii. Quantify levels of neuromuscular innervation in Ercc1$^{\Delta/-}$ mice at different ages.

Chapter 2 - General Materials and Methods

All materials and methods presented in this chapter are general, and have been used for experiments throughout this thesis. For detailed materials and methods pertaining to each specific results chapter, see individual chapter materials and methods.

2.1 Surgery

Mice were anaesthetised by inhalation of halothane (2% in 1:1 N_2O/O_2) before exposing the sciatic nerve in the thigh, the tibial nerve above the heel or the intercostal nerves following the line of the ribs. For nerve crush surgeries pressure was applied between a pair of fine-point forceps for 30 seconds. Nerves were checked to ensure a complete crush had been performed before suturing the skin and allowing the mouse to recover. For nerve cut experiments, a ~1mm section of nerve was removed to ensure complete transection. Post-operative mice were kept in standard animal house conditions.

2.2 Quantitative fluorescent (Li-COR) western blots

Total protein was isolated from distal nerve stumps, entire dissected sciatic nerves or spinal cords. Protein was separated by SDS/Polyacrylamide gel electrophoresis on 4-20% pre-cast NuPage 4-12% Bis Tris gradient gels (Invitrogen) and then transferred to PVDF membrane overnight. The membranes were blocked for 30 minutes using 5ml Odyssey blocking buffer (Li-

COR) and incubated overnight with 3µl primary antibody (Actin – Abcam; apoE - Millipore; Caspase 1 and CCL3 – Abcam; GFP – Millipore; STI1 – BD Biosciences). Secondary antibodies were added at a concentration of 1µl/ml in PBS and membranes were incubated for two hours (Donkey anti goat IRDye 680, goat anti mouse IRDye 800, goat anti mouse IRDye 680 and goat anti rabbit IRDye 680 - Odyssey). Blots were imaged using an Odyssey Infrared Imaging System (Li-COR Biosciences). Quantification was performed on single channels with the analysis software provided. Bands were identified by their molecular weight and normalised to controls. The arbitrary fluorescence intensity was calculated using Odyssey software.

2.3 Immunohistochemistry

Mice were sacrificed by inhalation of isofluorane (2% in 1:1 N_2O/O_2) or perfusion fixation with 0.1M PBS containing 4% paraformaldehyde. The levator auris longus (LAL; from the dorsal/ posterior surface of the neck; Murray et al., 2008a), transversus abdominis (TA; from the anterolateral abdominal wall; Murray et al., 2008b), first to third deep lumbricals (from the plantar surface of the hind-paw; Murray et al., 2010) and/or flexor digitorum brevis muscles (FDB; from the plantar surface of the hind-paw; Murray et al., 2010) were dissected in oxygenated mammalian physiological saline (mM: NaCl 120, Kcl 5, $CaCl_2$ 2, $MgCl_2$ 1, NaH_2PO_4 0.4, $NaHCO_3$ 23.8, D-glucose 5.6). Muscles were then fixed for 30 minutes in 0.1M PBS containing 4% paraformaldehyde (Electron Microscopy Science).

All non-FP muscles were exposed to α-bungarotoxin (BTX) conjugated to the fluorescent label tetramethyl-rhodamine isothiocyanate (TRITC-α-bungarotoxin; 5mg/ml, Molecular Probes) for 30 minutes to label post-synaptic acetylcholine receptors. Acetylcholine receptors in YFP muscles were labelled with α-bungarotoxin conjugated to Alexa Fluor® 647 (Alexa 647-α-BTX; 5mg/ml, Invitrogen).

Muscles were then immunohistochemically processed to allow visualisation of pre-synaptic nerve terminals. Muscles were blocked in 4% bovine serum albumin (BSA) and 1.5% TritonX in 0.1M PBS for 30 minutes before incubation in primary antibodies directed against 145kDa neurofilament proteins (1:300 dilution; Millipore) overnight. After washing for 2 hours in 0.1M PBS, non-FP muscles were incubated for 4 hours in a 1:30 dilution of swine anti-rabbit secondary antibody conjugated to the fluorescent label fluorescein isothiocyanate (FITC; Dako). YFP muscles were incubated for 4 hours in a 1:30 dilution of swine anti-rabbit secondary antibody conjugated to TRITC (Dako). Muscles were then whole-mounted in Mowoil® (Calbiochem) on glass slides and cover-slipped for subsequent imaging.

2.4 Microscopy

Fluorescently labelled muscle preparations were viewed using either a standard epi-fluorescence microscope equipped with a chilled CCD camera (40x objective; 0.8NA; Nikon IX71 microscope; Hammamatsu C4742-95), or a laser

scanning confocal microscope (63x objective; 1.4NA; Zeiss Axioskop). For confocal microscopy, the 488nm, 543nm and 647nm laser lines were used for excitation and confocal Z-series were merged using Zeiss software. All images were taken using sequential laser capture and with the excitation/emission spectra set to ensure no bleed-through between channels. Images were assembled for analysis using Adobe Photoshop.

2.5 Quantification of NMJs

A minimum of 50 NMJs, selected at random but spread across the entire muscle, were assessed in each muscle preparation. Muscles where antibody staining was too faint to quantify due to poor antibody penetration and muscles with damage to either the muscle fibres or nerves from dissection were excluded from further analysis. All analysis was performed blind to the genetic status of the material.

For occupancy counts endplates were categorised as vacant (no neurofilament overlying the endplate), partially occupied (neurofilament partially overlying the endplate) or fully occupied (neurofilament entirely overlying the endplate). For quantification of developmental synapse elimination or pathological levels of poly-innervation, fully occupied endplates were further subdivided based on the number of axonal inputs contacting the endplate. For neuromuscular reinnervation experiments, an individual endplate had to be fully occupied by an incoming single axon profile to be considered reinnervated.

2.6 Statistical analysis

All data were collected into Microsoft Excel spreadsheets and analysed using GraphPad Prism software. All bar charts shown are mean ± SEM. Statistical significance was considered to be $p<0.05$ for all analyses. Individual statistical tests used are detailed in figure legends.

Chapter 3 - YFP

3.1 Introduction

Green fluorescent protein (GFP) was first discovered, almost accidently, in 1961. Osamu Shimomura and colleagues were trying to purify aequorin, a protein from the jellyfish *Aequorea Victoria* that fluoresces blue in the presence of Ca^{2+} (Shimomura et al., 1962). During the purification of aequorin they noted a second protein in the jellyfish extract, which appeared "slightly greenish in sunlight". This protein was named GFP, and was hardly used again until Martin Chalfie realised that it might be useful as a fluorescent marker to study gene expression and protein localisation in *Caenorhabditis elegans* over thirty years later (Chalfie et al., 1994).

Work carried out in the Chalfie lab in the early 1990s showed that the formation of the GFP chromophore did not need any other substrates or enzymes from the jellyfish, and that it could be expressed in other species (Chalfie et al., 1994). Variants of GFP were then engineered by Roger Tsein to improve on the original wt-GFP, so that the fluorescent proteins used in research today have improved biophysical properties, such as more efficient protein folding, as well as a number of spectrally distinct colour variants (reviewed by Cubitt et al., 1995; Heim et al., 1994; Heim and Tsien 1996). These colour variants include yellow, cyan, red and blue, as well as the original green. Collectively the fluorescent proteins are termed XFPs.

From that time onwards GFP and its variants have been a hugely important biological marker/molecular imaging tool, and its discovery and refinement lead to Shimomura, Chalfie and Tsien receiving the Nobel Prize for Chemistry in 2008.

GFP has several advantages making it an excellent biological marker. First it is small – the peptide consists of only 298 amino acids (Prasher et al., 1992) and exists as a monomer, which allows it to diffuse through cells more easily than other, larger markers such as β-galactosidase. Second, GFP is heritable, meaning that GFP expressing strains could be established. Third, the chromophore (the part of the molecule responsible for giving GFP its colour) is encoded entirely by the polypeptide chain. This means that no other exogenous substrates or co-factors are needed to cause fluorescence and that living cells can be viewed non-invasively, simply by viewing them under blue light (Chalfie et al., 1994). Fourth, GFP can be fused to other proteins without loss of fluorescence, making it very valuable as a biological marker. Finally, different spectral variants of GFP have been developed (Cubitt et al., 1995; Heim and Tsein, 1996; Heim et al., 1994). These different fluorophores can be used in conjunction with each other, allowing for studies examining the co-expression of different genes.

In 1995 Ikawa et al produced the first lines of GFP transgenic mice. In trialling different promoters and different variants of GFP they produced mice that expressed GFP ubiquitously (Ikawa et al., 1995). The lines of mice used in the

current study express YFP selectively in neurons, and were generated in 2000 by Feng et al. (Feng et al., 2000). This group produced 25 lines of transgenic mice expressing each of the four spectral variants (GFP, YFP, CYP, RFP) under the control of the *thy1* promoter. *Thy1* is a cell surface glycoprotein which is part of the immunoglobulin superfamily (Gordon et al., 1987). Its name is derived from its expression in thymocytes, but it is also expressed on the surface of neurons throughout the nervous system (Morris, 1985) making it ideal for use as a neuronal-specific promoter. Although all of the founder *thy1*-YFP mice were generated using the same construct, each of the lines produced had a unique pattern of expression within the neurons that proved to be hereditable. This observation indicated that insertion site and / or copy number could play a role in XFP expression.

The variations in expression patterns in the *thy1*-XFP mice included differences in the intensity of the XFP labelling, different cell types expressing fluorescent protein, and variable proportions of neurons being labelled (Feng et al., 2000). In this study, two lines of the thy-1 mice have been used: YFP-16, which express YFP in all motor neurons, and YFP-H, in which only a minority of the motor neurons fluoresce. The YFP-H mice have the particular advantage of allowing the comparison of neurons expressing YFP and non-fluorescent neurons within the same muscles from individual mice, thereby eliminating any complications caused by background strain differences that may arise from using non-YFP mice for controls.

Feng et al (2000) assessed the toxicity and phototoxicity of YFP using in vivo imaging of YFP labelled NMJs. Identified NMJs were imaged over a time course of 8 weeks to 9 months. The only changes identified were those typically associated with aging, i.e. a change in the staining pattern with the staining of both the motor nerve terminal and endplate becoming 'spotty' (Balice-Gordon and Lichtman, 1990). Additional NMJs were imaged for longer sustained time periods and every 2 minutes during the process of reinnervation, but no changes were detected and the process of reinnervation continued as normal. Feng et al therefore concluded that expression of fluorescent proteins in neurons had no discernable effect on neuronal morphology or any detectable level of toxicity (Feng et al., 2000). This conclusion was in agreement with other reports that suggested that XFPs are biologically inert (Ikawa et al., 1998; Lichtman and Sanes, 2003; Okabe et al., 1997). Thus, the underlying assumption is that the presence of fluorescent protein has no effect on the cellular or molecular composition of the neuron.

Neurons in the *thy1*-XFP mice contain large amounts of a foreign protein, the presence of which has been shown to alter cellular and molecular characteristics of living cells in other experimental model systems *in vivo* and *in vitro*, triggering stress responses and pathological changes. In 1999 Liu et al noted a link between expression of GFP and induction of apoptosis in three cell lines, and noted that this finding "should promote studies of GFP cytotoxicity and attempt to isolate new non-toxic mutants of GFP" (Liu et al., 1999). When Huang et al introduced mice over-expressing GFP in the heart as an extra,

transgenic, control group for a study of cardiac hypertrophy they noticed that the 'control' GFP group developed dilated cardiomyopathy, and that the severity was dose-dependent (Huang et al., 2000). The effect of reporter genes on primary cortical neurons was directly investigated in 2002 by Detrait and colleagues (Detrait et al., 2002). They reported that GFP expression induced apoptotic cell death in the neurons more rapidly than other reporter genes (Detrait et al., 2002). Taken together, these studies potentially contradict the findings of Feng et al. (2000), indicating that XFPs are not inert, particularly when highly expressed. My hypothesis is therefore that YFP is not an inert reporter protein, but that its expression can influence the form and function of the PNS.

In order to test this hypothesis I have investigated whether expression of yellow fluorescent protein modifies the form and function of the healthy and pathological PNS *in vivo.* I have used RT-PCR, western blotting and immunohistochemistry to examine the levels of cell stress proteins in the spinal cord of YFP mice. I have also used immunohistochemistry and confocal microscopy to study the effect of expression of YFP on morphology of NMJs in healthy adult mice, and investigate the effect of YFP on the time course of Wallerian degeneration following nerve injury and in pathological dying-back neuropathy.

3.2 Materials and methods

3.2.1 Mice

Breeding colonies of *thy1*-YFP-H mice (Feng et al., 2000) and *thy1*-YFP-16 mice (hereafter referred to as YFP-H and YFP-16, respectively), both on a C57BL/6J background, were initially purchased as breeding pairs from Jackson Laboratories and established and maintained in animal care facilities at the University of Edinburgh. Young adult YHP-16 mice were compared with non-FP C57BL/6J mice from the same breeding colony. In experiments using YFP-H mice non-FP motor units within the same mice were used as internal controls. The YFP status of mice was ascertained by examining ear punches for evidence of YFP-labelled neurons innervating the skin. To determine the effects of YFP on dying-back pathology, YFP-H mice were crossed with *wasted* mice, a model of dying-back pathology (Murray et al., 2008b; Newbury et al., 2005). YFP-H mice were crossed with *wasted* mice for two generations in order to obtain homozygous *wasted* mice expressing YFP in a subset of neurons. *Wasted*/YFP-H mice were genotyped using standard PCR techniques. Primers used were:

Wasted wild-type	Forward:	TAGTGGCTCCTTGGAACAG
	Reverse:	CTACTCTCCCTGAATGCCTT
Wasted knockout	Forward:	ATAAGCTCCCCAATGGTAGAGAA
	Reverse:	CGCGCCATTCTTGTATTGTT

Wasted genotype was determined by presence or absence of a band of the appropriate size following separation by gel electrophoresis. *Wasted*/YFP-H mice were taken for analysis at post-natal day 24 (late-symptomatic). The

banked tissue from a previous, now defunct, colony of strongly expressing *thy1*-YFP-16 mice was obtained from mice originally supplied to Dr Simon Parson at the University of Leeds by Jackson Laboratories. Animals were housed in standard SPF conditions and all procedures were carried out under licensed authority from the UK Home Office.

3.2.2 Cell stress array

Mouse cell stress focused pathway arrays in a 96-well plate format (PAM-003A), compatible with an ABI 7000 real-time PCR machine, were used to assay changes in cell stress gene expression (three comparisons for YFP-16 and three for wild-type controls, each comparison composed of pooled tissue from three individual mice). Samples were added to the reaction plate and signal amplification by PCR was carried out using Sybr-Green '1 step qRT-PCR kit' (Invitrogen). Analysis was carried out using the Analysis Suite spreadsheet provided by Tebubio SuperArrays. Gene functions listed in table 3.1 were obtained from the SuperArray product specification sheets.

3.2.3 Quantitative fluorescent (Li-COR) western blots

See general materials and methods, section 2.2.

3.2.4 Spinal cord immunohistochemistry

Entire vertebral columns were removed and collected into 4% paraformaldehyde solution for 1 hour. The spinal cord was removed from the vertebral column and further fixed for 30mins before being washed in 1xPBS

and embedded in 2% low-melting point agarose. The embedded spinal cords were mounted on a vibratome and cut coronally at a thickness of ~200μm for immunohistochemical staining. Sections were blocked in 4% bovine serum albumin (BSA) and 1.5% TritonX in 0.1M PBS for 30 minutes before incubation in primary antibodies directed against caspase 1 (1:500 dilution; Abcam) overnight. Sections were washed for 2 hours in 0.1M PBS, and then incubated for 2 hours in a 1:30 dilution of swine anti-rabbit secondary antibody conjugated to the fluorescent label tetramethyl-rhodamine isothiocyanate (TRITC, Dako). Sections were co-stained with fluorescent nuclear dye (TO-PRO 3, Molecular Probes). Sections were then whole-mounted in Mowoil® (Calbiochem) on glass slides and cover-slipped for imaging.

3.2.5 NMJ Immunohistochemistry

See general materials and methods, section 2.3.

3.2.6 Surgery

See general materials and methods, section 2.1, for surgery overview. Intercostal nerve cuts have been used to obtain results presented in this chapter. Initially I attempted to study the effects of YFP expression on Wallerian degeneration using our standard nerve axotomy protocol – cutting the tibial nerve leading to denervation of the deep lumbrical muscles of the hind paw. Whilst immunohistochemistry confirmed that the nerve cut itself was successful very little YFP was expressed in the lumbrical muscles, both in terms of the number of motor units fluorescing and the levels of fluorescence seen. Despite a number

of attempts I was unable to use the lumbrical muscles to view Wallerian degeneration in the presence of YFP.

A different muscle preparation commonly used in the lab is the LAL muscle, which is innervated by the facial nerve. I next attempted to denervate this muscle, as previous work on YFP mice has shown that it often has a number of YFP expressing motor units in YFP-H mice (see Fig. 3.7 and 3.11 for confocal micrographs of YFP expression in the LAL). However, the nerve innervating it is relatively short and could only be accessed behind the ear of the mouse, making it very difficult to visualise and meaning that the muscle was often damaged in the surgery.

I then attempted to denervate the transversus abdominis muscle. Fewer motor units express YFP in this muscle compared to the LAL, but it has the advantage of being innervated by the intercostal nerves, which can be axotomised far enough from the TA to avoid damaging the muscle in the surgery. Once the intercostal nerves innervating the area of the TA that I was able to dissect out for immunohistochemistry were identified this preparation proved to be the most successful, and was the protocol I used to obtain nerve cut data comparing YFP and non-FP nerves in the same muscle (Fig. 3.1).

The high frequency of YFP-positive motor units and the high levels of fluorescence seen in the LAL muscle, in comparison to the infrequent, low intensity labelling in the lumbricals indicates a possible proximal to distal

gradient of YFP expression in these YFP-H mice. This is supported by the intermediate numbers of YFP-positive motor units observed in the TA, a muscle that is anatomically between the LAL and lumbricals (un-quantified observation).

Figure 3.1 – Adaptation of surgical protocol in YFP-H mice (over page). Flow chart showing the changes in method for nerve cut surgery to allow for both an accessible nerve and good YFP expression.

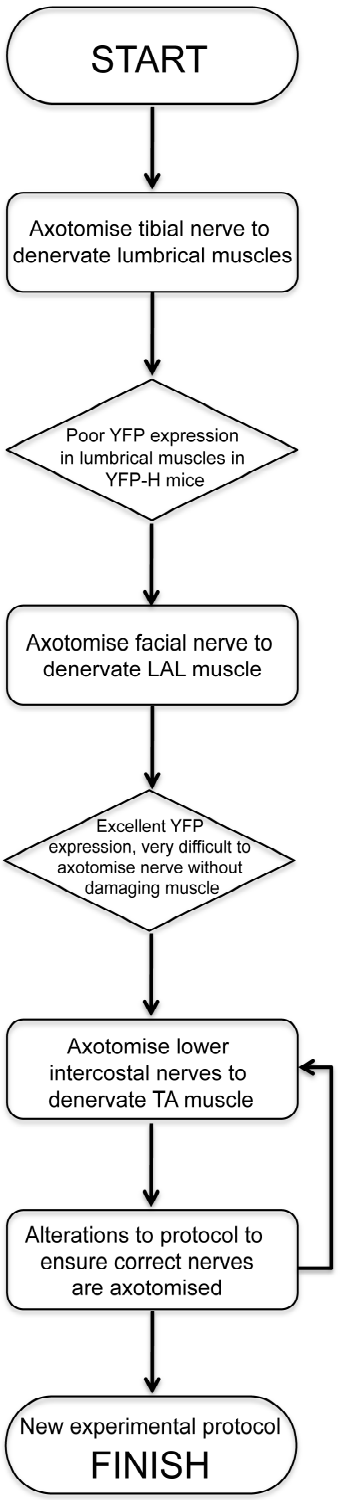
START
Axotomise tibial nerve to denervate lumbrical muscles
Poor YFP expression in lumbrical muscles in YFP-H mice
Axotomise facial nerve to denervate LAL muscle
Excellent YFP expression, very difficult to axotomise nerve without damaging muscle
Axotomise lower intercostal nerves to denervate TA muscle
Alterations to protocol to ensure correct nerves are axotomised
New experimental protocol
FINISH

3.2.7 Microscopy

See general materials and methods, section 2.4.

3.2.8 Quantification of NMJs

Quantitative analysis was performed on images obtained from the confocal microscope with the YFP channel initially excluded, so that the operator did not know the YFP status of the tissue being analysed. For analysis of neurofilament accumulation in normal tissue endplates were assigned a score between 0 and 5, with 0 being healthy NMJs with no evidence of neurofilament accumulation and 5 being nerve terminals with large aberrant accumulations of neurofilament. The YFP channel was revealed subsequent to quantification to determine the YFP status of each nerve terminal. For occupancy counts in *Wasted*/ YFP-H mice undergoing dying-back pathology, endplates were categorised as either partially occupied (neurofilament partially overlying the endplate) or fully occupied (neurofilament entirely overlying the endplate). Vacant endplates were excluded from analysis since there was no way to tell their YFP status.

3.2.9 Statistical analysis

See general materials and methods, section 2.6.

3.3 Results

3.3.1 YFP expression activates cell stress responses in neurons in vivo.

To begin with I investigated whether expression of yellow fluorescent protein modifies neuronal cell stress pathways *in vivo*, using cell stress pathway-specific RT^2 profiler PCR arrays. This allowed me to quantify and compare expression of known cell stress-related genes in the spinal cord of YFP-16 mice compared to C57-Bl6 wild-type controls. YFP-16 mice from our breeding colony appeared grossly identical to those previously reported in the literature, expressing YFP in the vast majority of neurons in the PNS (Feng et al., 2000). However, nearly half of all the cell stress genes (41 out of 84) examined on the PCR array were up-regulated more than 1.5-fold in spinal cord from YFP-16 mice compared to controls (table 3.1 and Fig. 3.2). Of these, 10 genes (24%) had expression levels increased greater than 2-fold, including genes involved in cell stress activation, inflammation, DNA damage and repair and apoptosis (table 3.1).

To confirm that the RNA changes observed in YFP-16 mouse spinal cord resulted in corresponding changes at the protein level, I selected two proteins which had greater than 2-fold up-regulation in YFP-16 mice, caspase 1 and CCL3, for validation using quantitative fluorescent western blot. Caspase 1 has a role in apoptosis signaling, and CCL3 in inflammation. A further stress inducible protein, STI1, which was not included on the PCR array, was also selected for western blot. Expression levels of both caspase 1 and CCL3 were dramatically increased in the YFP-16 spinal cord (1000 fold and 100 fold

respectively, when normalised to wild-type, Fig. 3.3), in agreement with the mRNA data. STI1 was expressed at an equivalent level in wild-type and YFP-16 tissue, showing that there was not a universal up-regulation of stress-related proteins in the YFP-16 spinal cord. YFP protein was found only in samples from YFP-16 mice, and not seen in the controls, confirming genotyping (Fig. 3.3A).

I verified that levels of YFP were directly responsible for the cell stress response by comparing the levels of caspase 1 in YFP-16 mouse spinal cord with levels in YFP-H mouse spinal cord. YFP-H mice only express YFP in a small subset of neurons, compared to the majority of neurons in the YFP-16 line. Increased expression of caspase 1 correlated directly with the amount of YFP present, as levels in YFP-16 mouse spinal cord were 70-fold higher than levels in YFP-H mice (Fig. 3.4).

I further confirmed the YFP expression in neurons was directly triggering cell stress responses by using immunohistochemistry for caspase 1 expression in YFP-H mouse spinal cord. Increased caspase 1 levels were restricted to cells expressing YFP (Fig. 3.5). It was important to ensure that there was no bleed-through between the channels imaging YFP and caspase 1, as this could lead to a signal being picked up in the TRITC channel that was actually due to the YFP rather than immunohistochemistry against caspase 1. To avoid this all images were taken using sequential laser capture and with the excitation/emission spectra set as narrowly as possible to avoid overlap between the channels. Lack of bleed-through was confirmed by the presence of information in the YFP

channel that was not seen in the TRITC channel. Similarly structures marked by the caspase immunohistochemistry have not all shown in the YFP channel (Fig. 3.6).

Taken together, these data demonstrate that expression of YFP in mouse neurons *in vivo* activates a robust cell stress response at both the RNA and protein level.

TABLE 3.1 - Mouse SuperArray data showing greater than 1.5 fold cell stress RNA expression changes in the spinal cord of YFP-16 mice compared with wild-type controls

Array cell	Symbol	Fold change	Role in cell stress
A09	Ccl4	3.26	Inflammation
C03	Cyp7a1	3.14	Oxidative or metabolic stress
A08	Ccl3	2.94	Inflammation
B04	Csf2	2.77	Inflammation
A05	Casp1	2.30	Apoptosis signalling
F06	Nfkbia	2.26	Apoptosis signalling
B11	Cyp2c29	2.23	Oxidative or metabolic stress
F01	Lta	2.18	Inflammation
A06	Casp8	2.11	Apoptosis signalling
B02	Chek2	2.07	DNA damage and repair
A01	Anxa5	1.95	Apoptosis signalling
A07	Ccl21b	1.94	Inflammation
C01	Cyp4a10	1.93	Oxidative or metabolic stress
G05	Tnfsf10	1.92	Apoptosis signalling
D05	Gpx2	1.90	Oxidative or metabolic stress
A03	Bax	1.89	Apoptosis signalling
B05	Cxcl10	1.84	Inflammation
D09	Hmox1	1.84	Oxidative or metabolic stress
B10	Cyp2b9	1.84	Oxidative or metabolic stress
F07	Nos2	1.79	Inflammation
D08	Gstm3	1.79	Oxidative or metabolic stress
B06	Cyp1a1	1.74	Oxidative or metabolic stress
F02	Mdm2	1.72	Growth arrest and senescence
C07	Egr1	1.72	Proliferation and carcinogenesis
C04	Ddit3	1.68	Growth arrest and senescence
F12	Rad50	1.67	DNA damage and repair
A02	Atm	1.66	DNA damage and repair
E11	Il1b	1.65	Inflammation
C02	Cyp4a14	1.64	Oxidative or metabolic stress
H01	Gusb	1.63	Oxidative or metabolic stress
B07	Cyp1b1	1.63	Oxidative or metabolic stress
G08	Ugt1a2	1.63	DNA damage and repair
C12	Fmo1	1.62	Oxidative or metabolic stress
A04	Bcl2l1	1.62	Apoptosis signalling
E02	Hspa4	1.60	Heat Shock
A11	Ccnd1	1.59	Proliferation and carcinogenesis
B03	Cryab	1.56	Oxidative or metabolic stress
B09	Cyp2b10	1.56	Oxidative or metabolic stress
B12	Cyp3a11	1.56	Oxidative or metabolic stress
F11	Rad23a	1.52	DNA damage and repair
G04	Tnfrsf1a	1.52	Apoptosis signalling

Table 3.1 - Mouse SuperArray data showing greater than 1.5 fold cell stress RNA expression changes in the spinal cord of YFP-16 mice compared with wild-type controls. Note that none of the genes on the array were found to be

significantly down-regulated 1.5 fold in YFP-16 mouse spinal cord. (Array cell refers to the location on the 3D bar chart in Fig. 3.2).

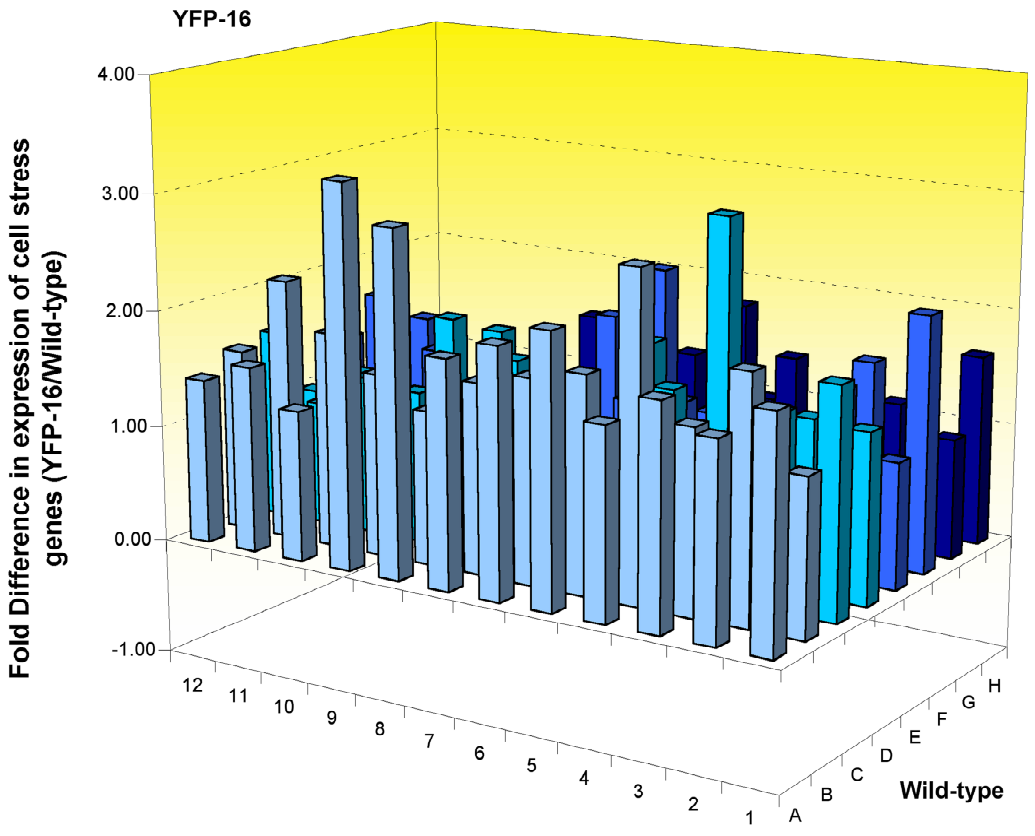

Figure 3.2 - YFP expression in neurons activates cell stress responses at the RNA level *in vivo*. 3D bar chart showing fold-differences in mRNA expression levels for 84 cell stress related genes comparing spinal cord from YFP-16 mice with wild-type (C57-Bl6) mice (N=3 samples, each consisting of pooled tissue from 3 mice. Each bar on the graph represents the mean of the 3 samples. The colours of the bars do not represent anything specific, but are intended to make viewing the graph clearer).

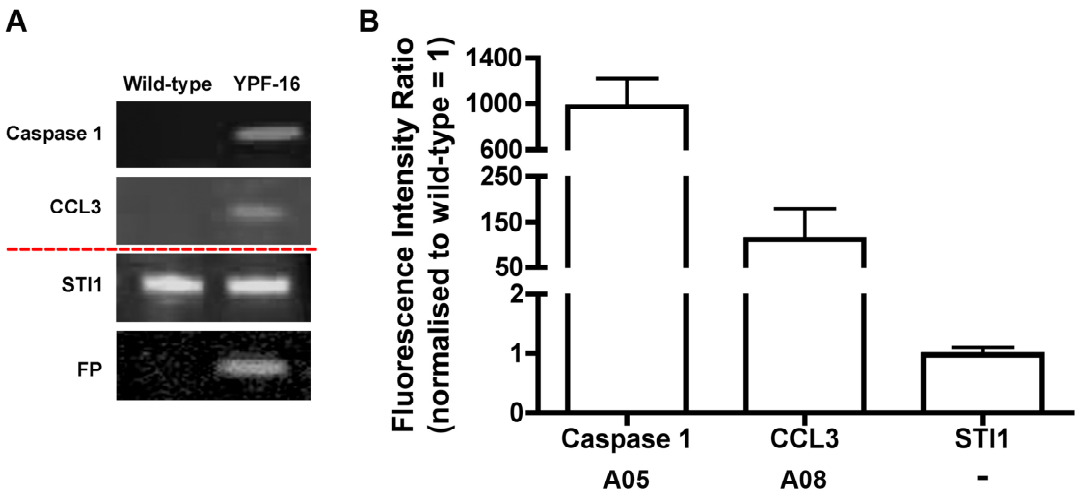

Figure 3.3 - YFP expression in neurons leads to corresponding up regulation of cell stress proteins. A: Representative fluorescent western blots for cell stress proteins in the spinal cord of wild-type and YFP-16 mice. Both caspase 1 and CCL3 had increased expression in YFP-expressing tissue, in agreement with RNA data (Fig. 3.2). A control cell stress protein, STI1, which did not appear in the SuperArray, remained at the same level as seen in wild-type mice. Western blots for GFP confirmed genotype. **B:** Bar chart (mean±SEM) showing quantification of protein expression levels in YFP-16 spinal cord (normalised to wild-type: fluorescence intensity ratio of 1 = same as wild-type), confirming a ~50-fold increase in levels of CCL3 and ~1000-fold increase in levels of caspase 1 (N=3 samples, each consisting of pooled tissue from 3 mice).

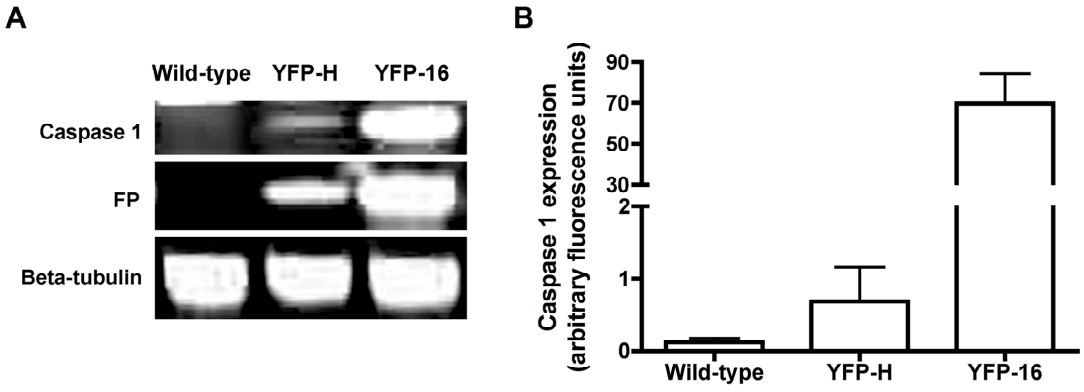

Figure 3.4 – Increased caspase 1 levels correlate with levels of YFP. A: Representative fluorescent western blots for caspase 1 and GFP in the spinal cord of wild-type, YFP-H and YFP-16 mice. Increased caspase 1 expression correlated directly with the amount of YFP present. **B:** Bar chart (mean±SEM) showing quantification of protein expression levels in wild-type, YFP-H and YFP-16 spinal cord (N=3 per genotype).

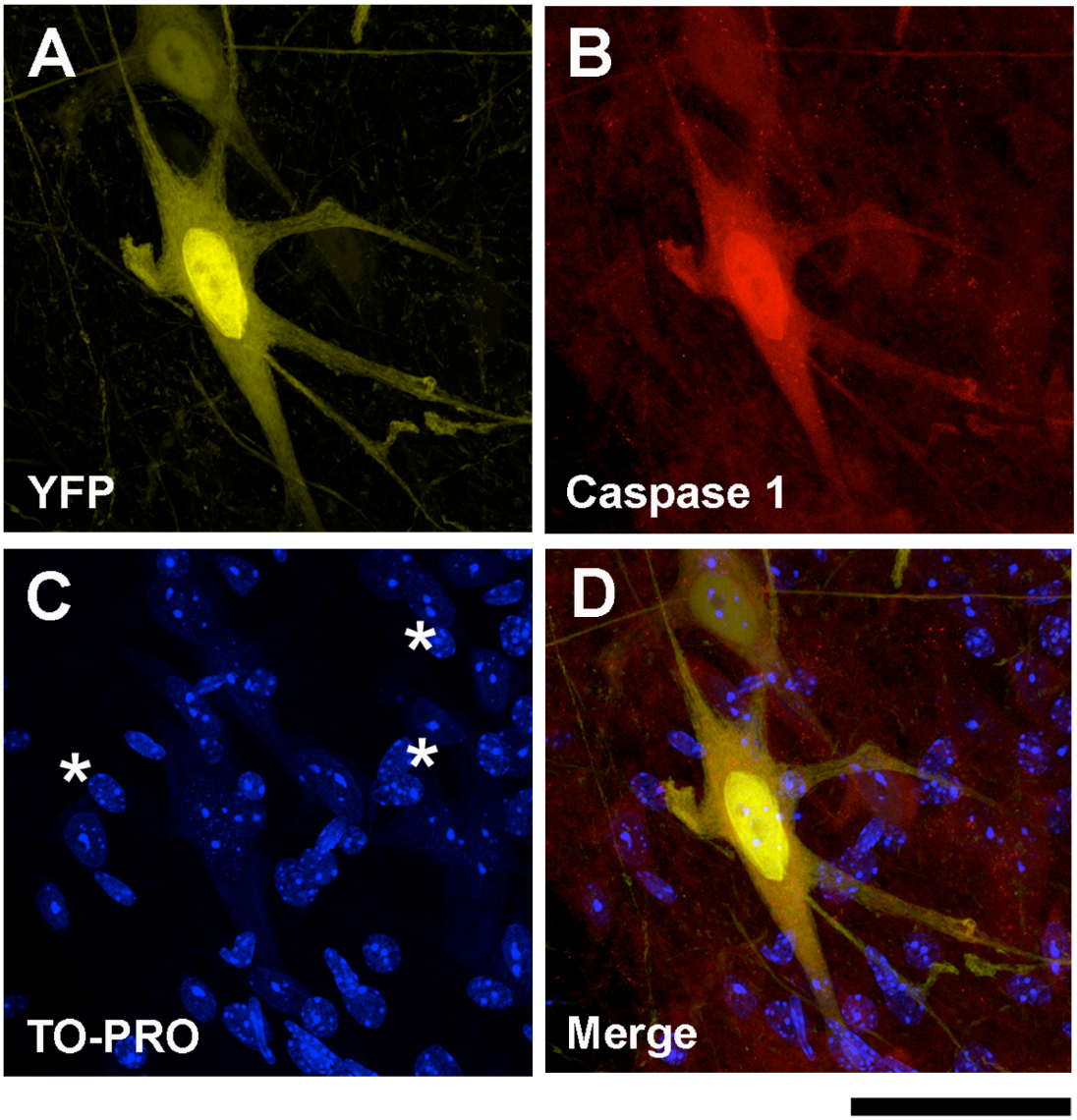

Figure 3.5 – Increased expression of caspase 1 is restricted to YFP expressing cells. Representative confocal micrograph showing caspase 1 immunohistochemistry in the spinal cord of a YFP-H mouse. **A:** Confocal micrograph showing endogenous YFP labelling of two cells in the spinal cord of

a YFP-H mouse. **B:** Caspase immunohistochemistry showing strong caspase labelling of the same two cells, indicating an up-regulation of caspase (a cell stress marker), which is restricted to YFP-positive neurons. **C:** TO-PRO staining for nuclear DNA, showing the nuclei of both the two YFP neurons and all other, negatively labelled, cells (three examples of which are marked with asterisks). **D:** Confocal micrograph showing panels A-C merged. Increased expression of caspase 1 was seen in YFP-positive neurons in all of the sections imaged (N=5 sections). Scale bar = 20μm.

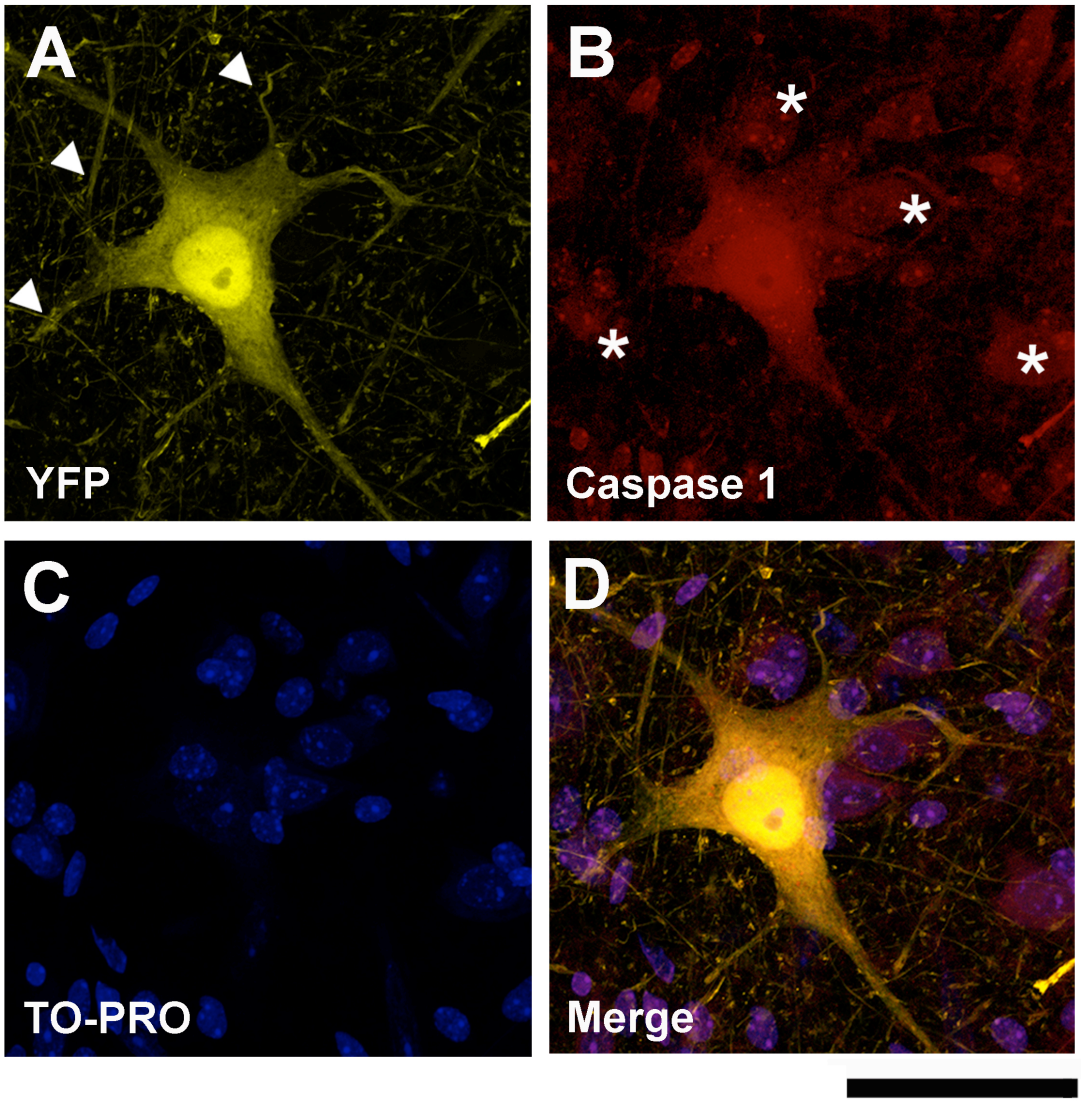

Figure 3.6 – Increased levels of caspase seen in YFP positive cells are not due to bleed-though. Representative confocal micrographs showing caspase 1 immunohistochemistry in the spinal cord of a YFP-H mouse. **A/B:** Lack of bleed-through between the yellow (YFP) and red (caspase 1/TRITC) channels is confirmed by the presence of information in the YFP channel which is not seen

in the TRITC channel (marked by arrows in panel A) and caspase staining in the TRITC channel which is not seen in the YFP channel (marked by asterisks in panel B). **C:** TO-PRO staining for nuclear DNA. **D:** Confocal micrograph showing panels A-C merged. Scale bar = 20μm.

3.3.2 YFP expression in motor neurons subtly disrupts neuronal morphology.

I next sought to establish whether activation of cell stress pathways in YFP-expressing neurons had any adverse effects on neuronal morphology. I first examined the morphology of lower motor neurons innervating the LAL muscle in YFP-H mice. The advantage of this strain of YFP mice is that they only express YFP in a fraction of motor neurons. This allowed me to compare YFP-expressing neurons with non-FP neurons side-by-side in the same muscle, eliminating any potential for background strain differences (Fig. 3.7A). Care was taken to ensure that all quantification was performed blind by first quantifying with the YFP channel removed from all confocal micrographs, thus basing analysis on the neurofilament staining alone for all NMJs. The YFP channel was then replaced in order to gain the YFP status of each NMJ.

As previously reported, all NMJs in 2-4 month old YFP-H mice were fully innervated by a single motor axon (Fig. 3.7A; Feng et al 2000). However, higher-resolution analysis showed a significant increase in abnormal accumulations of neurofilaments in distal axons and motor nerve terminals when YFP was present. NMJs were assigned a score between 0 (no neurofilament accumulation) and 5 (large accumulations of neurofilament). Non-FP NMJs only rarely had a score greater than 1, whereas YFP containing terminals frequently showed neurofilament accumulation that scored 3 or higher. This morphology is similar to cytoskeletal changes considered to represent early pathological changes in neurons (Fig. 3.7B-E; Mi et al., 2005; Murray et al., 2008a).

Retrospective examination of banked tissue from a now defunct YFP-16 mouse colony from the University of Leeds with very high YFP expression levels (~7 times greater than those found in our standard YFP-16 colony) revealed more severe morphological abnormalities. Motor neurons in these mice had both large swellings and vacuoles in pre-terminal axons and very high levels of neurofilament accumulation. This again suggests a dose-dependent effect of YFP (Fig. 3.8).

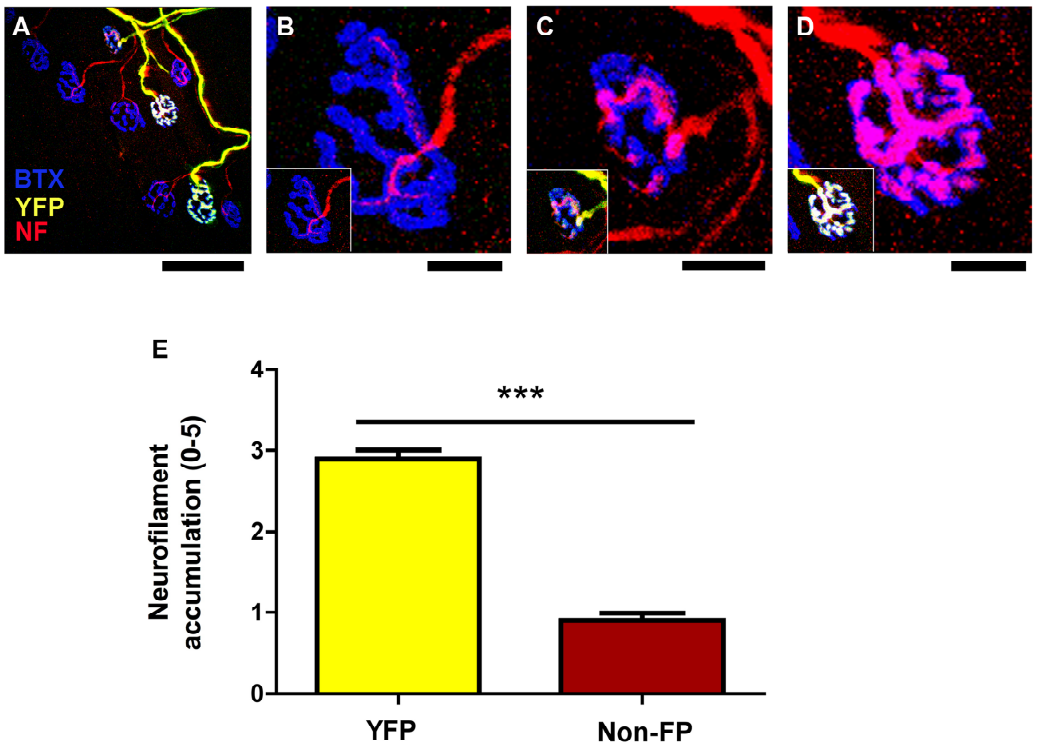

Figure 3.7 - YFP expression in motor neurons subtly disrupts neuronal morphology. A-D: Representative confocal micrographs of NMJs in the LAL muscle from a YFP-H mouse labelled to reveal neurofilaments (NF: red) and postsynaptic motor endplates (BTX: blue). Note how only a small proportion of motor axons were YFP-positive in these mice, but that all motor endplates were innervated (A). Panels **B-D** show high power micrographs of NMJs identified in panel A. The main panels show the respective NMJs with the YFP channel removed, as they were viewed for quantification. The insets show the same NMJs with the YFP channel replaced in order to ascertain the YFP status of the terminal. Note how YFP-positive NMJs had abnormal accumulations of NF in

the motor nerve terminal (compare C&D with B). **E**: Bar chart (mean±SEM) showing quantification of NF accumulation in motor nerve terminals from YFP-H mice (0=no accumulation; 5=large abnormal accumulation), revealing significant increases in NF accumulation in YFP-positive terminals ($P<0.001$; Mann-Whitney test, two-tailed; N=5 mice, n=9 muscles;). Scale bars = 80μm (A), 40μm (B-D). *Ailish Nimmo assisted with obtaining some data, during a summer project supervised by L.Comley.*

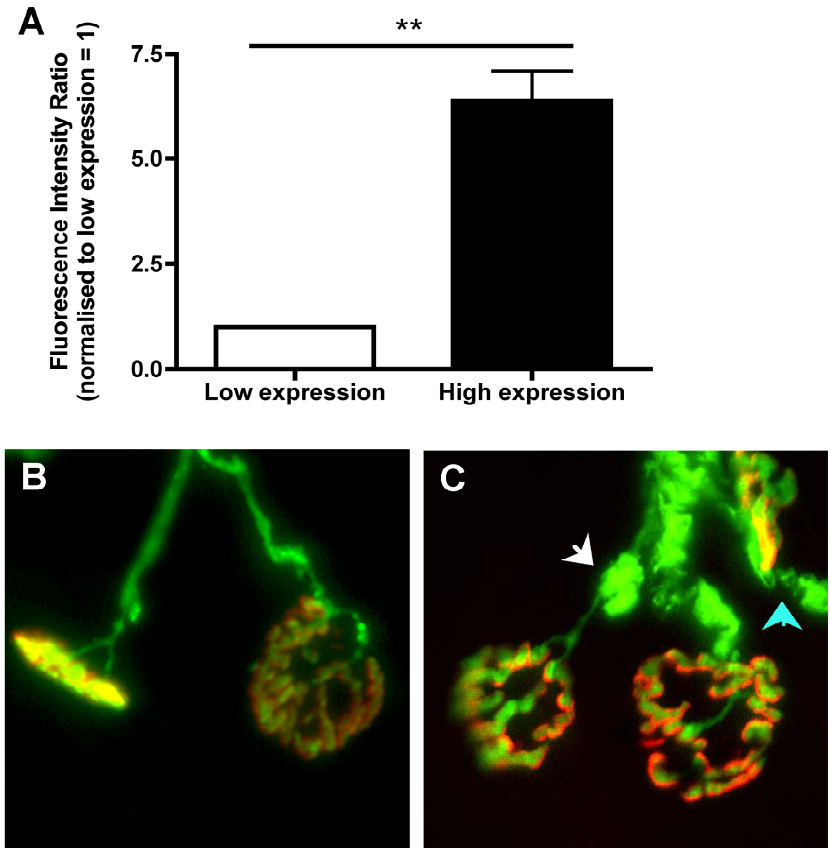

Figure 3.8 – Increased incidence of morphological abnormalities at the NMJ in tissue with increased expression of YFP. A: Bar chart (mean±SEM) showing fluorescent western blot quantification of YFP protein expression levels in the sciatic nerve of YFP-16 mice from the current Edinburgh colony (low expression) compared to levels in tissue banked from a high-expressing colony from the University of Leeds ($P<0.01$; unpaired two-tailed t-test; $N=3$ mice). **B-C**: Representative micrographs showing NMJ morphology in low-expressing YFP-16 mice (**B**) compared to high-expressing YFP mice (**C**). Note the presence

of both neurofilament accumulations (white arrow) and vacuoles (blue arrow) in the axons of the high-expressing mouse. *Tissue from the colony of high-expressing YFP-16 mice was obtained by Dr Simon Parson.*

3.3.3 YFP expression in neurons alters response to dying-back neuropathy but not Wallerian degeneration.

It has previously been suggested that modulation of cell stress pathways can alter the response of neurons to neurodegenerative stimuli (Wishart et al., 2008; Xu et al., 2005), therefore I next addressed whether YFP also affected neurodegeneration pathways *in vivo*. This was done using two neurodegenerative pathways with distinct molecular mechanisms: Wallerian degeneration and dying-back pathology (see general introduction, section 1.4).

In order to investigate the effect of YFP expression on Wallerian degeneration intercostal nerves were crushed in YFP-H mice (see materials and methods, section 3.2.6). The TA muscles, which these nerves innervate, were dissected and fixed 20 hours later. This allowed me to analyse nerve bundles containing both FP-positive and –negative axons at an intermediate state of degeneration. Fragmentation was occurring in both FP-positive and –negative axons at this time point, indicating that the time-course and morphological correlates of Wallerian degeneration following nerve lesion were not altered in YFP-expressing motor neurons (Fig. 3.9). However, in a number of cases the YFP protein itself appeared to be preserved, whereas viewing the muscle with only neurofilament staining and the YFP channel removed showed the same axons in a fragmented state (Fig. 3.10). This suggests that although YFP does not affect the time course of the degeneration process itself, it may be slower to be cleared away during debris clearance following breakdown than other cytoskeletal proteins such as neurofilaments.

In contrast, in *wasted* mice, where loss of translation elongation factor eEF1A2 is known to cause dying-back pathology (see general introduction, section 1.4.2; Murray et al., 2008b), the majority of YFP-expressing neurons remained intact whilst neighbouring non YFP-expressing neurons were in the final stages of degeneration, even at late-symptomatic ages (P24, Fig. 3.11). Therefore, dying-back pathology was significantly attenuated in YFP-expressing motor neurons. Quantification was performed with the YFP channel removed so occupancy was based solely on the amount of neurofilament overlying the endplate. This both minimized the potential for operator bias and removed the possibility that any retention of YFP as seen in the Wallerian degeneration study could lead to an over-estimation of occupancy in the YFP expressing terminals.

Taken together, these data show that YFP has differing effects on different neurodegenerative pathways, with unpredictable consequences.

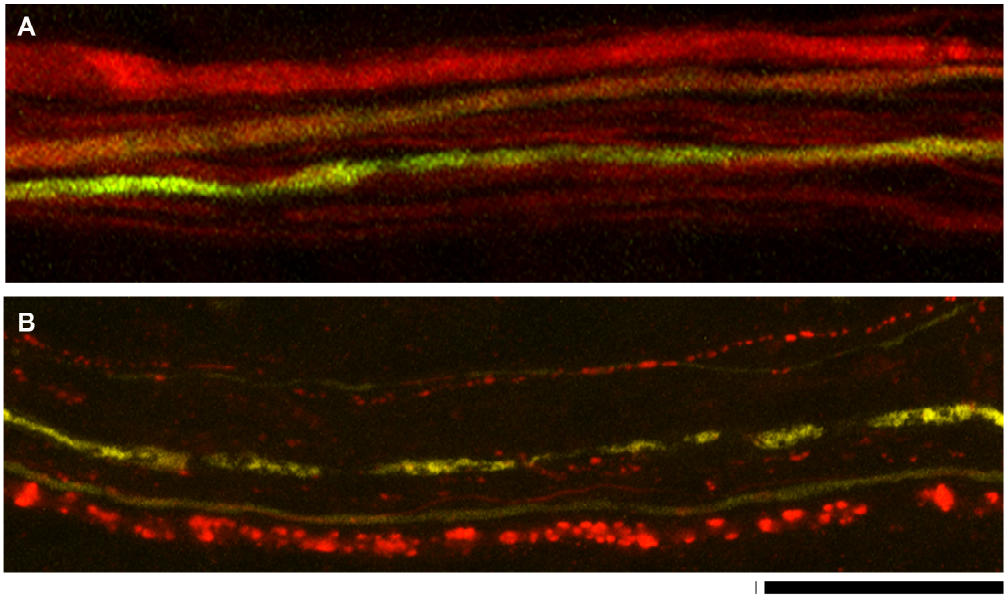

Figure 3.9 - YFP expression does not alter responses to Wallerian degeneration *in vivo*. **A-B**: Representative confocal micrographs of intramuscular axons supplying the transversus abdominis muscle from YFP-H mice (also labeled to reveal NFs; red), before (**A**) and 20 hours after (**B**) intercostal nerve lesion. The presence of YFP did not alter the time-course or morphological appearance of Wallerian degeneration after nerve injury, with NF fragmentation occurring in YFP-positive and –negative axons at the same rate in all nerves examined (N=6 mice, n=6 nerves). Scale bar = 30μm.

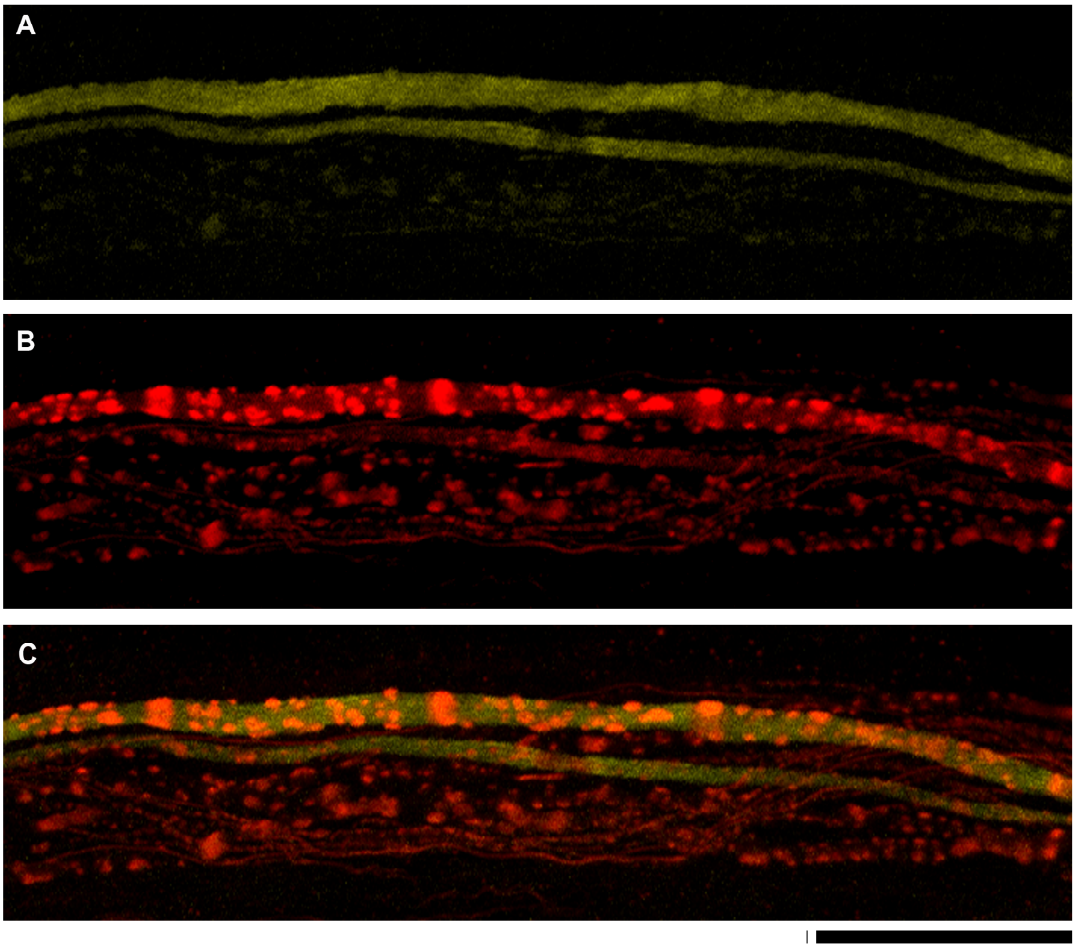

Figure 3.10 - YFP expression persists in axons undergoing Wallerian degeneration. A-C: Representative confocal micrograph of intramuscular axons supplying the transversus abdominis muscle from YFP-H mice 20 hours after intercostal nerve lesion. When viewed on just the YFP channel the axons expressing YFP appear to be preserved (**A**), but NF labeling reveals that the axons are already fragmented at this time point, and are indistinguishable from

YFP-negative axons (**B**). **C**: Merged image showing both YFP and NF channels. Scale bar = 30μm.

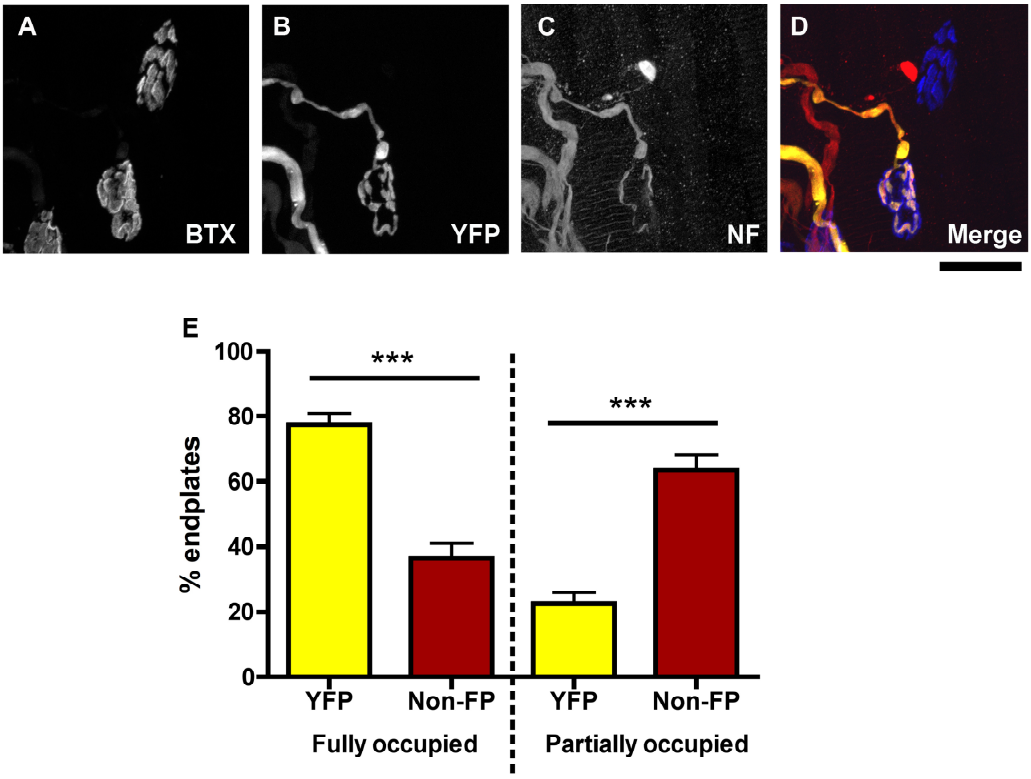

Figure 3.11 - YFP expression alters responses to dying-back pathology in *wasted* mice. A-D: Representative confocal micrographs of two NMJs in the LAL muscle from a late-symptomatic (P24) *wasted*/YFP-H mouse labeled to reveal NFs (red) and postsynaptic motor endplates (BTX: blue). Note how the motor axon with YFP (bottom NMJ) remained intact whereas the motor axon without YFP (top) was undergoing retraction, characteristic of a dying-back pathology. All quantification was performed with the YFP channel removed. **E**: Bar chart showing quantification of dying-back pathology at the NMJ in late-symptomatic (P24) *wasted*/YFP-H mice, revealing a significant attenuation of dying-back pathology in YFP expressing motor nerve terminals (i.e. a retention

of endplates fully occupied by overlying NFs and a reduction in the numbers of partially occupied endplates; $P<0.001$; Mann-Whitney test, two-tailed; N=4 mice, n=7 muscles). Scale bar = 50μm.

3.4 Discussion

In this chapter I have shown that expression of YFP in neurons *in vivo* activates a cell stress response, in contradiction with previous studies that have reported it to be biologically inert (Feng et al., 2000; Ikawa et al., 1998; Lichtman and Sanes, 2003; Okabe et al., 1997). I have used cell stress arrays, western blotting and immunohistochemistry to show that an up-regulation of cell stress responses in YFP mice is present at both the RNA and protein level, and that it is the presence of YFP itself which is causing this response. I have also shown that expression of YFP alters neuronal morphology in otherwise healthy nerves, and alters the time course of dying-back pathology in *wasted*-YFP-H mice, but does not delay the onset of Wallerian degeneration after nerve injury.

The finding that YFP induces a cell stress response is perhaps unsurprising, considering that neurons expressing YFP contain large amounts of a foreign fluorescent protein. Such fluorescent proteins are known to be capable of altering the cellular and molecular characteristics of living cells in other experimental model systems *in vivo* and *in vitro,* e.g. the cardiovascular system, triggering pathological changes (Huang et al., 2000; Liu et al., 1999). Huang and colleagues have previously reported a dose-dependent effect of GFP expression in the hearts of mice expressing GFP. In these mouse lines higher GFP levels gave rise to dilated cardiomyopathy (Huang et al., 2000). The force generating ability of isolated ventricular cardiomyocytes is also thought to be impaired by GFP expression (Nishimura et al., 2006). These muscle specific effects of XFP expression could be linked to impaired myosin-actin interactions in GFP

expressing myocytes – GFP binds preferentially to myosin heads disrupting the binding of actin (Agbulut et al., 2006; Agbulut et al., 2007).

My cell stress array picked up a greater than 1.5 fold increase in expression levels in 41 different cell stress genes in the YFP-16 spinal cord compared to wild-type. These genes are known to be involved in a number of different cell stress responses, including apoptosis. An early study on XFPs focused on the potential apoptotic effect of GFP (Liu et al., 1999). In setting out to look at how the brightness of fluorescence affected the rate of photo bleaching this group noticed that a high percentage of their cells "contracted, rounded up and disappeared". They went on to show that the presence of GFP in the cells was activating cell death through apoptosis (Liu et al., 1999). Detrait and colleagues also reported an apoptotic effect of GFP when comparing the effects of three different reporter genes on primary cortical neurons (Detrait et al., 2002). They also showed that the rate of cell death correlated with the level of expression of GFP. This is consistent with my finding that increased levels of YFP expression in the mouse spinal cord correlate with increased levels of caspase 1 (interleukin-1b converting enzyme), a protein known to be involved in the induction of cell death (Miura et al., 1993).

The increased levels of caspase and other genes relating to apoptosis in the YFP mice have implications for previous studies. Mahajan and colleagues used XFPs as biological markers to study the activation of specific caspases at the onset of apoptosis (Mahajan et al., 1999). Another group developed GFP expressing cells

lines as a tool for analysing apoptosis and necrosis *in vitro* (Strebel et al., 2001). In both cases, the up-regulation of apoptosis related genes in the YFP mice could impact on the results reported.

Over a third of up-regulated genes in the cell stress array had known roles in oxidative and metabolic stress pathways (15 out of 41). As long ago as 1996 it was reported that exciting GFP for extended periods of time could generate free radicals that are toxic to the cell and contribute to oxidative stress (Clontech user manual, 1996). Greenbaum and colleagues showed that photoactivation of GFP generated endogenous singlet oxygen, which damaged the chromophore and lead to photobleaching (Greenbaum et al., 2000). GFP has also been shown to increase the sensitivity of cell lines to cytotoxic drugs in assays of antineoplastic drugs by increasing oxidative stress (Goto et al., 2003). RNA for the heat shock 70-related protein APG-2 (hspa4) was up-regulated in the cell stress array. Elevating concentrations of GFP in the cytoplasm of endothelial cells causes a dose-dependent up-regulation of heat shock protein 70 (HSP70) mRNA and protein (Zhang et al., 2003). Synthesis of HSP70 is also specifically increased during cell stress conditions (Kiang and Tsokos, 1998).

Interestingly, Caine et al use GFP in a study of the Alzheimer's Aβ peptide, fusing Aβ to the fluorescent protein in order to monitor its expression in yeast (Caine et al., 2007). They showed a lower growth yield and increased heat shock response in their Aβ-GFP and GFP-Aβ cells compared to controls, and

concluded that this was due to the presence of Aβ. However, in studies such as this it would be preferable to use a different reporter molecule or immunocytochemistry when appropriate antibodies are available, in order to rule out any confounding effects of GFP on the results. YFP and GFP are also commonly used to tag mutant and wild-type SOD1 in order to visualise its intracellular localisation in ALS studies (Corti et al., 2004; Matsumoto et al., 2005; Zhang and Zhu, 2006). However, when Stevens and colleagues compared GFP-tagged wild-type and mutant SOD1 protein they found that the presence of GFP was altering some of the physiochemical properties of the SOD1 (Stevens et al., 2010). They highlight the need for other studies using GFP tagged proteins to interpret results carefully, and not to assume that untagged proteins will always behave in the same way.

My results show that at the molecular level, expression of YFP in neurons instigates cell stress pathways and is not biologically inert. This finding provides evidence, supported by a number of other studies, that expression of fluorescent proteins in cells and tissues can alter molecular composition. The precise molecular mechanisms by which this occurs are not yet known, but warrants further investigation.

The second part of this chapter looked at the effects of YFP expression on the form of the healthy and pathological PNS *in vivo*. YFP mice have been a valuable tool for morphological studies of the nervous system *in vivo* for over ten years. In particular, the YFP-H strain, in which approximately 3% of axons are labelled

(Beirowski et al., 2004; Feng et al 2000), has allowed visualisation of entire individual motor axons. The potential to reconstruct entire neurons in these mice has lead to breakthroughs such as a greater understanding of the asynchronous nature of synapse elimination (Keller-Peck et al., 2001).

Morphological abnormalities have previously been reported in YFP-H mice; Bridge and colleagues have shown that there is a dose-dependant increase in axonal swellings in the gracile system of these mice with age (Bridge et al., 2009). Accumulations of other proteins have also been shown to cause axonal swellings and neurodegeneration in several disease models including Parkinson's disease (Martin et al., 2006) and giant axonal neuropathy (Allen et al., 2005). Despite this YFP has been used as a tool for studying the mechanisms of neurodegeneration *in vivo* (Beirowski et al., 2004). Here I have shown that YFP causes morphological abnormalities at the NMJ, with accumulations of neurofilament, which increase in a dose dependant manner.

Expression of YFP also has unpredictable effects on degenerative pathways. YFP expressing axons in *wasted*/YFP-H mice had significantly attenuated dying-back pathology, and whilst the rate of Wallerian degeneration wasn't affected per se several axons retained YFP expression after neurofilament proteins had begun to fragment. It is not clear if the retained NMJs in the YFP-positive neurons in the *wasted*/YFP-H mice were still functional, or if the presence of YFP in these neurons was merely preventing retraction of the nerve terminal without preserving function. It is possible that the increased expression of cell stress

proteins, instead of being detrimental, actually leads to a priming response in the YFP-positive neurons, making them more able to cope when external stressors are applied to them. If this is the case then a pathological insult such as the loss of eEF1A2 in the *wasted* mice could have less of an effect on the YFP-positive neurons than on the non-FP controls. Further work is needed to confirm or deny this hypothesis, and to elucidate the mechanisms by which YFP is attenuating dying-back pathology in the *wasted*/YFP-H mice.

A limitation of this study is the lack of quantitative data for the rate of Wallerian degeneration in YFP-positive neurons compared to non-FP neurons. The difficulties in finding a nerve cut protocol to allow visualisation of this process restricted the time available for this, but ideally degeneration at the NMJ could be quantified to give further insights into what may be happening in YFP-positive neurons.

The morphological findings reported in this chapter highlight the need to use adequate controls to ensure that any findings are occurring as a result of experimental intervention and not due to the expression of YFP. Where possible immunohistochemical labelling of cytoskeletal proteins can be used to ensure that situations where YFP persists after other proteins have degenerated, as seen here during Wallerian degeneration, are recognised.

YFP is one of the most powerful tools in modern neuroscience, with advantages over other methods of visualising the nervous system. However, the findings

reported here support the hypothesis that XFPs are not innocuous, inert reporter proteins, and indicate that care should be taken when using them, particularly when studying molecular mechanisms or neurodegeneration in mice expressing fluorescent proteins in neurons. Further work is now needed in order to determine the mechanisms by which fluorescent proteins induce the cell stress response seen in neurons, and to discover if this is due to the presence of the protein itself, or due to its fluorescent properties.

Chapter 4 - ApoE

4.1 Introduction

Apolipoprotein E (apoE) is a 34kDa plasma protein that facilitates the transport of cholesterol and other lipids via its interactions with low-density lipoprotein receptors (Mahley, 1988). Initially called arginine-rich apoprotein, apoE was discovered in 1973 by Shore and Shore, as a protein component of lipoproteins (Shore and Shore, 1973). Early studies in a number of species highlighted the importance of apoE in cholesterol metabolism (Mahley, 1988). Throughout the last 40 years apoE has been the focus of intensive research which has highlighted roles for it in atherosclerosis and heart disease, as well as several biological processes which are potentially unrelated to its lipid transport role, including neurological disease, immunoregulation and susceptibility to infectious disease (for review see Mahley et al., 2009).

ApoE is polymorphic in humans (Utermann et al., 1977; Utermann et al., 1980; Zannis et al., 1981), although other non-human primates show no polymorphism, and express only one form of apoE (Zannis et al., 1985). The polymorphism in humans occurs as a result of three alleles, termed ε2, ε3 and ε4, that occur at a single locus. These three alleles give rise to one of three isoforms, apoE2, apoE3 or apoE4, which give six phenotypes - three homozygous phenotypes (E4/4, E3/3, and E2/2) and three heterozygous phenotypes (E4/3, E3/2, and E4/2, Zannis et al, 1982). The most common

phenotype is apoE3/3 and the distribution of alleles in the human population is thought to be approximately 8% for ε2, 75% for ε3 and 15% for ε4 (Utermann et al., 1982).

Analysis of the amino acid sequence of the three apoE isoforms identified the molecular basis of the polymorphism. The three isoforms differ from each other by two amino acid substitutions, at residues 112 and 158. ApoE3 has cysteine at residue 112 and arginine at residue 158, while apoE4 has arginine and apoE2 cysteine at both sites (Rall et al., 1982; Weisgraber et al., 1981). The entire apoE protein has two structural domains: an N-terminal domain consisting of four-helix bundle, which contains the receptor binding site of the protein, and a C-terminal domain containing the major lipid binding region. The two domains are linked by a flexible hinge region (Wetterau et al., 1988). Substitution of cysteine for arginine at residue 112 in apoE4 leads to a change in orientation of arginine-61, which then interacts with the C-terminal domain causing a change in conformation of the protein (Dong et al., 1994). This altered conformation distinguishes apoE4 from both the apoE2 and apoE3 isoforms, and is thought to be the cause of the isoform specific effects of apoE (Fig. 4.1).

ApoE is primarily synthesised in the liver, by hepatic parenchymal cells, but unlike other apolipoproteins apoE is also produced by many other tissues throughout the body (Elshourbagy et al., 1985). It is abundant in the brain, where expression levels reach approximately a third of those seen in the liver

(Elshourbagy et al., 1985). Within the CNS apoE is synthesised primarily by astrocytes and macrophages (Basu et al., 1981; Boyles et al., 1985; Pitas et al., 1987). However, neurons in certain regions of the brain have also been shown to be capable of synthesising apoE (Aoki et al., 2003; Xu et al., 1999). ApoE has also been shown to be the major apolipoprotein in CSF (Roheim et al., 1979). In the PNS apoE is known to be synthesised by non-myelinating Schwann cells and macrophages, though whether or not it can also be produced intraneuronally is yet to be established (Boyles et al., 1985; Stoll and Müller, 1986).

In 1993 Strittmatter and colleagues reported an association between APOE genotype and incidence of familial late-onset Alzheimer's disease (Strittmatter et al., 1993). In this study they showed that the frequency of the apoE ε4 allele was significantly higher in patients suffering from Alzheimer's than in age-matched controls. Since that time numerous studies have confirmed that APOE4 genotype is a major risk factor in Alzheimer's disease (Corder et al., 1993: Saunders et al., 1993a: Saunders et al., 1993b), as well as in several other CNS neurodegenerative conditions, including Parkinson's disease (Li et al., 2004a; Zareparsi et al., 1997). The APOE4 genotype is also associated with poor outcome after head injury, stroke, intracerebral haemorrhage and traumatic spinal cord injury (Alberts et al., 1995; Horsburgh et al., 2000; Jha et al., 2008; McColl et al., 2007; Millar et al., 2003; Teasdale et al., 1997). Conversely, APOE3 has been shown to provide a neuroprotective effect on CNS degeneration in conditions such as Wilson's disease (Schiefermeier et al., 2000a) and on

neurological outcome following cardiopulmonary resuscitation (Schiefermeier et al., 2000b).

In 1994 Nathan and colleagues reported that apoE affected neuronal growth *in vitro* in an isoform specific manner (Nathan et al., 1994). Cultured dorsal root ganglion neurons incubated with lipids had enhanced neurite outgrowth in the presence of apoE3, and inhibited neurite outgrowth in the presence of apoE4 (Nathan et al., 1994; Nathan et al., 1995). In order to produce these isoform specific effects apoE binds to and internalises lipoproteins, itself becoming intracellular in the process, where the different isoforms accumulate at different concentrations within the cells and have differing effects on the neuronal cytoskeleton (Ji et al., 1998; Nathan et al., 1995). ApoE3 is retained in both the cell bodies and neurites of neural cells *in vitro* at much higher concentrations than apoE4, and supports microtubular structure, whereas apoE4 is associated with microtubule depolymerisation within neurons (Nathan et al., 1995). These findings provided evidence that apoE had a role in neurobiology, and isoform specific effects on the nervous system.

Although the influence of apoE genotype on CNS injury and disease is well established, there is only a partial understanding of any potential influence of apoE genotype on the PNS *in vivo* (Bedlack et al., 2000; Geranmayeh et al., 2005). ApoE is expressed throughout the PNS, including at the NMJ (Akaabourne et al., 1994). Increased levels of apoE production have been noted during maturation of peripheral nerves in newborn rats (Müller et al., 1985) and a

several hundred-fold increase in synthesis and secretion has been reported in the distal segments of peripheral nerves following nerve injury and exposure to harmful environmental stimuli (Gelman et al., 1987; Ignatius et al., 1986; Skene and Shooter, 1983; Snipes et al., 1986). Up-regulation of apoE is also seen in the injured optic nerve and spinal cord; however, unlike in the PNS it fails to accumulate in the injured CNS (Skene and Shooter, 1983). The accumulation of apoE in the PNS following nerve injury occurs over the same time period as regeneration of the sciatic nerve (Skene and Shooter, 1983), and remains elevated if the nerve is prevented from regenerating by axotomy (Müller et al., 1985). These observations indicate a role for apoE in nerves undergoing growth or regeneration, potentially in the clearance of lipids from the site of injury during Wallerian degeneration, and in transferring them among macrophages, Schwann cells and axons during subsequent regeneration of peripheral nerves (Boyles et al., 1985; Boyles et al., 1989; Ignatius et al., 1986; Skene and Shooter, 1983).

An association between APOE genotype and disease outcome in the PNS has been demonstrated for diabetic neuropathies (Bedlack et al., 2003; Tsuzuki et al., 1998) and HIV-associated peripheral neuropathy (Corder et al., 1998). As within the CNS the ε4 allele is commonly associated with increased risk and faster progression of disease.

A number of studies have investigated the effect of APOE genotype on progression and outcome in motor neuron disease but the results have been

inconclusive. Some studies have reported an association between apoE genotype and MND or ALS: both Al-Chalabi et al and Drory et al found that the frequency of the ε4 allele was increased in the patient group compared to the ε3 or ε2 forms, and Drory and colleagues found that patients with an ε4 allele had a shorter survival time than those without (Al-Chalabi et al., 1996; Drory et al., 2001). Moulard and colleagues found no difference in the frequency of the genotypes between ALS patients and controls, but reported that apoE4 patients had an earlier age of onset, and that patients with an ε2 allele had a longer duration of disease (Moulard et al., 1996). A more recent study by Li and colleagues has also reported an association between apoE genotype and ALS, but this time found an effect only of the ε2 allele, which they showed was protective against an earlier age of onset (Li et al., 2004b). These studies support the protective role of apoE2 and deleterious role of apoE4 seen in studies of the CNS and the role of apoE in Alzheimer's disease. However, other studies have reported a lack of association between apoE genotype and either age of onset, frequency of each of the apoE alleles or duration of disease in ALS (Bachus et al., 1997; Mui et al., 1995; Siddique et al., 1998; Smith et al., 1996). One possible reason for the discrepancies between studies is that they are patient cohort studies, which often have small sample sizes, which can confound results. At present the influence of APOE genotype on events in the PNS remains controversial.

Previous studies using genetically-modified animals have investigated the effects of complete loss of apoE on regenerative events in the PNS, and have reported that regeneration occurs normally in the absence of apoE (Genden et al., 2002; Popko et al., 1993). However, these studies have not looked at the influence of loss of apoE on degeneration, nor have they looked at the effects of different APOE genotypes, as is seen in the human population, on degenerative or regenerative events. I have therefore examined the influence of apoE genotype on the PNS using a transgenic mouse model expressing human apoE3 or apoE4 isoforms, established by Xu and colleagues in 1996 (Xu et al., 1996). This group used a background strain of mice that lacked a functional mouse APOE gene (Piedrahita et al., 1992) to allow the study of the different human apoE isoforms without interference from endogenous mouse apoE. Founder mice for the human apoE isoforms were generated by micro-injection of human APOE genomic DNA fragments. These founder mice were then back-crossed with apoE knockout mice to produce mice that had a homozygous deletion of mouse apoE and were hemizygous for a human apoE transgene (either E2, E3 or E4). These mice express human apoE at physiological levels, and have expression patterns of apoE found in humans and other non-human primates (Xu et al., 1996). They also have the advantage of allowing us to study the influence of APOE genotype on the PNS with control over other confounding factors (such as genetic background) that can make human studies less reliable (Gerenmayeh et al., 2005).

Here, I have used apoE3 and apoE4 mice to investigate isoform-specific effects of human apoE on the form, function and molecular composition of the healthy and degenerating mouse PNS. ApoE2 mice were not used as they express apoE at levels much higher than the apoE3 or apoE4 mice (Xu et al., 1996); this would have made it impossible to determine whether any effects observed were due to the genotype or were simply occurring due to differences in expression levels of apoE. I have used immunocytochemistry, electrophysiology, confocal microscopy and electron microscopy to compare the processes of development, degeneration and regeneration of lower motor neurons in mice expressing apoE3 and apoE4, and iTRAQ proteomics to investigate potential molecular mechanisms regulating apoE-specific responses in the PNS *in vivo.*

Figure 4.1 – Model of the domain structure of apoE3 and apoE4 (over page). ApoE has two structural domains: an N-terminal domain consisting of four-helix bundle (red - helix 1; blue - helix 2; green - helix 3; yellow - helix 4), and a C-terminal domain modelled as a series of α-helices. The two domains are linked by a flexible hinge region. Helix 4 of the N-terminal domain contains the receptor binding site of the protein, and the C terminal domain contains the major lipid-binding region. The cysteine at residue 112 in apoE2 (not shown) and apoE3 (**A**) is replaced by arginine in apoE4 (**B**). This causes a reorientation of arg-61 to a position where it interacts with glu-255 in the C-terminal domain, giving apoE4 (**B**) a more compact structure, and distinguishing it from the more extended structure of both apoE2 and apoE3 (**A**). (Adapted from Zhong and Weisgraber, 2009).

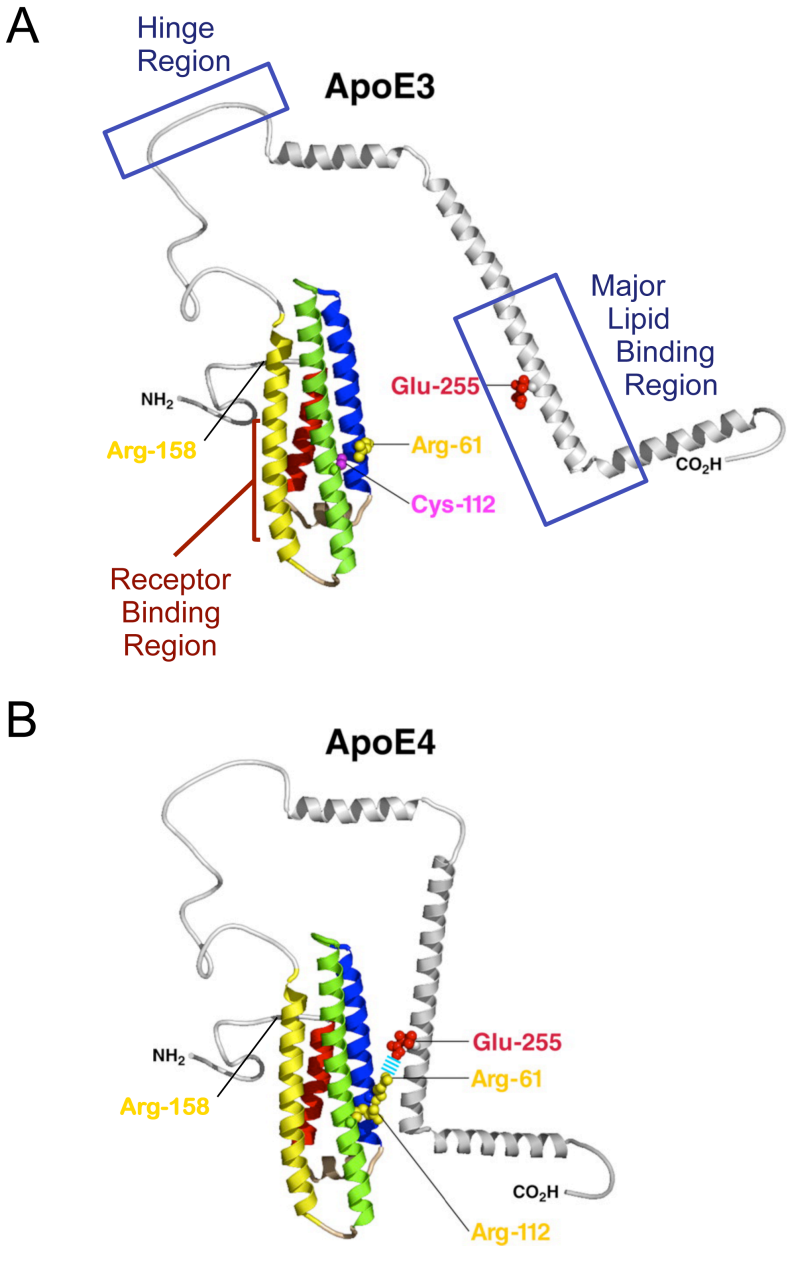
A
Hinge
Region
ApoE3
Major
Lipid
Binding
Region
NH2
Glu-255
Arg-158
Arg-61
CO2H
Cys-112
Receptor
Binding
Region
B
ApoE4
NH2
Glu-255
Arg-61
Arg-158
CO2H
Arg-112

4.2 Materials and methods

4.2.1 Mice

Young adult mice expressing human apoE4 were compared with non-apoE littermates (apoE-/-) or apoE3 mice. These mice lack endogenous mouse apoE to allow the study of the effects of the human isoforms without interference from mouse apoE. Mice were supplied via a collaboration with Dr. Allen Roses (Duke University) and breeding colonies established at the University of Edinburgh. Despite both apoE3 and apoE4 strains of mice being kept in identical conditions, the apoE3 colony produced litters much more infrequently than the apoE4 colony (unexplained observation). This has lead to the omission of apoE3 data from some experiments (detailed in results section for each specific experiment).

APOE knockout mice were generated on a C57Bl/6J background by disrupting the endogenous mouse APOE gene with the neomycin-resistance gene (Piedrahita et al., 1992). Human apoE4 and apoE3 transgenic mice have been generated on this apoE-deficient background by microinjection of human APOE genomic DNA fragments (Xu et al., 1996). As the precise regulatory elements necessary for the expression of APOE were unknown large upstream and downstream regions were included in the genomic DNA fragments in order to ensure the inclusion of the regulatory regions (Xu et al., 1996).

ApoE4 and apoE3 founder mice were backcrossed with apoE-knockout mice for more than 10 generations resulting in mice hemizygous for the human apoE transgenes E4 or E3 on a homozygous mouse apoE-knockout background. The apoE3 and apoE4 mouse lines used throughout this chapter have been shown to express apoE at physiological levels, similar to those found in humans (Horsburgh et al., 2000; Xu et al., 1996). ApoE was shown to be expressed in the brain, liver, kidney spleen, heart, skeletal muscle, intestine, serum and neurons in the transgenic mice (Xu et al., 1996).

The presence of human apoE transgenes on an established knockout background was determined by western blot analysis (See general materials and methods, section 2.2). All animals were housed in standard SPF conditions and all procedures were carried out under licensed authority from the UK Home Office.

For initial experiments apoE-/- mice were compared with age-matched C57Bl/6J (wild-type) mice in order to examine the influence of loss of apoE, and confirm that apoE-/- mice were functioning as expected prior to the addition of human apoE3 or apoE4. C57Bl/6J mice were used as non-littermate wild-type controls, as this is the background strain that the apoE-/- mice were produced from.

4.2.2 Quantitative fluorescent (Li-COR) western blots

See general materials and methods, section 2.2.

4.2.3 Electron microscopy

5mm sections of peripheral nerves (distal to the injury site if following surgery, see general materials and methods, section 2.1) were dissected out in 0.1M PBS and fixed in ice-cold 0.1M phosphate buffer containing 4% paraformaldehyde/2.5% glutaraldehyde. Nerves were post-fixed in 1% osmium tetroxide overnight. Following dehydration through an ascending series of ethanol solutions and propylene oxide, nerves were embedded in Durcupan resin. Ultrathin sections (~60 nm) were cut and collected on formvar-coated grids (Agar Scientific, UK), stained with uranyl acetate and lead citrate and then quantitatively assessed in a Philips CM12 transmission electron microscope (TEM) equipped with a Gatan camera (Comley et al., 2011; Gillingwater et al., 2002). Images were imported into ImageJ software for quantitative analysis. Individual high power micrographs were reconstructed to form entire nerve cross sections in Adobe Photoshop. Higher power images were taken to allow assessment of small myelinated and unmyelinated axon profiles (see section 4.2.4). All analysis was performed blind to the genetic status of the material to avoid bias.

4.2.4 Regenerating peripheral nerve quantification

Initially attempts to quantify regenerating axons were based solely on the number of myelinated profiles present in an entire nerve bundle (Fig. 4.2B). The disadvantage of this method was that it did not take into account the number of small unmyelinated profiles or any axons still in the early stages of myelination.

Thus, it was possible that the number of myelinated axons could remain relatively unchanged in apoE3 and apoE4 regenerating nerves, whilst the axon density or total axon number was altered.

To overcome this I next quantified individual high-resolution images from selected regions of a nerve in order to be able to count unmyelinated axons as well as the more obvious myelinated profiles. This produced a density measurement of axons in the sciatic nerve of each genotype, but did not take into consideration the fact that the total axon number could be altered by genotype due to a change in the overall size of the regenerating nerve (Fig. 4.2C).

As it was not possible to count the total number of axons in an entire nerve I then took measurements of the total cross sectional area of reconstructed sciatic nerves from apoE3 and apoE4 mice using image J software. This allowed me to scale up axon density counts from individual images to estimated total axon counts from entire nerves of different genotypes (Fig. 4.2D). This approach avoided the pitfalls of sampling only a subset of axons and so missing a change in total axon number, and overcame the possibility that packing density itself had not changed between the genotypes, but that overall number was changed due to smaller overall size of regenerating nerves. Ideally the total number of axons in a few nerves of each genotype could be counted in order to check for the accuracy of this approach, but time limitations prevented this.

Figure 4.2 – Adaptation of quantifying method of regenerating apoE3 and apoE4 peripheral nerves (over page). A: Flow chart showing progression of changes in method of quantifying regenerating peripheral nerves from apoE3 and apoE4 mice 3 weeks after sciatic nerve crush. **B:** Bar chart (mean±SEM) showing total number of myelinated axons in sciatic nerve of apoE3 and apoE4 mice 3 weeks after sciatic nerve crush ($P>0.05$; t-test, two-tailed; apoE3 N=3, apoE4 N=3; ns = not significant). **C:** Bar chart (mean±SEM) showing number of axons (myelinated and unmyelinated) per 2500μm^2 in sciatic nerve of apoE3 and apoE4 mice 3 weeks after sciatic nerve crush ($P>0.05$; t-test, two-tailed; apoE3 N=9, apoE4 N=7; ns = not significant). **D:** Bar chart (mean±SEM) showing a significant difference in estimated total axon number (myelinated and unmyelinated) in sciatic nerve of apoE3 and apoE4 mice 3 weeks after sciatic nerve crush 3 weeks ($P<0.05$; t-test, two-tailed; apoE3 N=11, apoE4 N=11).

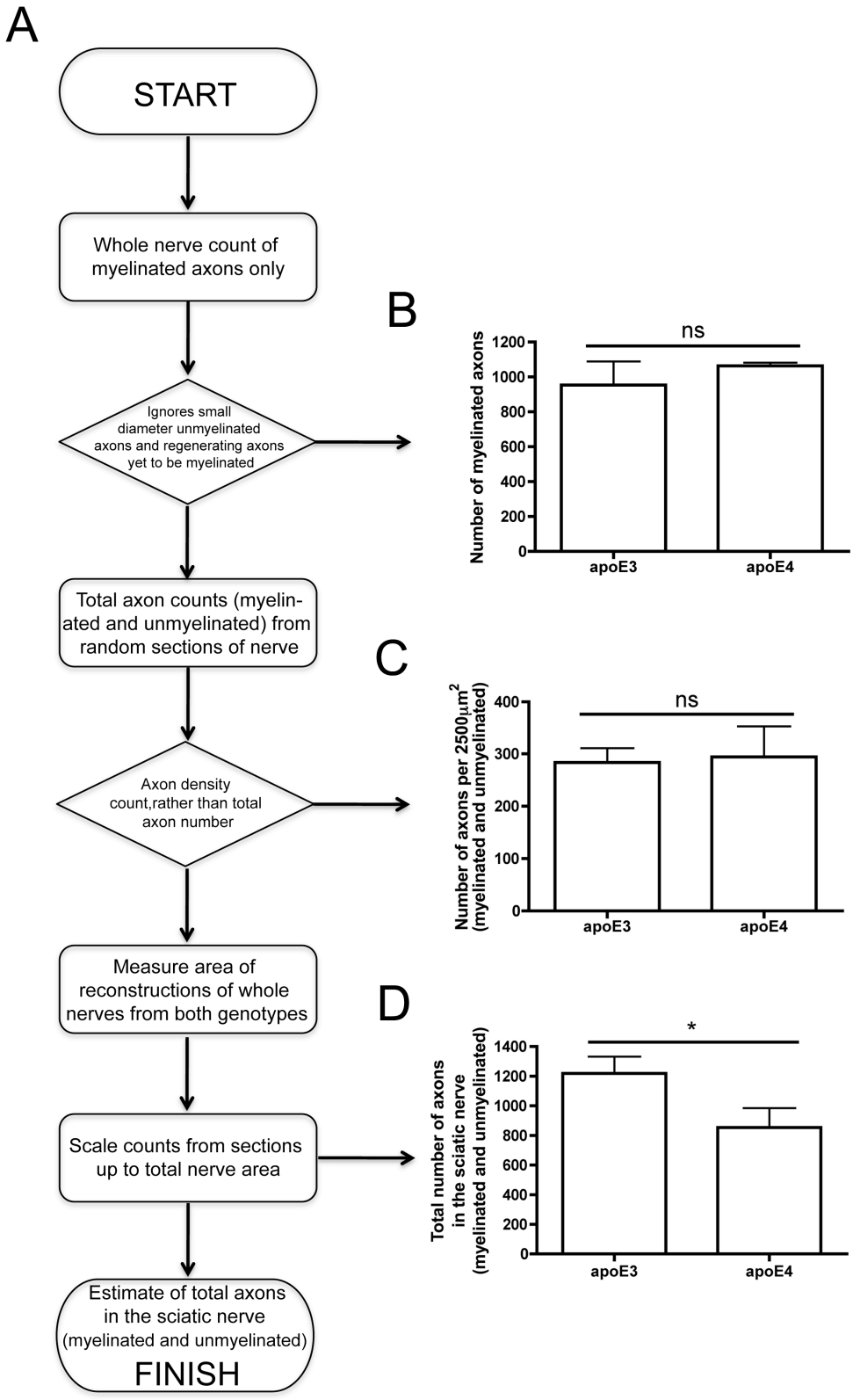
A
START
Whole nerve count of myelinated axons only
Ignores small diameter unmyelinated axons and regenerating axons yet to be myelinated
Total axon counts (myelinated and unmyelinated) from random sections of nerve
Axon density count,rather than total axon number
Measure area of reconstructions of whole nerves from both genotypes
Scale counts from sections up to total nerve area
Estimate of total axons in the sciatic nerve (myelinated and unmyelinated)
FINISH
B
Number of myelinated axons
ns
apoE3
apoE4
C
Number of axons per 2500μm2 (myelinated and unmyelinated)
ns
apoE3
apoE4
D
Total number of axons in the sciatic nerve (myelinated and unmyelinated)
*
apoE3
apoE4

4.2.5 Surgery

See general materials and methods, section 2.1. Tibial and sciatic nerve crushes and cuts have been used to obtain results presented in this chapter.

4.2.6 Immunohistochemistry

See general materials and methods, section 2.3.

4.2.7 Microscopy

See general materials and methods, section 2.4.

4.2.8 Quantification of NMJs

See general materials and methods, section 2.5.

4.2.9 Electrophysiology

Electrophysiological recordings were obtained with the technical support of Derek Thomson. Freshly dissected FDB muscles were used to obtain intracellular recordings of evoked endplate potentials (EPPs) and spontaneous miniature endplate potentials (mEPPs). FDB muscles were pinned out in a Sylgard lined bath (VWR International, Poole, UK) and perfused with oxygenated mammalian physiological saline (mM: NaCl 120; KCl 5; $CaCl_2$ 2; $MgCl_2$ 1; NaH_2PO_4 0.4; $NaHCO_3$ 23.8; D-glucose 5.6; bubbled with 5 % CO_2/95 % O_2 mixture.). Muscle contractions were reduced or eliminated by bathing the muscles in 2.5μM μ-conotoxin (μ-CTX) GIIIB (Scientific Marketing Associates,

UK) for 30–45 min (Gillingwater et al., 2002). 30 muscle fibres per muscle were sampled at random using glass microelectrodes filled with 5M potassium acetate (impedance ≈ 40 MΩ). Spontaneous and evoked EPPs were recorded using Axoclamp 2B amplifiers (Axon Instruments) and stored and analysed on a PC using WinWCP v3.9.5 software (developed and distributed by Dr John Dempster, Strathclyde University). Average frequency of spontaneous mEPP's was obtained from continuous records of 10-60 seconds duration. The quantal content was determined from measurements of peak EPP amplitude in trains evoked at stimulation frequencies of 0.5-2 Hz, using the variance method with correction for non-linear summation implemented in the WinWCP software package.

4.2.10 Statistical analysis

See general materials and methods, section 2.6.

4.2.11 *Proteomics*

Unlesioned tibial nerves from nine apoE3 mice and nine apoE4 mice were dissected and pooled into 3 groups for each genotype. The same was repeated for 9 mice of each genotype 3 weeks after tibial nerve crush injury. These samples underwent iTRAQ proteomic analysis. Nerves were extracted in a buffer containing 6 M urea, 2 M thiourea, 2% CHAPS and 0.5% SDS in dH2O. The proteins were then precipitated in ice-cold acetone at -20°C overnight. Precipitates were pelleted by centrifugation at 13,000 x g for 10 minutes at 4°C.

The supernatant was removed and pellets were allowed to air-dry, before being resuspended in 6M Urea in 50mM TEAB.

All proteomics experiments were performed at the Keele University Mass Spectrometry and Proteomics Facility, Wolfson Centre for Inherited Neuromuscular Disease, Oswestry. For detailed proteomics methodology see Appendix 8.1.

Tables of changes proteins were analysed at Edinburgh University. Only proteins identified with >95% total ion score confidence intervals and by two or more unique peptides were accepted as being robust and reliable enough for inclusion in further analysis. In order to gain insights into potential pathways modified by apoE genotype Ingenuity Pathway Analysis (IPA) software was used (Ingenuity Systems). IPA generates networks of proteins, based on 'hand-curated' data held in a database. Specific altered protein interaction networks were identified based on the number and percentage of candidate proteins contributing to the network.

4.3 Results

4.3.1 ApoE genotype has no effect on normal form or function of the mouse PNS.

Initially, it was important to confirm that apoE was expressed at similar levels in the PNS in both the apoE3 and apoE4 mice, to ensure that any differences observed were not simply due to differing expression from the transgenes. I therefore started by examining apoE expression levels in tibial nerves from mice expressing human apoE3 or apoE4 and comparing them to nerves from wild-type and apoE-/- mice. As expected, apoE protein was undetectable in peripheral nerves from wild-type mice and apoE-/- mice, as endogenous apoE is only expressed at low levels in the uninjured nervous system (Ignatius et al, 1986; Skene and Shooter, 1983). However, apoE protein generated from the human transgenes (apoE3 and apoE4) was expressed at near-identical levels in peripheral nerves from apoE3 and apoE4 mice (Fig. 4.3).

Based on the results of the previous chapter (YFP) it was also important to consider how introducing a transgene into these mice could affect any changes seen. However, unlike YFP, apoE protein is normally expressed in mice, albeit without the polymorphism. Moreover, the majority of the results reported in this chapter are from comparisons between apoE3 and apoE4 mice. As both mice are expressing a transgene differences seen are more likely to be due to the differences between the isoforms of apoE, rather than expression of the transgene *per se.*

Once I had established that the transgenes were expressed at similar levels I examined peripheral nerves and NMJs from young healthy mice of all four genotypes (wild-type, apoE-/-, apoE3 and apoE4) to see if complete removal of apoE or expression of the human transgenes had any effect on normal neuronal morphology in the PNS. Equivalent numbers of myelinated axon profiles were seen in the tibial nerves of mice of each of the genotypes (Fig. 4.4). The majority of NMJs (>98%) were fully occupied and mono-innervated (the normal adult state) in all genotypes (Fig. 4.5). Therefore no qualitative or quantitative differences were observed in the morphological appearance of either the tibial nerve or NMJs between mice of each of the different genotypes.

Electrophysiological measurements also suggested normal neuromuscular function in mice lacking apoE (apoE-/-) and mice expressing a human transgene (in this case apoE4. ApoE3 mice were excluded from this analysis due to problems with the breeding colony at the time). Both apoE-/- and apoE4 mice had robust EPPs in the flexor digitorum brevis muscle in response to tibial nerve stimulation. There was no significant difference in amplitude of EPPs, quantal content or rate of spontaneous mEPPs between apoE-/- and apoE4 mice (Fig. 4.6).

Thus, expression of the human apoE3 or apoE4 isoform had no detrimental effect on the form or function of the uninjured mouse PNS.

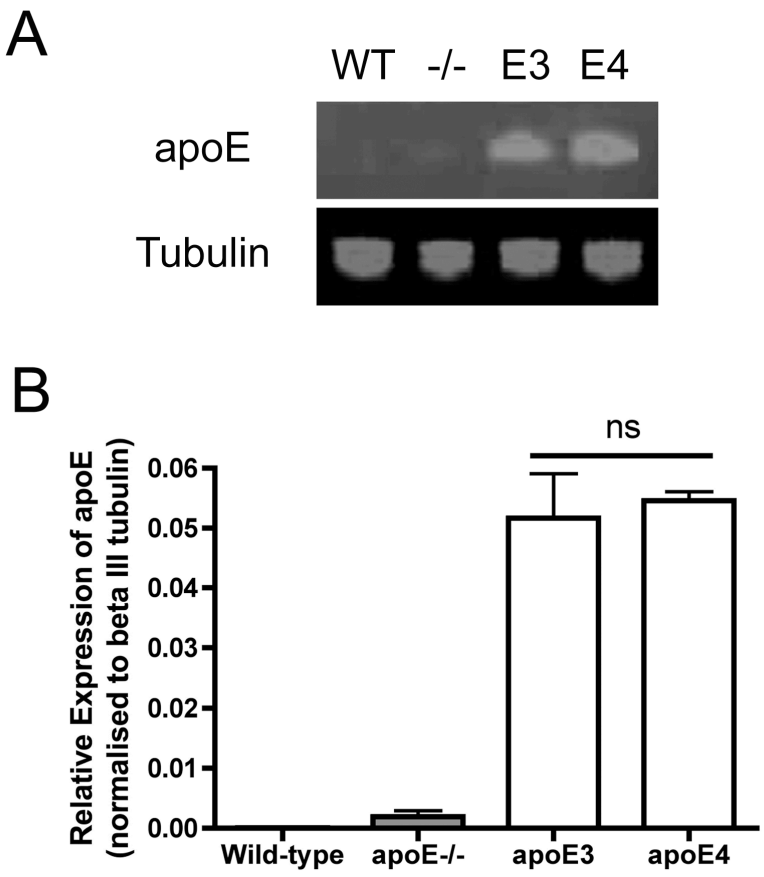

Figure 4.3 - ApoE3 and apoE4 isoforms are expressed at equivalent levels in unlesioned peripheral nerves from apoE3 and apoE4 transgenic mice. A: Representative fluorescent western blot for apoE protein in the uninjured sciatic nerve of wild-type (WT), apoE-/- (-/-), apoE3 (E3) and apoE4 (E4) mice, showing a lack of apoE in the wild-type and apoE-/- nerves, and comparable levels of protein expression in the apoE3 and apoE4 nerves. **B:** Bar chart (mean±SEM) showing quantification of apoE expression levels normalised to beta III tubulin (loading control), confirming no difference in expression levels between apoE3 and apoE4 ($P>0.05$ apoE3 vs apoE4; one-way ANOVA with Tukey's post-hoc test; N=3 for each genotype; ns = not significant).

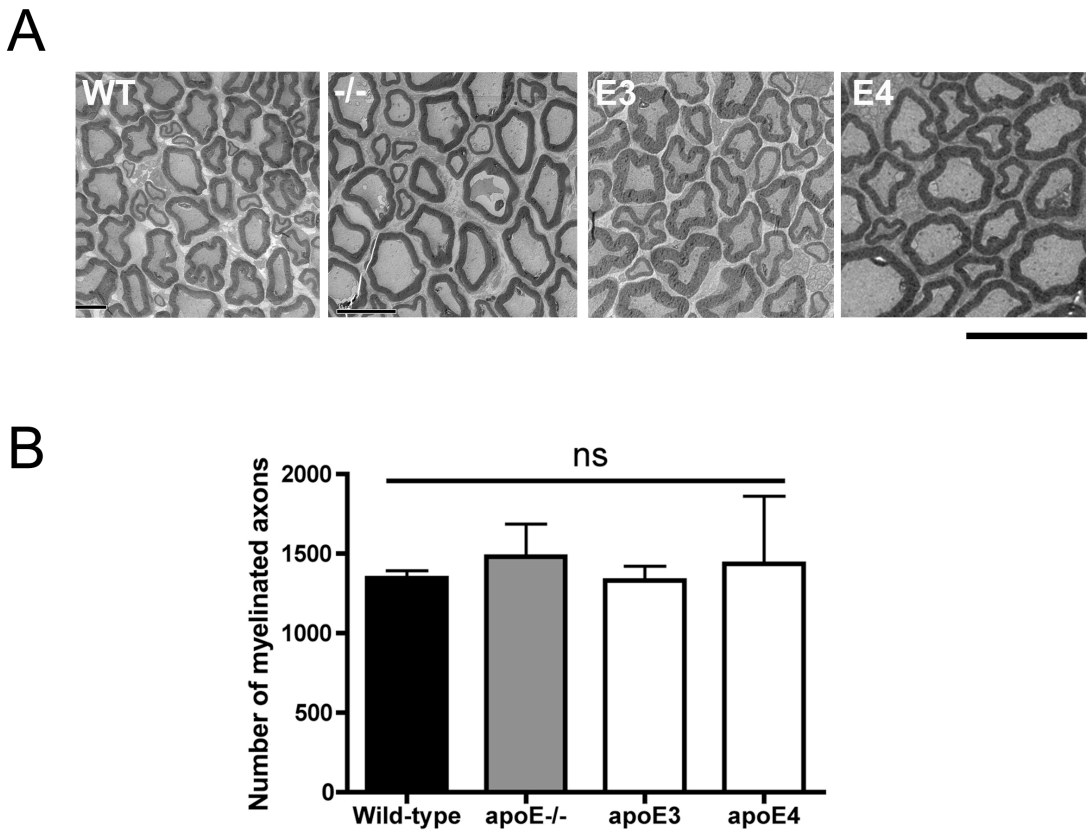

Figure 4.4 - Expression of the apoE4 isoform has no effect on normal peripheral nerve morphology. A: Representative electron micrographs of cross-sections from adult sciatic nerves in wild-type (WT), apoE-/- (-/-), apoE3 (E3) and apoE4 (E4) mice. All four genotypes had healthy myelinated axon profiles. Scale bar = 10μm. **B:** Bar chart (mean±SEM) showing quantification of myelinated axon profiles. There was no significant difference in the number of myelinated axons in wild-type, apoE-/-, apoE3 and apoE4 mice ($P>0.05$; one-way ANOVA with Tukey's post-hoc test; wild-type N=3, apoE-/- N=5, apoE3 N=5, apoE4 N=3).

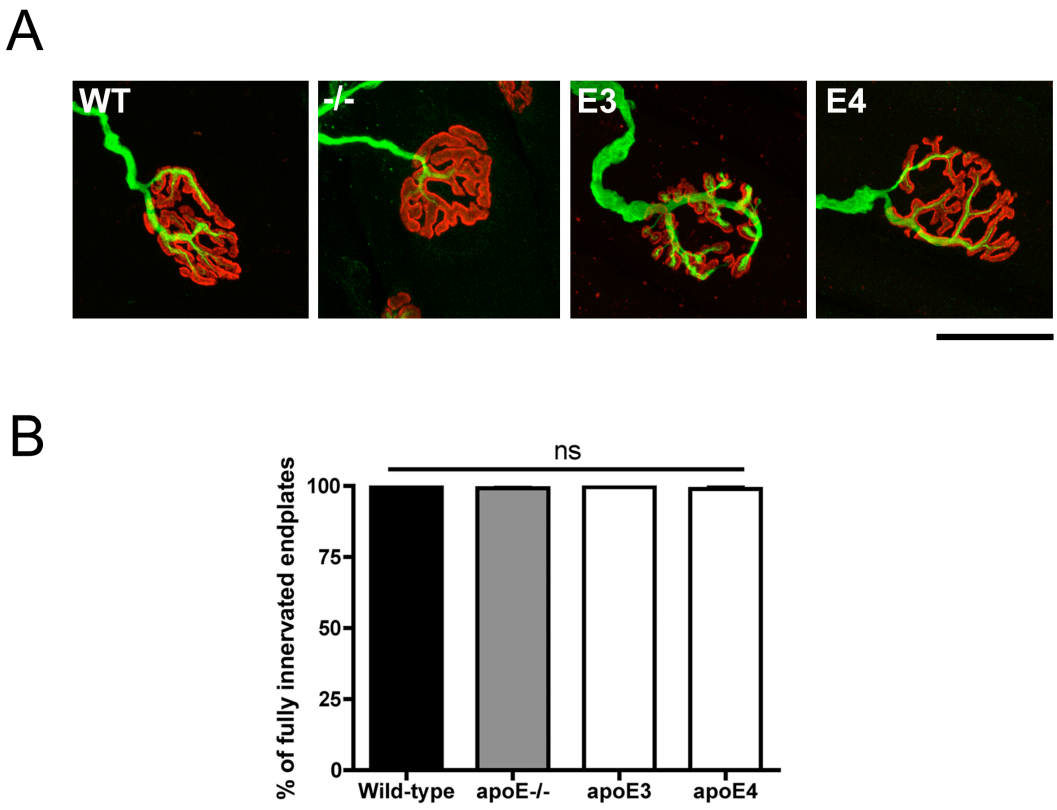

Figure 4.5 - Expression of the apoE4 isoform has no effect on normal neuromuscular junction morphology. A: Representative confocal micrographs showing immunohistochemically labelled NMJs in LAL muscles showing mono innervated, fully occupied endplates in wild-type (WT), apoE-/- (-/-), apoE3 (E3) and apoE4 (E4) mice (pre-synaptic axons and motor nerve terminals are shown in green and post-synaptic acetylcholine receptors labelled with α-bungarotoxin are shown in red). >98% of NMJs in all muscles examined, regardless of genotype, showed this morphology, characteristic of normal healthy adult NMJs. Scale bar = 30μm. **B:** Bar chart (mean±SEM) showing no

significant difference in the percentage of fully occupied, mono-innervated wild-type, apoE-/-, apoE3 and apoE4 mice ($P>0.05$; Kruskal-Wallis test with Dunn's post-hoc test; wild-type N=8, apoE-/- N=7, apoE3 N=7, apoE4 N=7).

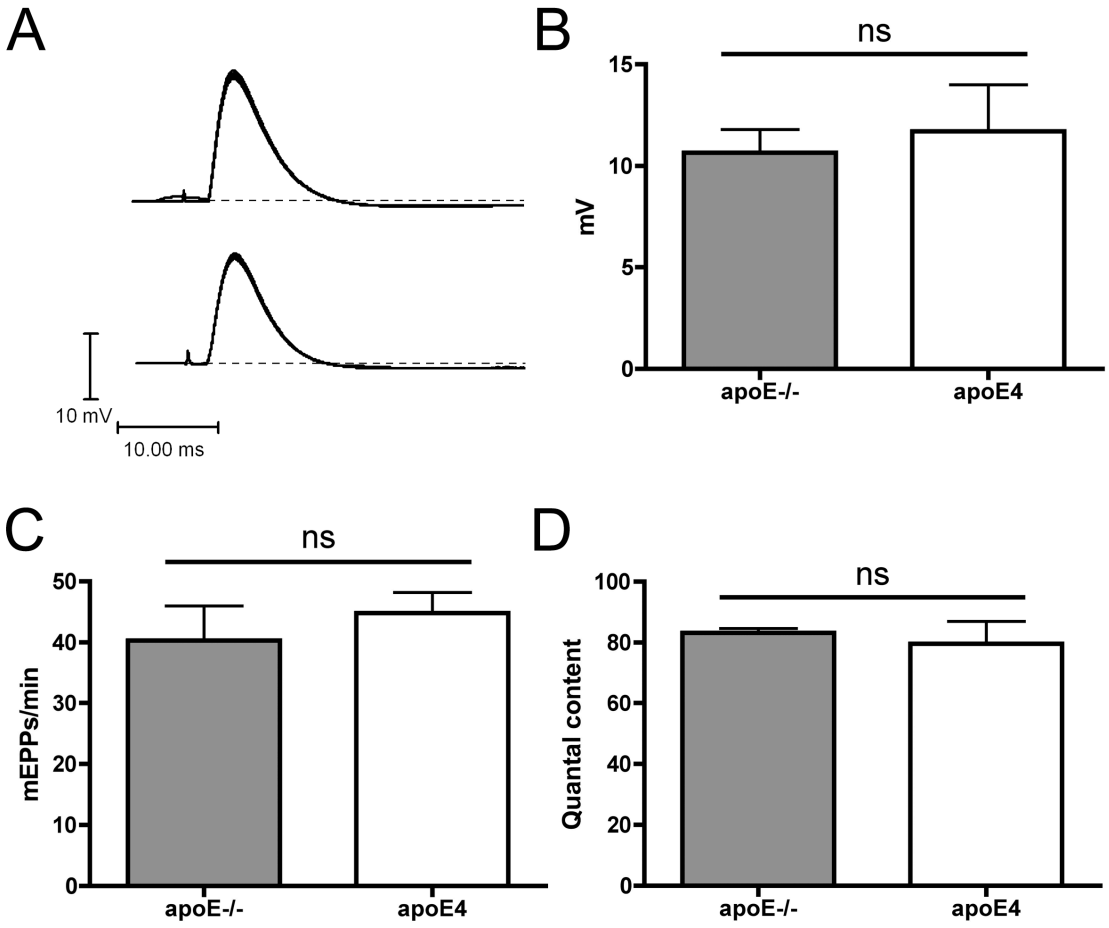

Figure 4.6 - Expression of human apoE4 has no effect on normal neuromuscular function. A: apoE-/- and apoE4 mice both showed robust EPPs in response to tibial nerve stimulation of the flexor digitorum brevis muscle. **B:** Muscles of both genotypes (apoE-/- and apoE4) had EPPs of equivalent amplitudes ($P>0.05$; t-test, two tailed; apoE-/- n=73 fibres N=3 mice, apoE4 n=75 fibres N=3 mice). **C:** There was no significant difference in the rate of

mEPPs between the genotypes (P>0.05; t-test, two tailed; apoE-/- n=78 fibres N=3 mice, apoE4 n=80 fibres N=3 mice). **D:** There was no significant difference in quantal content between apoE-/- and apoE4 mice (P>0.05; t-test, two tailed; apoE-/- n=48 fibres N=3 mice, apoE4 n=32 fibres N=3 mice).

4.3.2 ApoE4 expression at physiological levels has no effect on developmental plasticity at the NMJ.

At birth NMJs are innervated by multiple inputs, which are gradually pruned back until each NMJ is mono-innervated. This process is known as synaptic elimination and in mice is complete by two weeks after birth (Wyatt and Balice-Gordon, 2003). ApoE4 has previously been shown to modulate synaptic plasticity in the CNS (Arendt et al., 1997; Korwek et al., 2009), so I next wanted to know whether apoE genotype could influence developmental synaptic plasticity in the PNS. I quantified the progression of neonatal synapse elimination (for review see Wyatt and Balice-Gordon, 2003) by counting the number of axonal inputs to motor endplates at NMJs in the LAL and TA muscles of apoE4 and apoE-/- mice at time points over the first two postnatal weeks (Fig. 4.7 A/B). ApoE3 mice were omitted from this analysis due to problems with the breeding colony at the time. The presence of apoE4 did not modify the morphological correlates or time-course of synapse elimination at any time-point examined (Fig. 4.7 A-C). Thus, the apoE4 genotype did not influence developmental synaptic plasticity.

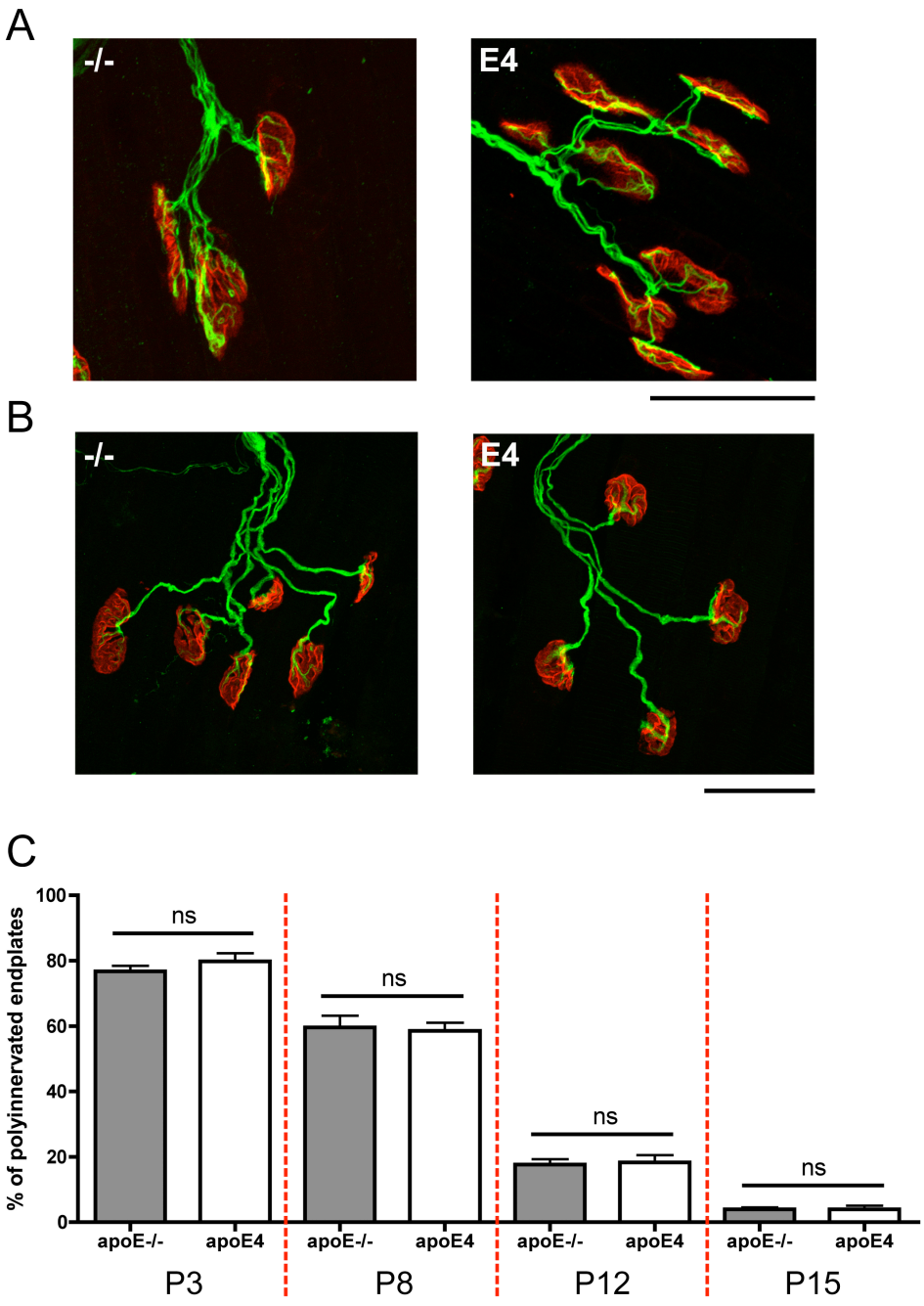

Figure 4.7 - Expression of the apoE4 isoform has no effect on developmental plasticity at the NMJ. A/B: Representative confocal micrographs showing immunohistochemically labelled NMJs in LAL muscles from apoE-/- (-/-) and

apoE4 (E4) mice at postnatal day 3 (**A**) and 15 (**B**). Note the presence of poly-innervated endplates (multiple axons (green) converging on a single motor endplate (red)) at P3 (**A**). Scale bar=30μm. By P15 the process of neonatal synapse elimination has remodelled the vast majority of NMJs into the adult mono-innervated state (only one incoming axon per endplate) (**B**). Scale bar=30μm **C:** Bar chart (mean±SEM) showing no significant difference in the progression of neonatal synapse elimination in apoE4 mice compared to apoE-/- controls at any time-point examined ($P>0.05$ for all time points; Mann-Whitney test, two tailed; P3 apoE-/- N=8, apoE4 N=10; P8 apoE-/- N=12, apoE4 N=20; P12 apoE-/- N=4, apoE4 N=25; P15 apoE-/- N=50, apoE4 N=11; ns = not significant).

4.3.3 ApoE4 expression has no effect on Wallerian degeneration of axons or NMJs following peripheral nerve injury.

ApoE4 has previously been shown to modulate neurodegenerative events in the CNS (Horsburgh et al., 2000; Malek et al., 2005; Tesseur et al., 2000), so I next asked whether apoE genotype could influence degeneration in the PNS.

I first quantified the extent of Wallerian degeneration occurring at motor nerve terminals in the 1st to the 3rd deep lumbrical muscles from wild-type and apoE-/- mice after a tibial nerve crush injury in order to find out if loss of apoE had any effect on degeneration (Fig. 4.8). To chart the time course of degeneration I examined two time points – 18 hours post crush for an intermediate stage of degeneration (Fig. 4.8A/B), and 24 hours for late stage of degeneration (Fig. 4.8C). At this later time point the majority of endplates are vacant in wild-type mice so any delay in degeneration would be very obvious (Gillingwater and Ribchester, 2001; Miledi and Slater, 1970).

At 18 hours post nerve crush there were significantly fewer vacant (denervated) endplates in apoE-/- mice compared to wild-type controls (expressing endogenous mouse apoE): only 52.9±3.9% of motor endplates had lost their pre-synaptic motor nerve terminals in apoE-/- mice compared to 91.5±1.3% in wild-type mice (Fig. 4.8A/B). However, by 24 hours post-crush almost all motor nerve terminals in mice from both genotypes were vacant similar to previous descriptions of Wallerian degeneration in wild-type mice (Gillingwater and Ribchester, 2001; Miledi and Slater, 1970), showing that the modest delay in

degeneration seen at 18 hours post crush was only transient and that the loss of apoE did not significantly influence the eventual conclusion of Wallerian degeneration.

I next compared degeneration in mice expressing the human apoE3 and apoE4 transgenes to apoE-/- littermates. Examination of motor nerve terminals at 18 hours post-crush revealed a subtle but significant increase in the percentage of denervated motor endplates in apoE4 muscles compared to apoE-/- muscles (Fig. 4.9A). However, the previous observation that loss of apoE delayed degeneration at 18 hours compared to wild-type mice (expressing endogenous mouse apoE (Fig. 4.8A/B)) suggested that the difference observed between apoE4 and apoE-/- mice was caused by the loss of apoE, rather than presence of apoE4. In order to further confirm that the apoE4 isoform specifically was not influencing Wallerian degeneration, I also compared degeneration rates between apoE4 mice and apoE3 mice 18 hours after nerve lesion. No significant differences were observed between apoE3 and apoE4 mice (Fig. 4.9A).

As with the wild-type and apoE-/- mice the vast majority of motor endplates in apoE3 and apoE4 mice were denervated by 24 hours post nerve crush (Fig. 4.9B). No significant differences in rate of degeneration were observed between any of the genotypes at this time point.

Likewise, Wallerian degeneration of axons in the sciatic nerve 1 week after nerve crush occurred at the same rate in apoE3, apoE4 and apoE-/- mice (Fig.

4.10). Thus, whilst complete loss of apoE had a very subtle and transient effect on the early stages of Wallerian degeneration, neither the apoE3 or apoE4 transgene had a significant effect on Wallerian degeneration pathways in the PNS.

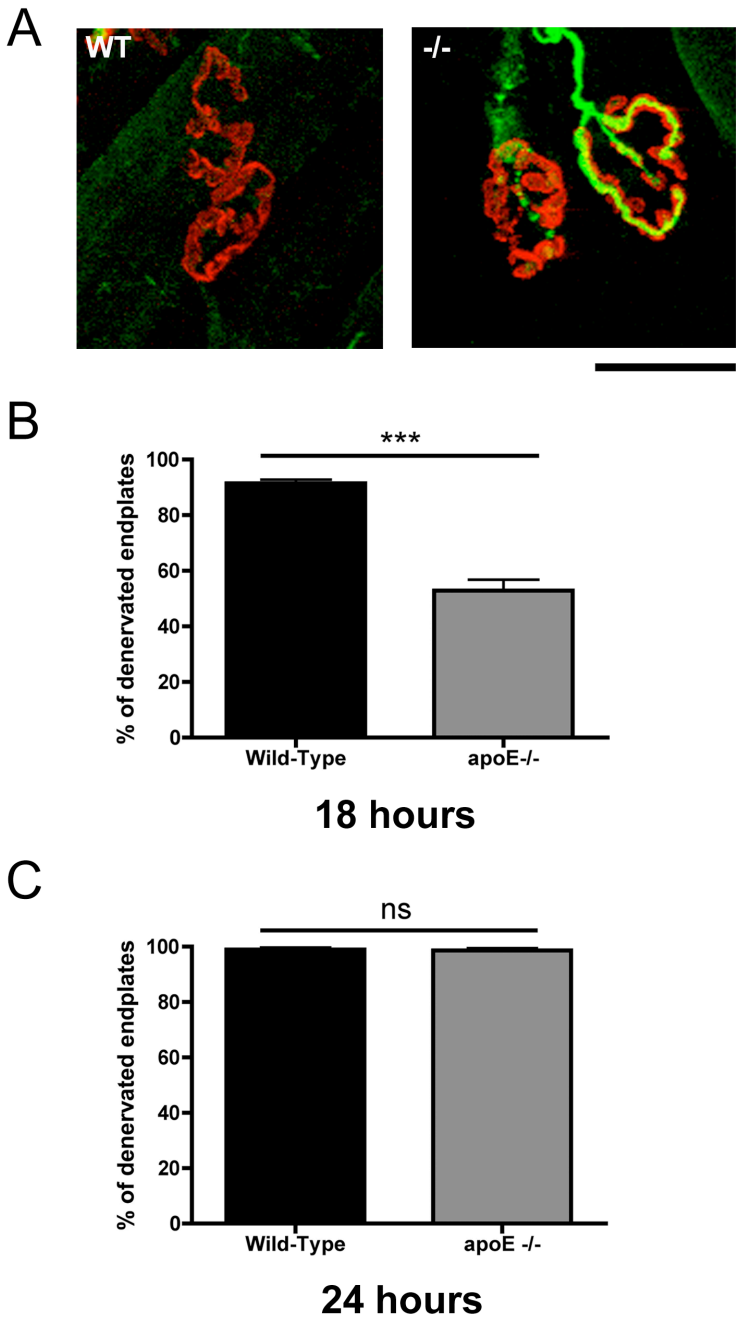

Figure 4.8 - Loss of apoE transiently delayed Wallerian degeneration of NMJs following peripheral nerve crush injury. A: Representative confocal micrographs showing a difference in the morphological appearance of NMJs in

apoE-/- (-/-) lumbrical muscles compared to wild-type (WT) controls 18 hours after a tibial nerve crush (pre-synaptic axons and motor nerve terminals are shown in green and post-synaptic acetylcholine receptors are shown in red). Note how all pre-synaptic elements (green) have undergone degeneration in wild-type mice whereas some pre-synaptic nerve terminals remain intact in apoE-/- mice at 18 hours post crush. Scale bar = 30μm. **B:** Bar chart showing significantly fewer denervated endplates in apoE-/- muscles compared to wild-type controls 18 hours after tibial nerve crush ($P<0.001$; Mann-Whitney test, two tailed; wild-type n=28 muscles N=5 mice, apoE-/- n=33 muscles N=6 mice). **C:** Bar chart showing no significant difference between the percentage of denervated endplates observed in wild-type and apoE-/- mice 24 hours post tibial nerve crush ($P>0.05$; Mann-Whitney test, two tailed; wild-type n=15 muscles N=4 mice, apoE-/- n=9 muscles N=4 mice).

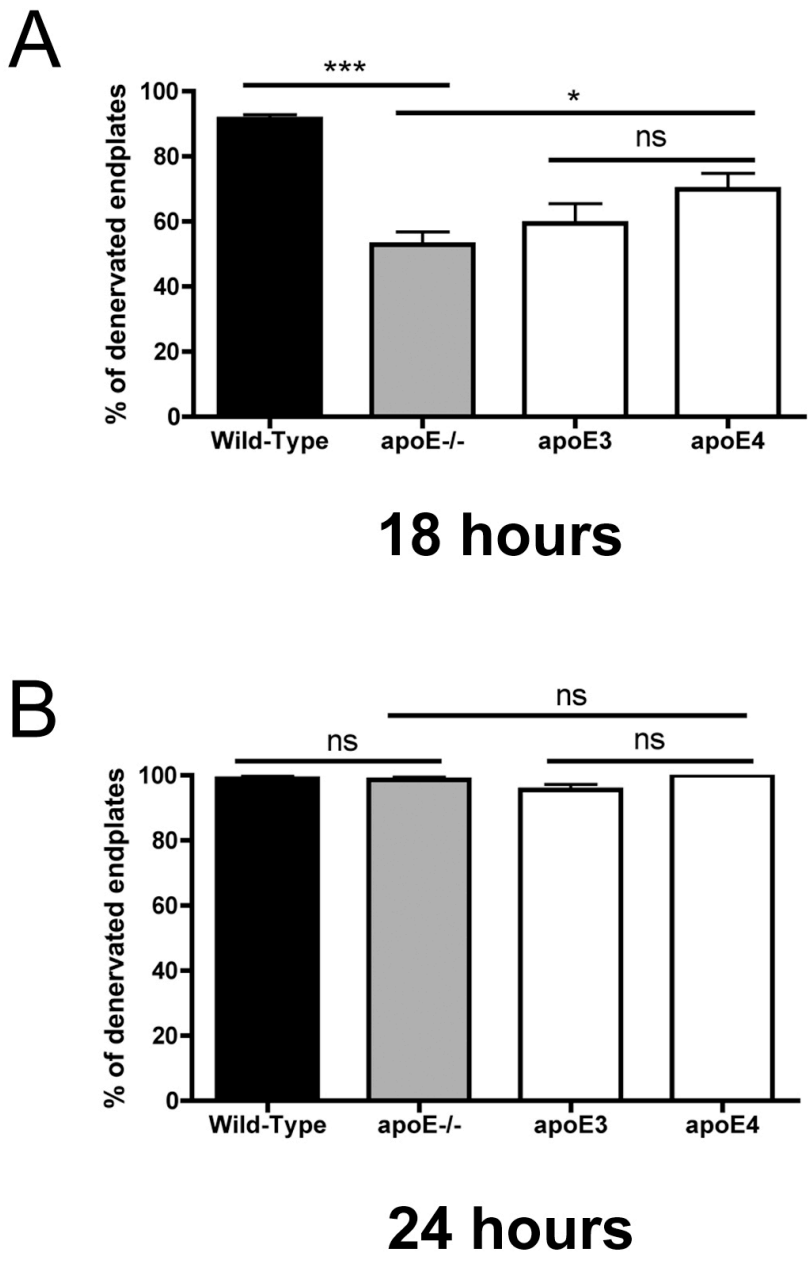

Figure 4.9 - Wallerian degeneration following nerve crush was subtly modified by presence of apoE. A: Bar chart (mean±SEM) showing levels of pre-synaptic degeneration in wild-type, apoE-/-, apoE3 and apoE4 lumbrical

muscles, 18 hours after a tibial nerve crush. At this time point significantly more endplates in apoE4 muscles were denervated compared to apoE-/- muscles ($P<0.05$; Kruskal-Wallis test with Dunn's post-hoc). However, there was no significant difference in the levels of denervation between apoE3 and apoE4 mice, indicating that the increase in the rate of degeneration in the apoE4 compared to apoE-/- mice is more likely to be as a consequence of loss of apoE in the apoE-/- mice, rather than and isoform specific effect of apoE4 ($P>0.05$; Kruskal-Wallis test with Dunn's post-hoc; wild-type N=5, apoE-/- N=6, apoE3 N=5, apoE4 N=4 mice). **B:** Bar chart (mean±SEM) showing no significant difference between the percentage of denervated endplates observed in wild-type, apoE-/-, apoE3 and apoE4 lumbrical muscles 24 hours post tibial nerve crush ($P>0.05$; Kruskal-Wallis test with Dunn's post-hoc test; wild-type N=4, apoE-/- N=4, apoE3 N=5, apoE4 N=3 mice).

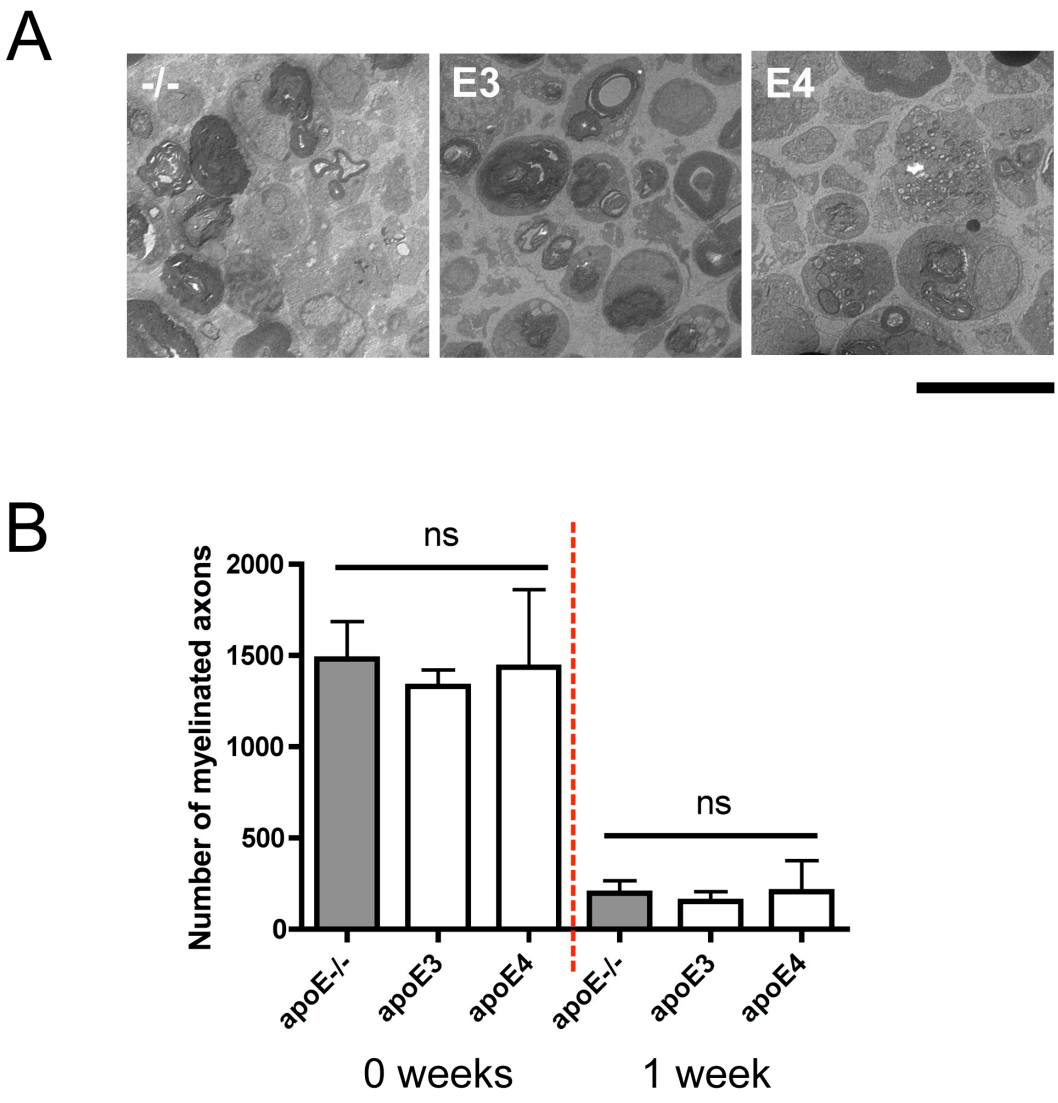

Figure 4.10 - Expression of the apoE4 isoform has no effect on Wallerian degeneration of axons following peripheral nerve crush injury. A: Representative electron micrographs of cross-sections from adult sciatic nerves in apoE-/- (-/-), apoE3 (E3) and apoE4 (E4) mice, 1 week after sciatic nerve

crush. Scale bar = 10μm. **B:** Bar chart (mean±SEM) showing reduced numbers of myelinated axons in apoE-/-, apoE3 and apoE4 sciatic nerves 1 week after nerve crush injury, but no significant difference in number of myelinated axons between the genotypes at either time point. (0 weeks $P>0.05$; one-way ANOVA with Tukey's post-hoc test; apoE-/- N=5, apoE3 N=5, apoE4 N=3. 1 week $P>0.05$; one-way ANOVA with Tukey's post-hoc test; apoE-/- N=3, apoE3 N=3 mice, apoE4 N=2).

4.3.4 ApoE4 significantly delays nerve regeneration and neuromuscular reinnervation following peripheral nerve injury.

Previous studies reported that complete loss of apoE did not affect regeneration of peripheral axons following nerve injury (Genden et al., 2002; Popko et al., 1993). To confirm and extend these findings to include functional reinnervation, I examined NMJs in deep lumbrical muscles from apoE-/- and wild-type mice following tibial nerve crush. As expected, there was no significant difference in the levels of NMJ reinnervation between apoE-/- and wild-type control mice at 2 or 3 weeks post nerve crush (Fig. 4.11). These data therefore support the findings of previous studies (Genden et al., 2002; Popko et al., 1993) and suggest that apoE *per se* is not essential for nerve regeneration and subsequent reinnervation of NMJs.

However, the more biologically relevant question is whether apoE genotype can influence regeneration and subsequent functional reinnervation in the PNS following nerve crush injury. I therefore used electron microscopy to quantify axon regeneration in the sciatic nerve of apoE3 and apoE4 mice at 2 and 3 weeks following sciatic nerve injury (Fig. 4.12). At one week post-injury (the time when regeneration is beginning following Wallerian degeneration *in vivo*: see above) there was no difference in the number of axons in the sciatic nerves of apoE3 and apoE4 mice. However, at 2 weeks post-injury, apoE4 mice showed significantly reduced numbers of regenerating axons in the sciatic nerve compared to apoE3 mice (only 63% regeneration when compared with apoE3

mice, P<0.05; fig 4.12). This significant delay in regeneration persisted in apoE4 mice 3 weeks after injury, where regeneration was almost complete in apoE3 mice, but had only reached 70% of these levels in apoE4 mice (P<0.05; Fig. 4.12).

To confirm that the delay in axon regeneration in apoE4 mice also resulted in delayed reinnervation of peripheral targets by the regenerating axons, I then quantified reinnervation of NMJs in the lumbrical muscles (innervated by the tibial nerve) of apoE3 and apoE4 mice following tibial nerve injury. 2 weeks after nerve injury, lumbrical muscles in apoE4 mice had significantly fewer reinnervated endplates compared to both apoE3 mice and apoE-/- mice (32% reinnervation compared with apoE3 mice, P<0.001; Fig. 4.13).

As expected, the reinnervation process progressed in both apoE-/- and apoE4 muscles between two (Fig. 4.13) and three (Fig. 4.14) weeks post crush, manifesting as an increase in the numbers of reinnervated endplates. However, neuromuscular reinnervation was still significantly delayed in apoE4 mice compared to apoE-/- controls three weeks after tibial nerve crush (Fig. 4.14).

Surprisingly, however, reinnervation did not appear to progress at all between the two and three week time-points in apoE3 mice (~65% of endplates were reinnervated at both 2 and 3 weeks after nerve crush; Fig. 4.13B and Fig. 4.14). As a result, the enhanced levels of reinnervation observed in these mice at 2 weeks were lost, leaving a significantly reduced number of reinnervated NMJs

compared to apoE-/- mice, with levels comparable to those observed in apoE4 mice.

To be sure that the delay in axon regeneration and neuromuscular reinnervation observed in apoE4 mice was not occurring due to differing expression levels of human apoE transgenes after nerve injury I used fluorescent quantitative western blotting to measure the levels of apoE protein in tibial nerves from apoE3 and apoE4 mice two weeks after nerve crush (Fig. 4.15). Expression levels of apoE protein were identical in apoE3 and apoE4 nerves. As expected there was no expression of apoE in the apoE-/- mice, and an up-regulation of the protein in the injured wild-type nerves (Fig. 4.3A compared to Fig. 4.15A).

Taken together, these data show that apoE4 selectively delays nerve regeneration and subsequent neuromuscular reinnervation in the PNS.

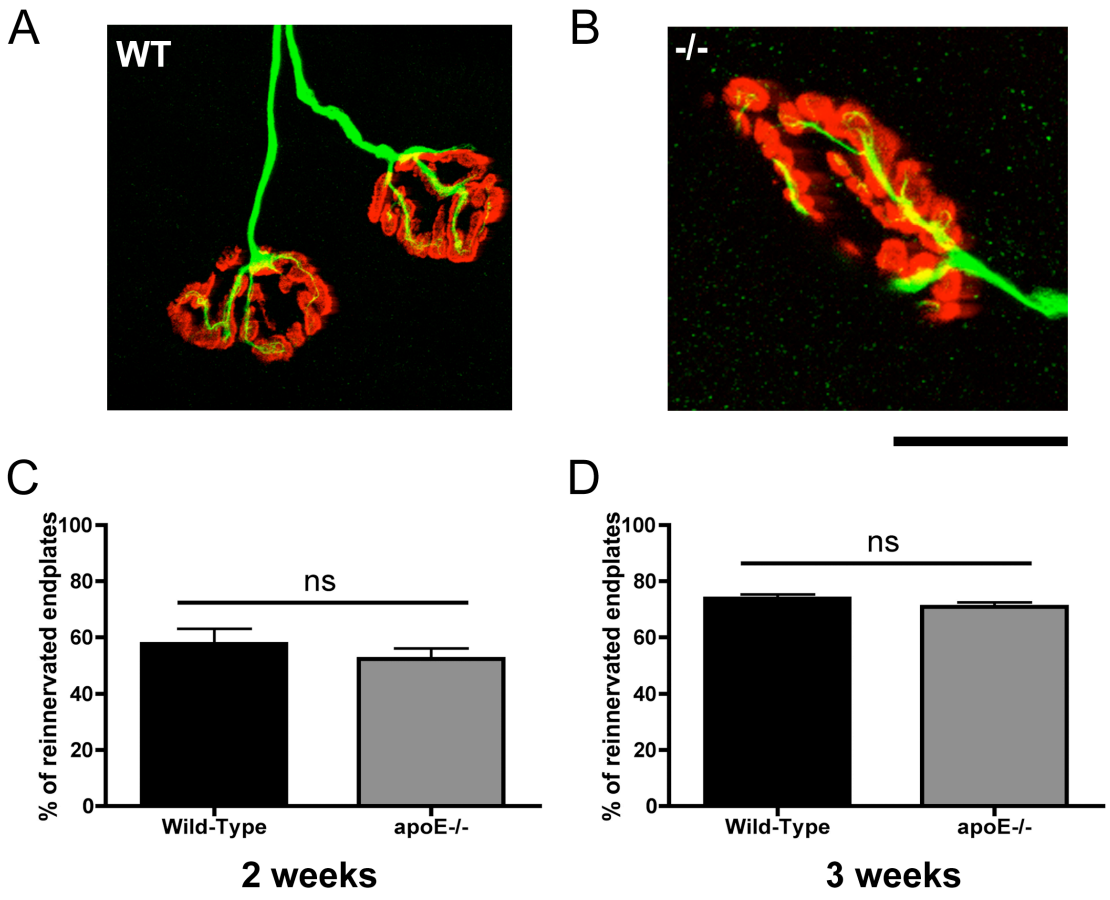

Figure 4.11 - Complete loss of apoE has no effect on neuromuscular reinnervation following nerve crush injury. A/B: Representative confocal micrographs showing fully reinnervated endplates in immunohistochemically labelled wild-type (**A**) and apoE-/- (**B**) lumbrical muscles three weeks after a tibial nerve crush. Scale bar = 30μm. **C:** Bar chart (mean±SEM) showing no significant difference in the level of neuromuscular reinnervation in lumbrical muscles from apoE -/- mice compared to wild-type controls two weeks after a

tibial nerve crush (P>0.05; Mann-Whitney test, two tailed; wild-type N=5 mice, apoE-/- N=6 mice). **D:** Bar chart showing no significant difference in the level of neuromuscular reinnervation in lumbrical muscles from apoE -/- mice compared to wild-type controls three weeks after a tibial nerve crush (P>0.05; Mann-Whitney test, two tailed; wild-type N=8, apoE-/- N=12 mice).

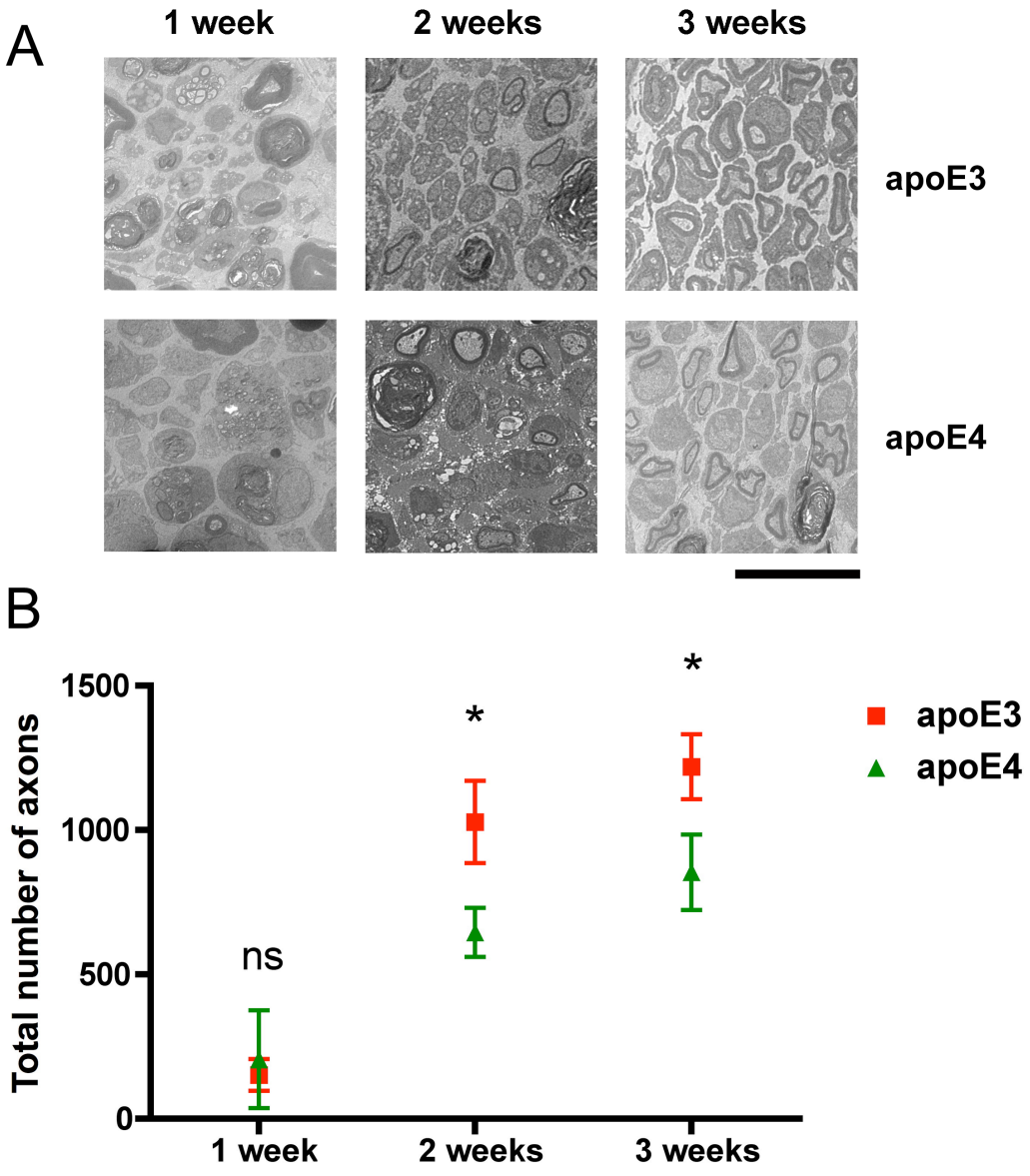

Figure 4.12 – The apoE4 isoform significantly delays nerve regeneration following sciatic nerve injury. A: Representative electron micrographs showing cross-sections from adult sciatic nerves in apoE3 (E3) and apoE4 (E4) mice, one, two and three weeks after sciatic nerve crush. Scale bar = 10μm. **B:** Scatter plot

(mean±SEM) showing time course of axonal regeneration in apoE3 and apoE4 sciatic nerves following sciatic nerve crush. At both two and three weeks post-crush apoE4 significantly delays regeneration (63% and 70% that of the levels of apoE3 axon regeneration at the same time points, respectively; 1 week $P>0.05$; t-test, two-tailed; apoE3 N=3, apoE4 N=2; 2 weeks $P<0.05$; t-test, two-tailed; apoE3 N=6 apoE4 N=6. 3 weeks $P<0.05$; t-test, two-tailed; apoE3 N=11, apoE4 N=11).

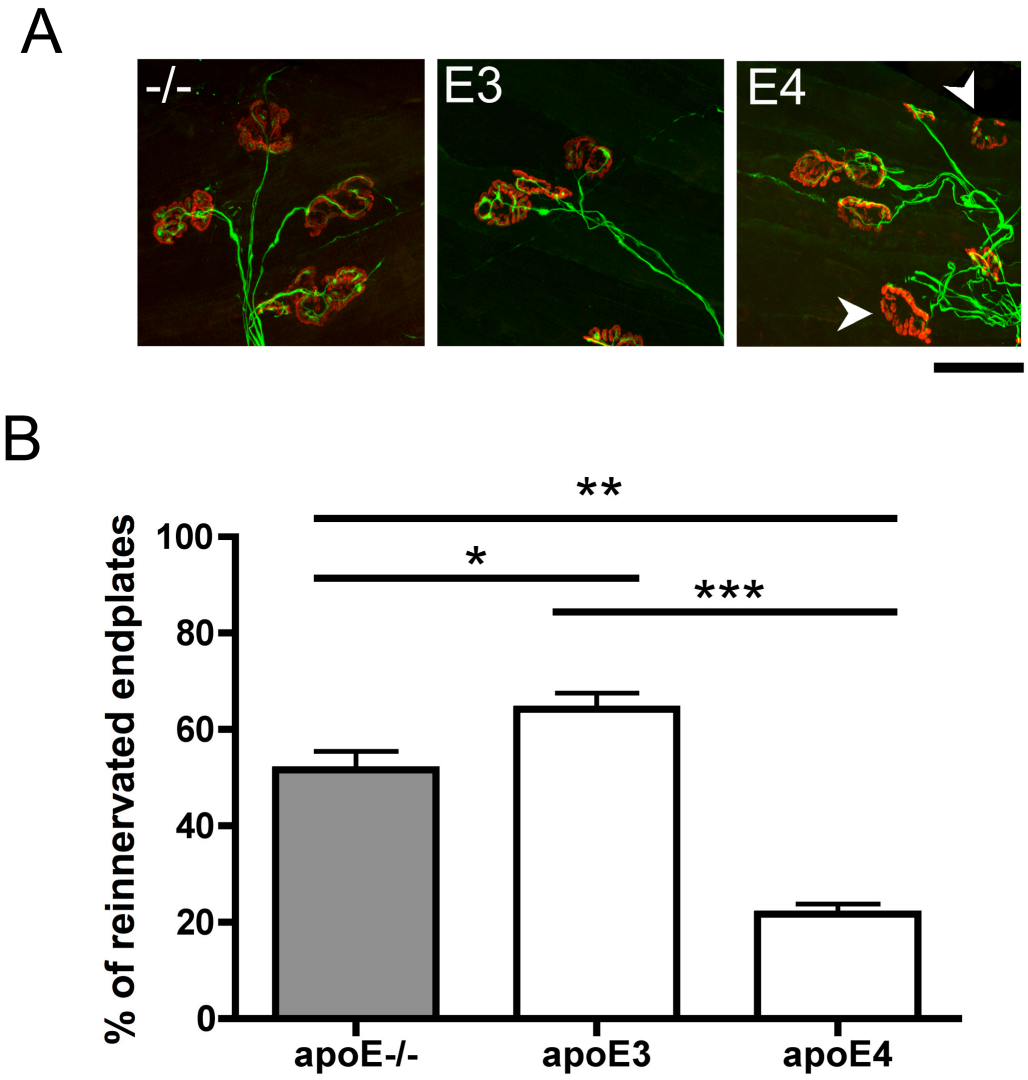

Figure 4.13 - ApoE4 significantly delays neuromuscular reinnervation following tibial nerve crush injury. A: Representative confocal micrographs showing NMJs from apoE-/-, apoE3 and apoE4 lumbrical muscles two weeks after a tibial nerve crush (pre-synaptic axons and motor nerve terminals shown

in green and post-synaptic acetylcholine receptors labelled with α-bungarotoxin are shown in red). Note how all endplates in the field of view in the apoE-/- and apoE3 muscles have been reinnervated, whereas in the apoE4 muscle some endplates are still awaiting reinnervation (white arrowheads). Scale bar = 30μm. **B:** Bar chart (mean±SEM) showing levels of neuromuscular reinnervation in lumbrical muscles 2 weeks after a tibial nerve crush. Reinnervation was significantly delayed in apoE4 mice compared to both apoE-/- and apoE3 mice ($P<0.01$ and $P<0.001$ respectively; Kruskal Wallis test with Dunn's post-hoc test; apoE-/- N=6, apoE3 N=5, apoE4 N=5).

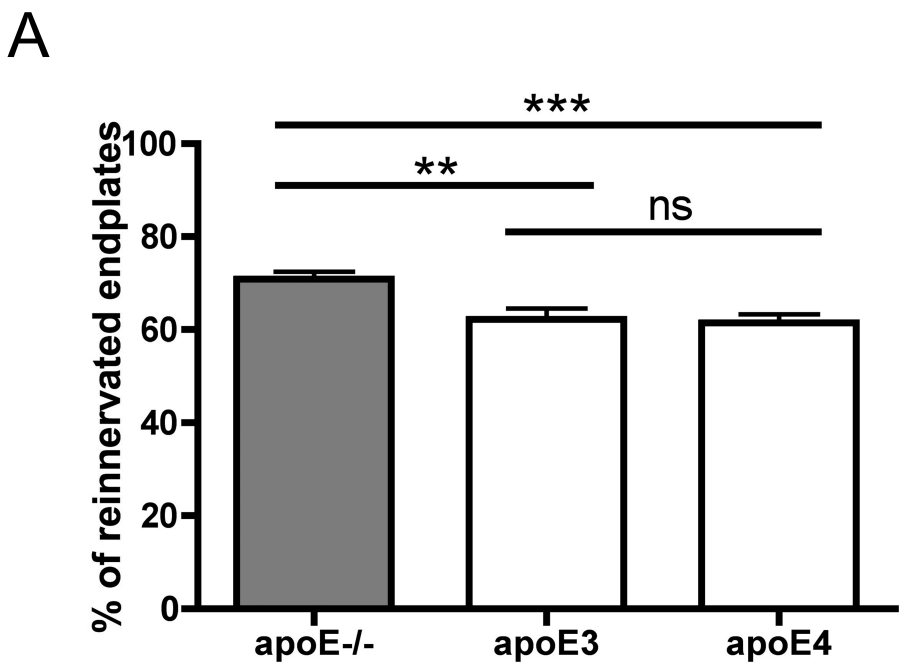

Figure 4.14 - ApoE4 significantly delays neuromuscular reinnervation following nerve crush injury in the mouse PNS. Bar chart showing levels of reinnervation in lumbrical muscles 3 weeks after a tibial nerve crush. Neuromuscular reinnervation was still significantly delayed in apoE4 muscles compared to apoE-/- muscles. ($P<0.001$; Mann-Whitney test, two tailed; apoE-/- n=63 muscles N=12 mice, apoE4 n=34 muscles N=6 mice).

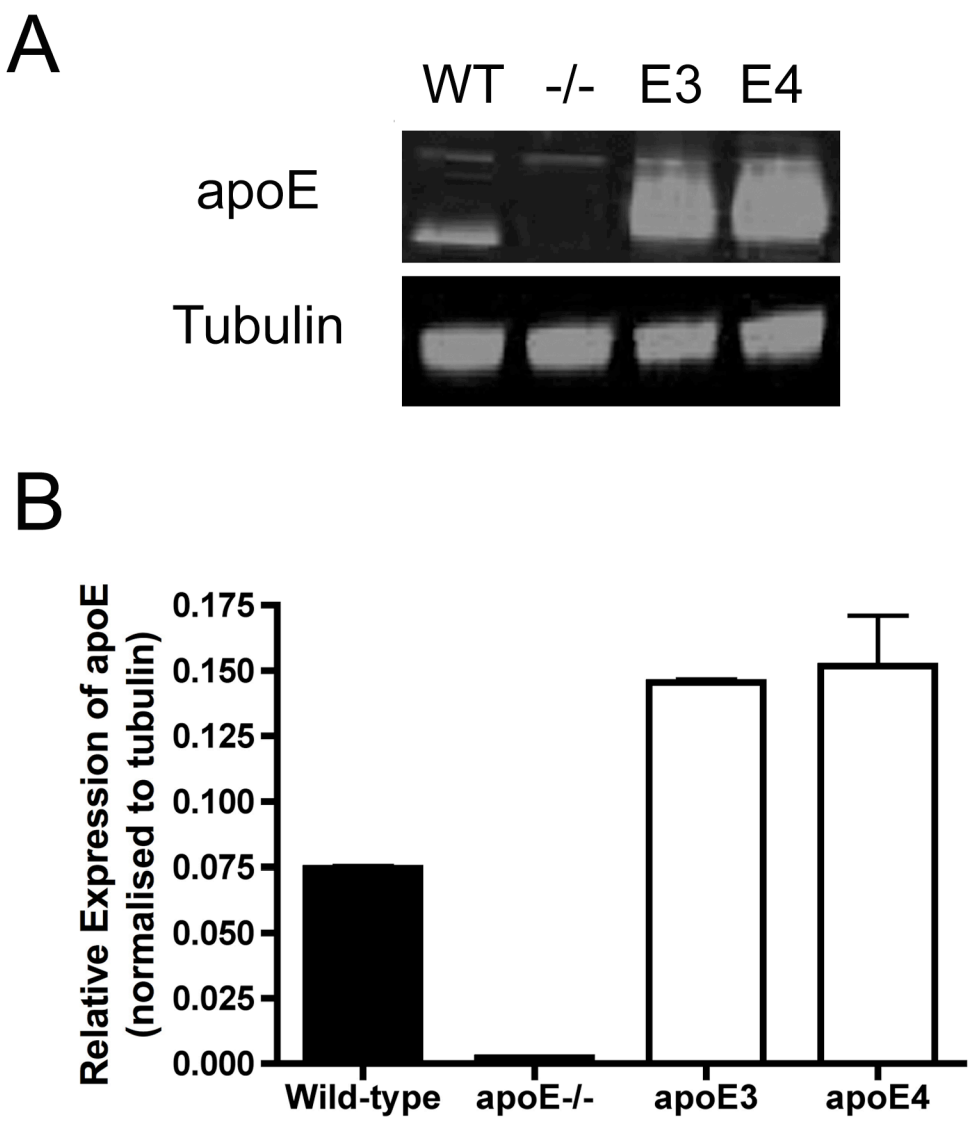

Figure 4.15 – The delayed axon regeneration and neuromuscular reinnervation seen in apoE4 mice is a specific response to the E4 isoform of apoE, and is not due to differing expression levels from human apoE transgenes after nerve injury. A: Representative fluorescent Western blots showing levels of apoE and tubulin (loading control) protein extracted from sciatic nerves 3 weeks after

nerve injury. There is no obvious difference in the levels of apoE protein expression between apoE3 and apoE4 isoforms. **B:** Bar chart (mean±SEM) showing quantification of Western blots, confirming no difference in the levels of apoE3 and apoE4 protein expressed in distal nerve stumps (N=2 per genotype).

4.3.5 ApoE genotype modifies expression levels of proteins associated with cellular outgrowth and blood-nerve barrier integrity in peripheral nerve in vivo.

Given the finding that apoE genotype modifies nerve regeneration in the mouse PNS *in vivo*, I next wanted to identify potential molecular mechanisms underlying the genotype specific response. To do this I first used iTRAQ proteomics to compare protein expression levels in tibial nerves from apoE3 and apoE4 mice. As these were uninjured nerves these experiments were designed to pick up any changes in the peripheral nerve proteome occurring solely as a result of the presence of different isoforms of apoE, in the absence of any external stimuli (e.g. nerve degeneration or regeneration following nerve crush injury). The peripheral nerve preparations used were whole nerves, so contained all cell types present in the peripheral nerve (glial cells, capillaries, extracellular matrix etc.) as well as axons. These cell types make up the local microenvironment, which needs to be conducive for nerve regeneration to occur, so was important to consider in this experiment.

Using stringent inclusion criteria (see Materials and methods, 4.2.11), 62 proteins showed expression levels increased >20% in uninjured apoE4 peripheral nerves compared to apoE3 peripheral nerves (Table 4.1), and 40 proteins had expression levels decreased >20% in peripheral nerves in the apoE4 mice (Table 4.2). Neither of the protein products from the apoE3 or apoE4 transgenes were picked up as they are human proteins and the analysis was set to identify mouse proteins.

Proteins identified with differing expression levels were then analysed using Ingenuity Pathway Analysis software to look for potential clustering of functions or interactions. Systems level analysis of protein expression changes highlighted interaction networks of myosin and actin proteins, associated with regulation of tissue and cell morphology (Fig. 4.16). Networks associated with haematological regulation, including the integrity of the blood brain barrier (BBB) and blood nerve barrier (BNB) were also identified as being changed in the apoE4 mice compared to apoE3 (Fig. 4.17). These data show that even in normal healthy nerve, expression of the different apoE isoforms can lead to significant modifications in the peripheral nerve proteome, likely to have implications for form and function.

Within the myosin/actin interaction network there were changes in several myosin proteins in the uninjured peripheral nerve in apoE4 mice, in the absence of any corresponding changes in actin. Myosin proteins within these myosin/actin networks are essential for neurite outgrowth and as molecular motors are responsible for transporting actin to parts of the cell where it is needed for cell growth (Brown and Bridgman 2003; Chantler and Wylie, 2003; Wylie et al., 1998). However, corresponding changes in levels of actins would be necessary for the pathway to lead to alterations in cell morphology in uninjured nerves (Arnold 2009; Brown and Bridgman 2004; Chantler and Wylie, 2003). This finding was therefore consistent with the earlier morphological data showing that expression of apoE4 does not affect the form or function of the uninjured PNS *in vivo* (see section 4.3.1, and Figs. 4.4 and 4.5). These changes in

levels of myosin proteins in the uninjured nerve may however represent a 'priming' response, which has no effect on the healthy PNS, but could result in a change in actin dynamics following nerve injury.

To test whether changes in myosin levels lead to corresponding changes in actin levels in the regenerating peripheral nerve the iTRAQ proteomics experiments were repeated using nerves from apoE3 and apoE4 mice 3 weeks after sciatic nerve crush injury. As in the experiments on uninjured nerves, large numbers of proteins had altered expression levels in the apoE4 regenerating nerves compared to the apoE3 nerves. 28 proteins showed increased expression levels >20% in regenerating peripheral nerves from apoE4 mice compared to apoE3 peripheral nerve (Table 4.3), and 81 proteins had decreased expression levels >20% in regenerating apoE4 peripheral nerves (Table 4.4). Many of the proteins altered in the regenerating nerves were similar to those identified in the uninjured nerves, such as the proteins involved in haematological regulation, e.g. orosomucoid 1 and haptoglobin. However, even more dramatic changes were seen in the expression levels of both myosin and actin proteins in the apoE4 regenerating nerves (Table 4.4). The proteins altered in the regenerating nerves were also analysed using Ingenuity Pathway Analysis software to look for potential clustering of functions or interactions. 71% of the proteins in a myosin / actin network had altered levels of expression in the uninjured nerves (Fig. 4.16), whereas 83% and 86% of proteins in two separate myosin / actin networks had altered expression levels in the regenerating apoE4 nerves (Fig. 4.18 and 4.19).

The myosin/actin pathways are key pathways for cellular reorganisation in processes such as nerve regeneration following nerve injury (Arnold, 2009; Brown and Bridgman, 2004; Chantler and Wylie, 2003). The reduction in the levels of so many of these proteins in apoE4 peripheral nerve compared to apoE3 is therefore likely to be playing a significant role in reducing the regenerative capacity of these mice following nerve injury.

Table 4.1 - iTRAQ identification of proteins with >20% increased expression and peptide count >1 in the unlesioned sciatic nerve from ApoE4 mice compared to ApoE3 mice

Protein Name	Accession Number	Protein MW	Protein PI	Peptide Count	Total Ion Score C.I. %	Best Ion Score	Avg ratio (E4/E3)	StdDev (E4/E3)
haptoglobin precursor	8850219	42455.7	5.9	7	100.00	67.94	3.39	1.42
Orosomucoid 1	15215270	26393.8	5.4	5	100.00	58.65	2.05	0.53
myomesin 2	170763465	179757.5	5.6	11	100.00	72.44	1.80	0.35
PK-120 precursor	2739028	112522.4	6.1	2	100.00	52.16	1.67	0.03
myosin, heavy polypeptide 4, skeletal muscle	67189167	254149.5	5.6	85	100.00	127.38	1.67	0.44
hemopexin precursor	160358829	55053.3	7.9	15	100.00	95.47	1.63	0.42
muscle glycogen phosphorylase	6755256	104509.5	6.7	18	100.00	93.56	1.63	0.33
Myosin-binding protein C, fast-type	81910387	143381.3	6.0	10	100.00	100.37	1.62	0.49
ATPase, Ca++ transporting, ubiquitous	74215005	116671.4	5.5	2	100.00	48.16	1.61	0.09
major urinary protein	295910	22495.3	4.9	3	100.00	85.86	1.59	0.23
Major Urinary Protein	13276755	22609.4	5.0	3	100.00	85.86	1.58	0.21
MUP	755765	17535.8	4.9	2	100.00	62.95	1.53	0.12
Myh7 protein	187956918	252607.1	5.6	20	100.00	91.72	1.51	0.56
alpha cardiac myosin heavy chain	191618	253883.5	5.6	18	100.00	91.72	1.48	0.58
muscle creatine kinase	6671762	48101.2	6.6	14	100.00	101.99	1.45	0.34
S100 calcium binding protein A9 (calgranulin B)	6677837	14907.5	6.6	2	100.00	69.01	1.45	0.09
solute carrier family 4 (anion exchanger), member 1	74138529	108215.2	5.4	2	100.00	50.97	1.45	0.01
fibrinogen, gamma polypeptide	74143561	55480.4	5.4	6	100.00	84.66	1.43	0.09
titin	123232572	3312853.3	6.2	2	100.00	37.84	1.43	0.05
fibrinogen beta chain precursor	33859809	60169.0	6.7	12	100.00	78.56	1.41	0.29
myosin, heavy polypeptide 8, skeletal muscle, perinatal	71143152	253848.8	5.7	46	100.00	106.43	1.40	0.58
parvalbumin	31980767	14372.8	5.0	5	100.00	88.79	1.40	0.19
Myosin, heavy polypeptide 8, skeletal muscle, perinatal	187956525	253835.8	5.7	46	100.00	106.43	1.39	0.57
hemoglobin, beta adult major chain	31982300	17513.4	7.1	13	100.00	107.43	1.36	0.22
clusterin precursor	214010170	56451.5	5.5	4	100.00	82.73	1.36	0.47
mCG18455	148678485	256334.6	5.5	22	100.00	84.80	1.36	0.71
troponin T	2340048	34082.0	9.4	4	100.00	78.26	1.35	0.16
hemoglobin alpha, adult chain 2	145301549	16878.0	8.0	9	100.00	101.60	1.35	0.25
ATPase, Ca++ transporting, cardiac muscle, fast twitch 1	148685412	116243.4	5.3	12	100.00	114.25	1.35	0.24
actinin alpha 3	7304855	110400.7	5.3	34	100.00	112.37	1.34	0.46
Phosphofructokinase, muscle	13529638	92278.8	8.2	8	100.00	67.00	1.34	0.11
collagen, type VI, alpha 1 precursor	6753484	117555.5	5.2	7	100.00	91.16	1.33	0.17
glutamine synthetase	31982332	45842.4	6.6	2	100.00	67.62	1.33	0.04
myomesin 1 isoform 2	145279198	194032.5	6.0	7	100.00	81.84	1.33	0.13
sarcalumenin, isoform CRA_a	148664814	59761.7	6.2	4	100.00	60.15	1.31	0.25
ATPase, Ca++ transporting, slow twitch 2 isoform a	158635979	124907.5	5.2	5	100.00	68.51	1.31	0.33
histone cluster 1, H1c	9845257	29755.8	11.0	2	100.00	75.68	1.30	0.17
mCG2006, isoform CRA_a	148680420	187536.8	6.3	2	100.00	60.73	1.30	0.12
Glycogen phosphorylase, liver form	20178036	107417.7	6.6	5	100.00	58.28	1.29	0.20
phosphoglycerate mutase 2	9256624	31972.9	8.7	8	100.00	89.17	1.29	0.17
enolase 3, beta muscle, isoform CRA_a	148680653	54402.9	6.8	15	100.00	112.63	1.28	0.28
sorbitol dehydrogenase	22128627	42431.2	6.6	2	100.00	54.45	1.28	0.23
RIKEN cDNA 1810020D17, isoform CRA_c	148684357	17880.5	7.8	2	100.00	44.25	1.27	0.04
unnamed protein product	26345578	19080.7	10.5	3	100.00	67.62	1.26	0.17
cullin 1	7549752	100115.9	8.2	2	100.00	53.35	1.26	0.23

Table 4.1 -iTRAQ identification of proteins with >20% increased expression and peptide count >1 in the unlesioned sciatic nerve from ApoE4 mice compared to ApoE3 mice (Continued)

Protein Name	Accession Number	Protein MW	Protein PI	Peptide Count	Total Ion Score C.I. %	Best Ion Score	Avg ratio (E4/E3)	StdDev (E4/E3)
hormone-sensitive lipase [Mus musculus domesticus]	677885	87018.7	6.5	2	100.00	60.78	1.25	0.03
epoxide hydrolase 1	6753762	57724.5	8.4	2	100.00	53.93	1.24	0.10
collagen, type VI, alpha 2 precursor	22203747	118822.8	6.0	11	100.00	63.77	1.24	0.16
Aldolase A, fructose-bisphosphate	42490830	43401.8	8.5	11	100.00	91.23	1.23	0.10
preprocomplement component C3	309122	205041.7	6.4	6	100.00	56.08	1.23	0.18
phosphatidylinositol-4-phosphate 5-kinase type II beta	17223780	50243.1	6.4	2	100.00	52.71	1.23	0.27
fast skeletal myosin alkali light chain 1 isoform 1f	29789016	23699.5	5.0	14	100.00	97.84	1.22	0.18
adenylate kinase 1	10946936	26311.9	5.7	5	100.00	77.64	1.22	0.24
fibrinogen, alpha polypeptide, isoform CRA_b	148683477	68946.6	7.0	6	100.00	64.58	1.21	0.23
lactate dehydrogenase A isoform 1	6754524	40772.0	7.6	13	100.00	74.65	1.21	0.13
Chain B, X-Ray Structure Of The Nucleosome Core Particle	27573730	12958.6	11.4	4	100.00	53.05	1.21	0.14
2',3'-cyclic nucleotide 3' phosphodiesterase isoform 2	226423907	53755.9	9.1	24	100.00	122.44	1.21	0.17
ATPase, H+ transporting, lysosomal V1 subunit H	14318722	60928.4	6.2	2	100.00	61.01	1.20	0.02
chaperonin	460317	64225.7	8.2	2	100.00	98.95	1.20	0.15
tyrosyl-tRNA synthetase	165377181	68152.2	6.6	2	100.00	40.36	1.20	0.14
Glyoxalase 1	19354350	23702.3	5.2	2	100.00	47.51	1.20	0.33
xanthine dehydrogenase	187954915	159925.8	7.6	3	100.00	51.62	1.20	0.06

Table 4.2 - iTRAQ identification of proteins with >20% decreased expression and peptide count >1 in the unlesioned sciatic nerve from ApoE4 mice compared to ApoE3 mice

Protein Name	Accession Number	Protein MW	Protein PI	Peptide Count	Total Ion Score C.I. %	Best Ion Score	Avg ratio (E4/E3)	StdDev (E4/E3)
myosin, light polypeptide 6B	26986555	25852.8	5.4	4	100.00	69.41	0.19	0.12
myoglobin	21359820	20131.1	7.1	10	100.00	143.49	0.49	0.07
myosin, light polypeptide 3, isoform CRA_a	148677054	27359.4	5.0	5	100.00	54.09	0.51	1.25
h1-calponin alpha	1069994	36759.9	8.8	4	100.00	68.12	0.54	0.03
Igh protein	62028521	56919.8	7.5	3	100.00	71.06	0.57	0.08
Ig H-C allotype gamma2b	223428	40724.8	7.2	2	100.00	90.21	0.61	0.03
h-caldesmon	17017241	43428.3	5.3	2	100.00	70.01	0.63	0.25
light chain of the monoclonal antibody MST2	1617395	27982.7	7.0	2	100.00	55.34	0.66	0.03
skeletal muscle LIM protein	2880031	38678.1	8.8	2	100.00	78.07	0.67	0.02
heat shock protein, alpha-crystallin-related, B6	59958370	18132.5	5.6	3	100.00	54.71	0.68	0.09
Chain A, Crystal Structure Of Mouse Transthyretin	161172183	15211.9	5.8	3	100.00	94.87	0.69	0.08
actinin alpha 2	157951643	112009.7	5.3	23	100.00	112.37	0.69	0.22
LIM domain binding 3 isoform b	84872213	76092.4	8.3	3	100.00	70.38	0.70	0.10
filamin, alpha	125347376	305825.3	5.7	29	100.00	89.05	0.71	0.09
fibromodulin precursor	10946680	44933.6	5.9	2	100.00	43.37	0.71	0.13
milk fat globule-EGF factor 8 protein isoform 2	113865977	50796.5	6.7	5	100.00	83.22	0.71	0.08
transgelin	6755714	25201.2	8.9	8	100.00	88.00	0.71	0.04
myosin	1945080	253502.8	5.4	17	100.00	83.10	0.72	0.15
PDZ and LIM domain protein 3	7948997	36807.6	8.1	3	100.00	68.49	0.72	0.17
myosin regulatory light polypeptide 9	198278553	22033.0	4.9	6	100.00	74.98	0.72	0.04
Collagen alpha-1(XIV) chain	146345398	206682.6	5.0	8	100.00	93.04	0.74	0.05
procollagen, type I, alpha 2 precursor	111120329	136953.2	9.3	8	100.00	77.32	0.75	0.17
destrin, isoform CRA_b	148696488	28666.5	9.0	5	100.00	66.15	0.76	0.08
LIM domain containing preferred translocation partner in lipoma	225543157	71700.8	7.2	4	100.00	52.29	0.76	0.09
Actinin alpha 2	58476244	111806.5	5.3	20	100.00	112.37	0.76	0.27
Ig gamma-3 chain C region	121044	47963.7	6.7	3	100.00	46.58	0.76	0.03
proteasome alpha 6 subunit	6755198	30608.7	6.3	3	100.00	75.58	0.77	0.21
protein phosphatase 1	471976	42247.5	5.8	2	100.00	43.57	0.77	0.01
Chain A, Crystal Structure Of The Ap-2 Clathrin Adaptor Alpha	5822376	29953.4	6.9	2	100.00	49.31	0.78	0.06
Gfap protein	72679718	51278.8	5.1	3	100.00	45.03	0.78	0.19
albumin precursor	163310765	77836.5	5.8	36	100.00	121.79	0.78	0.12
Probable ATP-dependent RNA helicase DDX5	2500527	74734.3	9.1	2	100.00	50.01	0.78	0.02
adipsin precursor	7304867	29317.2	6.2	2	100.00	44.03	0.79	0.05
PDZ and LIM domain 5, isoform CRA_c	148680118	57492.2	8.2	3	100.00	82.11	0.79	0.09
heterogeneous nuclear ribonucleoprotein L	183980004	68765.9	7.3	3	100.00	77.22	0.79	0.03
Fibulin 2	13529413	134192.5	4.6	2	100.00	43.20	0.79	0.02
EF hand domain containing 2	31981086	28253.9	5.0	2	100.00	43.24	0.79	0.17
serpin peptidase inhibitor, clade C, member 1 precursor	18252782	57428.0	6.1	3	100.00	49.87	0.79	0.12
mKIAA0777 protein	28972395	139280.4	8.4	4	100.00	88.73	0.79	0.23
carboxylesterase	192854	65222.7	5.0	8	100.00	84.01	0.80	0.11

Table 4.3 - iTRAQ identification of proteins with >20% increased expression and peptide count >1 in lesioned sciatic nerve from ApoE4 mice compared to ApoE3 mice

Protein Name	Accession Number	Protein MW	Protein PI	Peptide Count	Total Ion Score C.I. %	Best Ion Score	Avg ratio (E4/E3)	StdDev (E4/E3)
haptoglobin precursor	8850219	42455.7	5.9	7	100.00	67.94	3.33	0.12
Orosomucoid 1	15215270	26393.8	5.4	5	100.00	58.65	1.90	0.15
PK-120 precursor	2739028	112522.4	6.1	2	100.00	52.16	1.87	0.01
hemopexin precursor	160358829	55053.3	7.9	15	100.00	95.47	1.51	0.12
calpain small subunit	19705421	24752.3	5.1	3	100.00	41.83	1.42	0.13
unnamed protein product	26345578	19080.7	10.5	3	100.00	67.62	1.41	0.17
laminin B1 subunit 1	114326497	221889.2	4.9	13	100.00	77.25	1.39	0.13
fibrinogen, alpha polypeptide, isoform CRA_b	148683477	68946.6	7.0	6	100.00	64.58	1.38	0.09
fibrinogen, gamma polypeptide	148683478	55480.4	5.4	6	100.00	84.66	1.38	0.09
CD10 neutral endopeptidase 24.11	192459	93776.9	5.7	2	100.00	52.20	1.37	0.23
fibrinogen beta chain precursor	33859809	60169.0	6.7	12	100.00	78.56	1.35	0.12
C4 complement protein	50242	137077.1	6.5	2	100.00	47.28	1.34	0.13
2',3'-cyclic nucleotide 3' phosphodiesterase isoform 2	226423907	53755.9	9.1	24	100.00	122.44	1.33	0.13
aspartyl-tRNA synthetase isoform 1	211065507	61980.2	6.1	2	100.00	63.91	1.33	0.03
PREDICTED: similar to major urinary protein 1	149252557	28801.5	5.1	4	100.00	85.86	1.32	0.08
PREDICTED: hypothetical protein isoform 2	82886943	18543.3	10.3	3	100.00	58.44	1.31	0.12
Hypoxanthine-guanine phosphoribosyltransferase	2499938	26555.9	5.7	3	100.00	48.91	1.30	0.08
neural cell adhesion molecule 1 isoform 1	124517689	101275.8	4.8	3	100.00	46.03	1.29	0.13
glutamine synthetase	31982332	45842.4	6.6	2	100.00	67.62	1.28	0.05
nucleoside phosphorylase	7305395	34057.1	5.8	3	100.00	67.49	1.28	0.06
Auh protein	20072952	36020.8	9.6	2	100.00	56.44	1.27	0.04
preprocomplement component C3	309122	205041.7	6.4	6	100.00	56.08	1.27	0.15
microtubule-associated protein 6 isoform 1	113204613	107716.5	9.5	5	100.00	70.91	1.27	0.10
nidogen 1 precursor	171543883	143072.8	5.2	23	100.00	76.48	1.27	0.10
Fbxo2 protein	20072543	34278.6	4.3	6	100.00	82.62	1.27	0.17
laminin, alpha 2	117647249	376116.8	5.8	26	100.00	107.74	1.26	0.15
breast carcinoma amplified sequence 1	123233481	58733.9	6.2	4	100.00	83.08	1.26	0.09
solute carrier family 44, member 2	22779895	86584.2	9.1	2	100.00	66.29	1.25	0.15

Table 4.4 - iTRAQ identification of proteins with >20% decreased expression and peptide count >1 in lesioned sciatic nerve from ApoE4 mice compared to ApoE3 mice

Protein Name	Accession Number	Protein MW	Protein PI	Peptide Count	Total Ion Score C.I. %	Best Ion Score	Avg ratio (E4/E3)	StdDev (E4/E3)
myosin, light polypeptide 3, isoform CRA_a	148677054	27359.4	5.0	5	100.00	54.09	0.38	1.11
troponin T	2340048	34082.0	9.4	4	100.00	78.26	0.39	0.50
myozenin 1	10946924	34319.7	8.6	3	100.00	58.73	0.41	0.23
Myosin-binding protein C	81910387	143381.3	6.0	10	100.00	100.37	0.41	0.71
myosin light chain, phosphorylatable, fast skeletal muscle	7949078	21485.1	4.8	11	100.00	99.81	0.42	0.94
myomesin 2	170763465	179757.5	5.6	11	100.00	72.44	0.42	0.63
Calsequestrin 1	127798794	49034.3	3.9	3	100.00	83.23	0.43	0.28
troponin C	6678371	19609.3	4.1	4	100.00	106.88	0.43	0.27
fast skeletal myosin alkali light chain 1 isoform 1f	29789016	23699.5	5.0	14	100.00	97.84	0.43	0.82
troponin I, skeletal, fast 2	123242973	25972.9	9.1	3	100.00	65.23	0.46	0.60
LIM domain binding 3 isoform f	84872217	33857.8	9.2	2	100.00	93.78	0.47	0.55
muscle creatine kinase	6671762	48101.2	6.6	14	100.00	101.99	0.47	0.56
myomesin 1 isoform 2	145279198	194032.5	6.0	7	100.00	81.84	0.48	0.54
actinin alpha 3	7304855	110400.7	5.3	34	100.00	112.37	0.49	0.69
nebulin	123857937	157734.8	8.8	2	100.00	45.87	0.51	0.63
titin	123232572	3312853.3	6.2	2	100.00	37.84	0.53	0.25
Igh protein	62028521	56919.8	7.5	3	100.00	71.06	0.54	0.34
alpha cardiac myosin heavy chain	191618	253883.5	5.6	18	100.00	91.72	0.55	0.25
Myh7 protein	187956918	252607.1	5.6	20	100.00	91.72	0.56	0.26
myosin, heavy polypeptide 4, skeletal muscle	67189167	254149.5	5.6	86	100.00	127.38	0.56	0.38
LIM domain binding 3 isoform b	84872213	76092.4	8.3	3	100.00	70.38	0.56	0.10
calcium/calmodulin-dependent protein kinase II alpha isoform 1	6753250	24580.7	6.5	1	99.85	50.17	0.56	0.02
myosin, heavy polypeptide 8, skeletal muscle, perinatal	71143152	253848.8	5.7	46	100.00	106.43	0.56	0.41
myosin heavy chain IIa	205830428	254268.0	5.6	58	100.00	123.29	0.56	0.38
Myosin, heavy polypeptide 8, skeletal muscle, perinatal	187956525	253835.8	5.7	47	100.00	106.43	0.57	0.40
alpha-tropomyosin	157787199	38470.8	4.7	14	100.00	105.62	0.58	0.35
myosin, heavy polypeptide 1, skeletal muscle, adult	82524274	254200.7	5.6	71	100.00	127.38	0.58	0.38
Ig H-C allotype gamma2b	223428	40724.8	7.2	2	100.00	90.21	0.59	0.26
sarcalumenin, isoform CRA_a	148664814	59761.7	6.2	4	100.00	60.15	0.60	0.36
mCG18455	148678485	256334.6	5.5	22	100.00	84.80	0.60	0.39
tropomyosin 1, alpha, isoform CRA_b	148694194	37823.3	4.7	12	100.00	105.62	0.60	0.39
PREDICTED: similar to tropomyosin 2 (beta) isoform 2	73971296	38348.4	4.6	17	100.00	86.54	0.61	0.30
adenylate kinase 1	10946936	26311.9	5.7	5	100.00	77.64	0.63	0.25
tropomyosin 1, alpha isoform i	78000203	32304.2	4.7	11	100.00	105.62	0.63	0.44
muscle glycogen phosphorylase	6755256	104509.5	6.7	18	100.00	93.56	0.63	0.32
myoglobin	21359820	20131.1	7.1	10	100.00	143.49	0.64	0.43
RIKEN cDNA 8030451F13, isoform CRA_c	148689541	142202.0	5.7	4	100.00	52.26	0.64	0.50
enolase 3, beta muscle, isoform CRA_a	148680653	54402.9	6.8	15	100.00	112.63	0.64	0.60
actin, alpha 1, skeletal muscle	4501881	45181.8	5.2	12	100.00	91.76	0.65	0.46
mCG2006, isoform CRA_a	148680420	187536.8	6.3	2	100.00	60.73	0.65	0.06
Actinin alpha 2	58476244	111806.5	5.3	20	100.00	112.37	0.65	0.39
ATPase, Ca++ transporting, ubiquitous isoform a	254039658	116671.4	5.5	2	100.00	48.16	0.66	0.09
alpha actin 1 proprotein	4885049	45033.8	5.2	12	100.00	91.76	0.66	0.45
alpha 2 actin	4501883	45185.8	5.2	12	100.00	91.76	0.66	0.48
methylthioadenosine phosphorylase, isoform CRA_b	148699009	36228.5	6.5	2	100.00	43.65	0.67	0.19
actinin alpha 2	157951643	112009.7	5.3	23	100.00	112.37	0.67	0.34
myosin	1945080	253502.8	5.4	17	100.00	83.10	0.67	0.39

Table 4.4 - iTRAQ identification of proteins with >20% decreased expression and peptide count >1 in lesioned sciatic nerve from ApoE4 mice compared to ApoE3 mice (Continued)

Protein Name	Accession Number	Protein MW	Protein PI	Peptide Count	Total Ion Score C.I. %	Best Ion Score	Avg ratio (E4/E3)	StdDev (E4/E3)
heat shock protein, alpha-crystallin-related, B6	59958370	18132.5	5.6	3	100.00	54.71	0.67	0.17
sarcomeric mitochondrial creatine kinase precursor	38259206	51557.9	8.6	2	100.00	46.62	0.69	0.37
adenylosuccinate synthase like 1	6671519	54920.1	8.6	2	100.00	81.76	0.69	0.07
growth factor receptor bound protein 2	6680083	27765.1	5.7	2	100.00	45.66	0.69	0.41
ATPase, Ca++ transporting, cardiac muscle, fast twitch 1	148685412	116243.4	5.3	12	100.00	114.25	0.70	0.14
PDZ and LIM domain protein 3	7948997	36807.6	8.1	3	100.00	68.49	0.70	0.13
mCG147612, isoform CRA_b	148686595	58853.2	5.8	4	100.00	49.09	0.70	0.24
h1-calponin alpha	1069994	36759.9	8.8	4	100.00	68.12	0.72	0.23
Myosin, light polypeptide kinase	55930915	237267.2	6.0	2	100.00	46.40	0.72	0.24
parvalbumin	31980767	14372.8	5.0	5	100.00	88.79	0.72	0.41
UDP-glucose ceramide glucosyltransferase-like 1	45946485	190971.6	5.4	2	100.00	43.57	0.72	0.02
PREDICTED: similar to tropomyosin 3 isoform 1	149751320	32645.1	4.8	10	100.00	80.10	0.74	0.37
carboxylesterase	192854	65222.7	5.0	8	100.00	84.01	0.74	0.09
phosphoglycerate mutase 2	9256624	31972.9	8.7	8	100.00	89.17	0.74	0.54
skeletal muscle LIM protein	2880031	38678.1	8.8	2	100.00	78.07	0.75	0.23
RIKEN cDNA 1810020D17, isoform CRA_c	148684357	17880.5	7.8	2	100.00	44.25	0.75	0.09
Aldolase A, fructose-bisphosphate	42490830	43401.8	8.5	11	100.00	91.23	0.75	0.17
albumin precursor	163310765	77836.5	5.8	36	100.00	121.79	0.77	0.26
SH3P9	1438563	53597.8	5.1	4	100.00	62.83	0.77	0.12
creatine kinase, mitochondrial 1, ubiquitous, isoform CRA_c	148696104	50564.3	8.5	2	100.00	59.05	0.77	0.04
milk fat globule-EGF factor 8 protein isoform 2	113865977	50796.5	6.7	5	100.00	83.22	0.77	0.20
ATPase, Ca++ transporting, slow twitch 2 isoform a	158635979	124907.5	5.2	5	100.00	68.51	0.78	0.32
proteasome alpha 6 subunit	6755198	30608.7	6.3	2	100.00	75.58	0.78	0.18
liver glycogen phosphorylase	18875342	107417.7	6.6	5	100.00	58.28	0.78	0.28
solute carrier family 4 (anion exchanger), member 1	6755560	108215.2	5.4	2	100.00	50.97	0.78	0.06
coagulation factor II	123227411	76215.8	6.0	4	100.00	61.55	0.79	0.08
TRIO and F-actin binding protein isoform 3	88501749	234306.2	8.4	2	100.00	36.79	0.79	0.04
Ig gamma-3 chain C region	121044	47963.7	6.7	3	100.00	46.58	0.79	0.01
filamin, alpha	125347376	305825.3	5.7	29	100.00	89.05	0.79	0.20
glyceraldehyde-3-phosphate-dehydrogenase isoform 1	149272161	40122.8	7.1	3	100.00	86.97	0.79	0.05
Phosphoglucomutase 2	55824767	66748.2	6.0	10	100.00	75.31	0.80	0.23
C-1-tetrahydrofolate synthase, cytoplasmic	34921990	110015.8	6.9	2	100.00	40.34	0.80	0.31
alpha actinin 1a	82659196	111086.8	5.3	32	100.00	112.37	0.80	0.33
Acyl-CoA thioesterase 2	39992610	52675.7	7.2	2	100.00	53.32	0.80	0.22

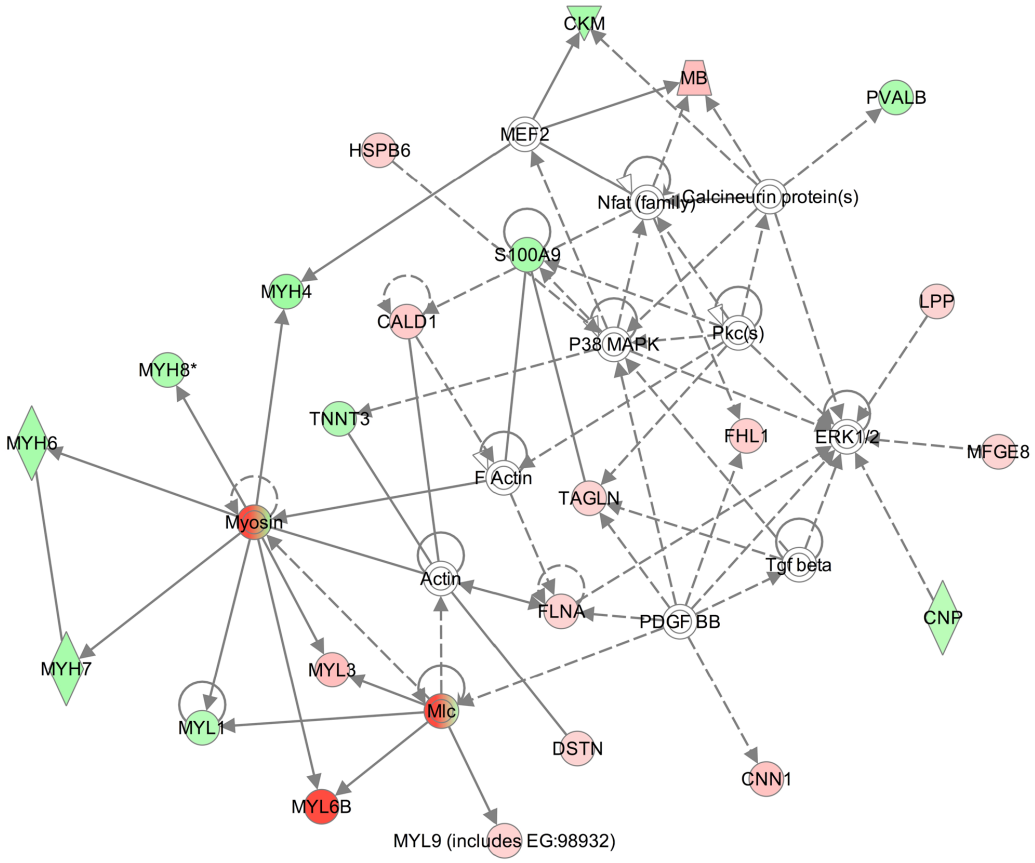

Figure 4.16 - Modification of myosin and actin protein interaction pathways in uninjured apoE4 peripheral nerves. Protein interaction network (generated by Ingenuity Pathway Analysis) showing interactions of myosin and actin proteins involved in regulation of tissue and cell morphology. 71% of proteins had modified expression levels in apoE4 uninjured peripheral nerves compared to apoE3 tissue (green = up in apoE4 vs apoE3; red = down in apoE4 vs apoE3;

grey = unchanged). Solid connecting lines indicate the presence of a direct interaction and dashed connecting lines indicate an indirect interaction.

Key to proteins - Actin; **calcineurin proteins**; **CALD1** – h-caldesmon; **CKM** – muscle creatine kinase; **CNN1** – h1-calponin alpha; **CNP** - 2',3'-cyclic nucleotide 3' phosphodiesterase isoform 2; **DSTN** – destrin isoform CRA_b; **ERK1/2** – extracellular signal-regulated kinase; **F Actin** – filamentous actin; **FHL1** - skeletal muscle LIM protein; **FLNA** - filamin alpha; **HSPB6** - heat shock protein, alpha-crystallin-related, B6; **LPP** - LIM domain containing preferred translocation partner in lipoma isoform 1; **MB** – myoglobin; **MEF2** – myocyte enhancer factor 2; **MFGE8** - milk fat globule-EGF factor 8 protein isoform 2; **MLC** - mKIAA0777 protein; **MYH4** - myosin, heavy polypeptide 4, skeletal muscle; **MYH6** - alpha cardiac myosin heavy chain; **MYH7** - Myh7 protein; **MYH8** - myosin, heavy polypeptide 8, skeletal muscle, perinatal; **MYL1** - fast skeletal myosin alkali light chain 1 isoform 1f; **MYL3** - myosin, light polypeptide 3, isoform CRA_a; **MYL6B** - myosin, light polypeptide 6B; **MYL9** (includes EG:98932) - myosin regulatory light polypeptide 9; **Myosin** - Myosin-binding protein C, fast-type; **Nfat family** – nuclear factor of activated T-cells; **P38 MAPK** - P38 mitogen-activated kinase; **PDGF BB** – platelet-derived growth factor beta polypeptide; **Pkc(s)** – protein kinase C; **PVABL** – parvalbumin; **S100A9** - S100 calcium binding protein A9 (calgranulin B); **TAGLN** – transgelin; **Tgf beta** – transforming growth factor beta; **TNNT3** - troponin T.

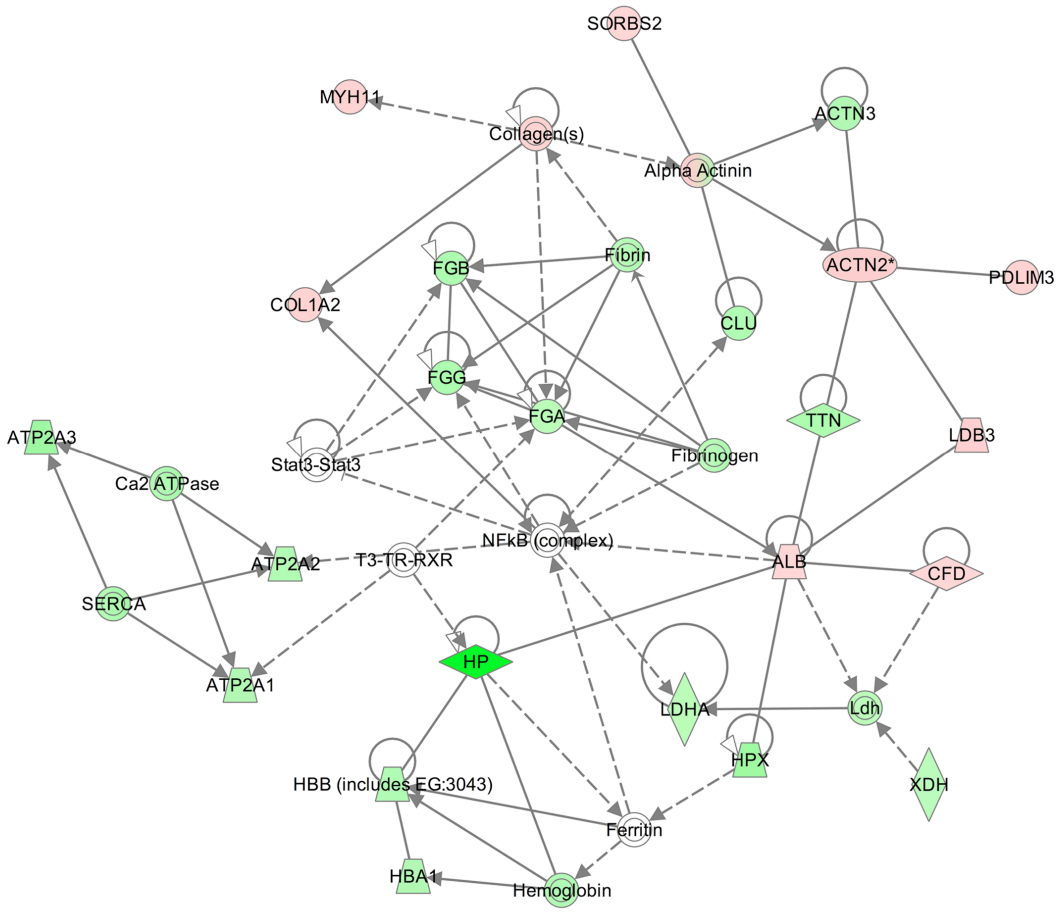

Figure 4.17 - Modification of protein interaction pathways involved with haematological regulation in uninjured apoE4 peripheral nerves Protein interaction network (generated by Ingenuity Pathway Analysis) showing interactions of proteins involved in haematological regulation (including integrity of the blood-brain/blood-nerve barrier). 91% of proteins had modified expression levels in apoE4 uninjured peripheral nerves compared to apoE3

tissue (green = up in apoE4 vs apoE3; red = down in apoE4 vs apoE3; grey = unchanged). Solid connecting lines indicate the presence of a direct interaction and dashed connecting lines indicate an indirect interaction.

Key to proteins - ACTN2* - actinin alpha 2; **ACTN3** - actinin alpha 3; **ALB** - albumin precursor; **Alpha Actinin** - Actinin alpha 2; **ATP2A1** - ATPase, Ca++ transporting, cardiac muscle, fast twitch 1, isoform CRA_c; **ATP2A2** - ATPase, Ca++ transporting, slow twitch 2 isoform a; **ATP2A3** (aka SERCA); **Ca2 ATPase** – ATPase, Ca++ transporting, ubiquitous; **CFD** - adipsin precursor; **CLU** - clusterin precursor; **COL1A2** - procollagen, type I, alpha 2 precursor; **Collagen(s)** - Collagen alpha-1(XIV) chain; **Ferritin**; **FGA** - fibrinogen, alpha polypeptide, isoform CRA_b; **FGB** - fibrinogen beta chain precursor; **FGG** - fibrinogen, gamma polypeptide; **Fibrin; Fibrinogen; HBA1** - haemoglobin alpha, adult chain 2; **HBB (includes EG:3043)** - haemoglobin, beta adult major chain; **Haemoglobin; HP** - haptoglobin precursor; **HPX** - hemopexin precursor; **LDB3** - LIM domain binding 3 isoform b; **Ldh -** lactate dehydrogenase**; LDHA** - lactate dehydrogenase A isoform 1; **MYH11 -** myosin, heavy chain 11, smooth muscle**; NFkB (complex)** - nuclear factor of kappa light polypeptide gene enhancer in B-cells; **PDLIM3** - PDZ and LIM domain protein 3; **SERCA** – (aka ATP2A3); **SORBS2** - mKIAA0777 protein; **Stat3-Stat3** - signal transducer and activator of transcription 3; **T3-TR-RXR** – thyroid hormone receptor/retinoid X receptor heterodimer; **TTN** – titin; **XDH** - xanthine dehydrogenase.

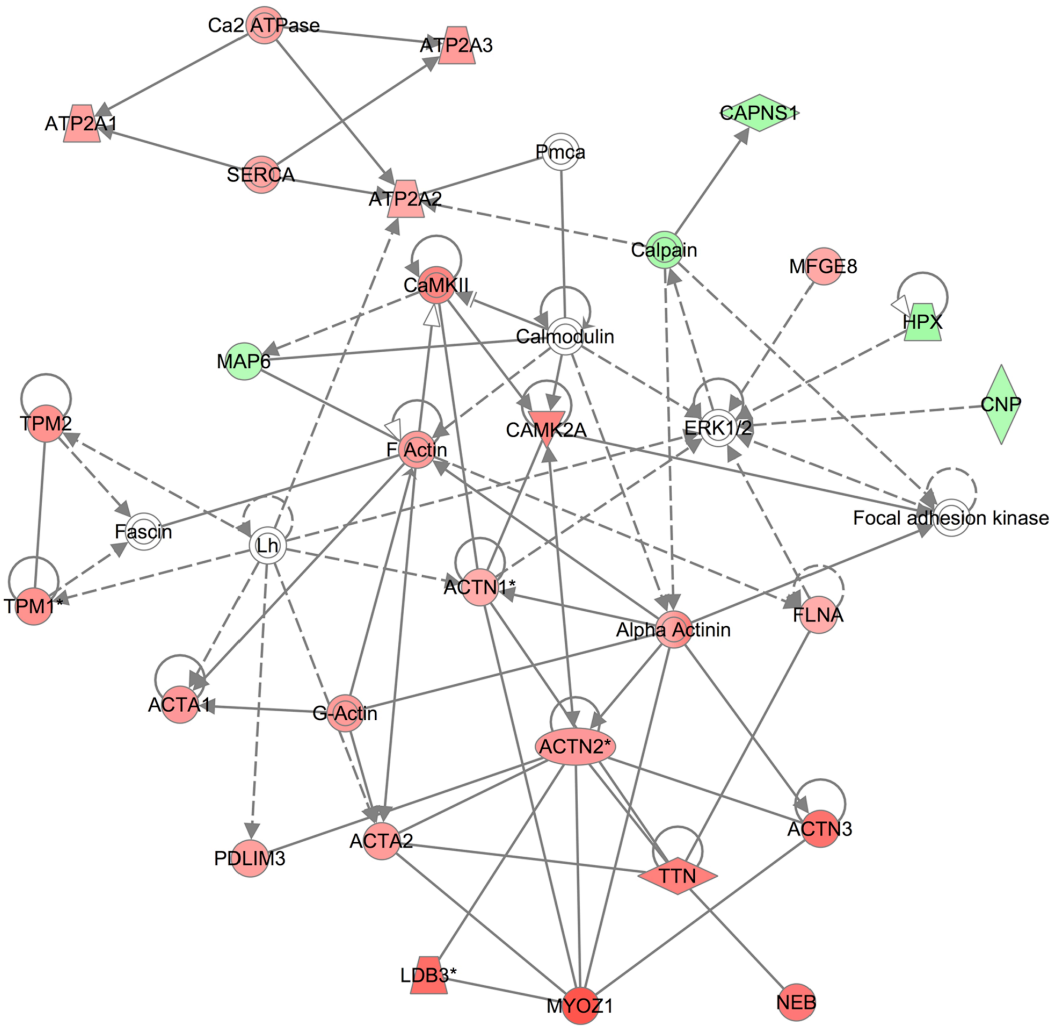

Figure 4.18 - Modification of actin protein interaction pathways in regenerating apoE4 nerves 3 weeks after nerve crush injury. Protein interaction network (generated by Ingenuity Pathway Analysis) showing interactions of proteins involved in actin-based regulation of tissue and cell morphology. 83% of proteins had modified expression levels in regenerating

apoE4 peripheral nerves compared to apoE3 tissue. (green = up in apoE4 vs apoE3; red = down in apoE4 vs apoE3; grey = unchanged). Solid connecting lines indicate the presence of a direct interaction and dashed connecting lines indicate an indirect interaction.

Key to proteins - ACTA1 - actin, alpha 1, skeletal muscle**; ACTA2 -** alpha 2 actin**; ACTN1* -** actinin, alpha 1; **ACTN2* -** actinin alpha 2; **ACTN3 -** actinin alpha 3; **Alpha Actinin -** Actinin alpha 2; **ATP2A1 -** ATPase, Ca++ transporting, cardiac muscle, fast twitch 1, isoform CRA_c; **ATP2A2 -** ATPase, Ca++ transporting, slow twitch 2 isoform a; **ATP2A3 -** ATPase, Ca++ transporting, ubiquitous**; Ca2 ATPase; Calmodulin**; **Calpain; CaMKII; CAMK2A -** calcium/calmodulin-dependent protein kinase II alpha isoform 1; **CAPNS1 -** calpain small subunit**; CNP -** 2',3'-cyclic nucleotide 3' phosphodiesterase isoform 2; **ERK1/2 -** extracellular signal-regulated kinase**; F Actin; Fascin**; **FLNA -** filamin, alpha; **Focal adhesion kinase; G-Actin; HPX-** hemopexin precursor; **LDB3* -** LIM domain binding 3 isoform b; **MAP6 -** microtubule-associated protein 6 isoform 1; **MFGE8 -** milk fat globule-EGF factor 8 protein isoform 2; **MYOZ1 -** myozenin 1; **NEB –** nebulin; **PDLIM3 -** PDZ and LIM domain protein 3; **Pmca** - plasma membrane Ca^{2+} ATPase; **SERCA; TPM1* -** tropomyosin 1, alpha isoform I**; TPM2 -** tropomyosin 1, alpha, isoform CRA_b; **TTN –** titin.

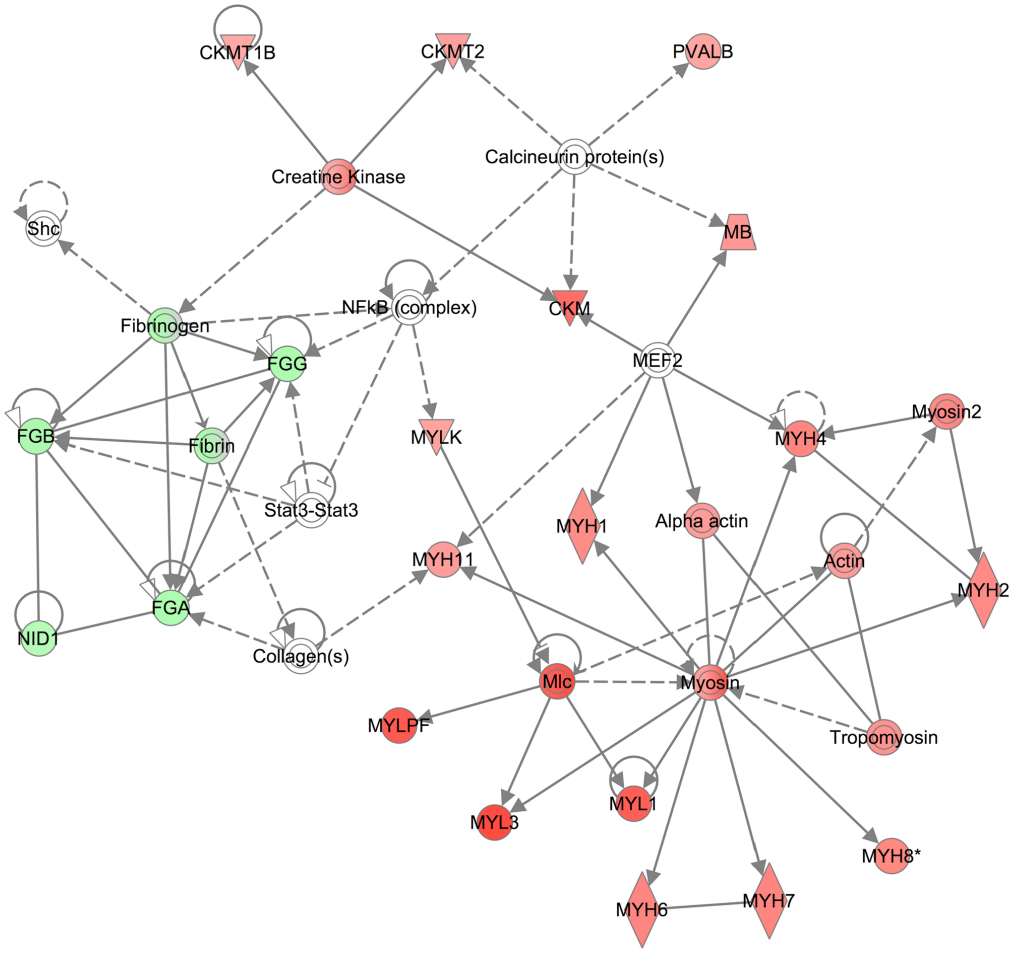

Figure 4.19 - Modification of actin and myosin protein interaction pathways in regenerating apoE4 nerves 3 weeks after nerve crush injury. Protein interaction network (generated by Ingenuity Pathway Analysis) showing interactions of proteins involved in actin/myosin-based regulation of tissue and cell morphology. 86% of proteins had modified expression levels in regenerating apoE4 peripheral nerves compared to apoE3 tissue (green = up in apoE4 vs

apoE3; red = down in apoE4 vs apoE3; grey = unchanged). Solid connecting lines indicate the presence of a direct interaction and dashed connecting lines indicate an indirect interaction.

Key to proteins in fig 4.19 - Actin; Alpha actin - actin, alpha 1, skeletal muscle; **calcineurin proteins; CKM -** muscle creatine kinase; **CKMT1B -** creatine kinase, mitochondrial 1, ubiquitous, isoform CRA_c; **CKMT2; Collagen(s); Creatine Kinase; FGA** - fibrinogen, alpha polypeptide, isoform CRA_b; **FGB** - fibrinogen beta chain precursor; **FGG** - fibrinogen, gamma polypeptide; **Fibrin; Fibrinogen; MB –** myoglobin; **MEF2 -** myocyte enhancer factor 2; **MYH1 -** myosin, heavy polypeptide 1, skeletal muscle, adult; **MYH2 -** myosin heavy chain IIa**; MYH4 -** myosin, heavy polypeptide 4, skeletal muscle**; MYH6 -** myosin, heavy polypeptide 6, skeletal muscle**; MYH7 -** Myh7 protein; **MYH8* -** myosin, heavy polypeptide 8, skeletal muscle, perinatal; **MYH11 -** myosin, heavy polypeptide 11, skeletal muscle**; MYL1 -** myosin, light polypeptide 1**; MYL3 -** myosin, light polypeptide 3, isoform CRA_a; **MYLK -** Myosin, light polypeptide kinase; **MYLPF -** myosin light chain, phosphorylatable, fast skeletal muscle; **Myosin**; **Myosin2; NFkB (complex)** - nuclear factor of kappa light polypeptide gene enhancer in B-cells**; NID1 –** nidogen 1 precursor; **PVALB –** parvalbumin; **Shc -** Src homology 2 domain containing) transforming protein 1**; Stat3-Stat3** - signal transducer and activator of transcription 3**; Tropomyosin -** tropomyosin 1, alpha isoform I.

4.4 Discussion

In this chapter I have shown an apoE genotype-dependent regulation of nerve regeneration in the PNS *in vivo*. I have shown that the presence of the apoE4 isoform selectively delays peripheral nerve regeneration and neuromuscular reinnervation, in the absence of any effect on normal form or function. Comparative iTRAQ proteomics revealed significant changes in the proteome of apoE4 peripheral nerve compared to that in apoE3 mice, both before and after nerve crush. Proteins associated with the regulation of cellular outgrowth and regeneration (myosin / actin pathways) and haematological regulation have modified expression levels in apoE4 peripheral nerves compared to apoE3.

The most notable finding in this study is the impaired axonal regeneration and neuromuscular reinnervation following peripheral nerve injury in apoE4 mice. This finding is in agreement with previous *in vitro* studies on cultured dorsal root ganglia and hippocampal neurons. In these studies the neuronal cell lines were incubated with a lipid source and either apoE3 or apoE4. The cells incubated with apoE3 showed increased levels of neurite outgrowth, whereas cells incubated with apoE4 had reduced levels of neurite outgrowth (Bellosta et al., 1995; Nathan et al., 1994; Teter et al., 2002). Bellosta and colleagues also showed that this effect was dose dependent: increasing E3 levels lead to increased sprouting, whereas increasing E4 decreased levels of sprouting (Bellosta et al., 1995).

The finding that a complete loss of apoE did not affect regeneration in the PNS is also in agreement with previous studies which showed no influence of loss of apoE on peripheral nerve regeneration (Genden et al., 2002; Popko et al., 1993). This has also been shown in the CNS; following a lesion in the entorhinal cortex both wild-type and apoE-/- mice showed similar levels of synaptic remodelling (Anderson et al., 1998). As apoE is one of several lipoproteins in the nervous system it has been hypothesised that other apolipoproteins could functionally compensate for a loss of apoE in the apoE-/- mice, leading to a null result in these regeneration studies (Anderson et al., 1998). In contrast, my results showed that complete loss of apoE did subtly affect the process of Wallerian degeneration following nerve injury, transiently reducing the rate compared to mice expressing apoE. This effect was subtle and did not persist beyond 18 hours, but suggests that apoE, which is up-regulated quickly following nerve injury (Ignatius et al., 1986; Skene and Shooter, 1983), can influence early stages of Wallerian degeneration, although its absence is not sufficient to delay the process by more than a few hours.

One slightly puzzling result from this study was the time course of neuromuscular reinnervation in the apoE3 mice following tibial nerve crush. ApoE3 significantly enhanced the initial stages of reinnervation, in agreement with the previous studies showing that it significantly enhances neurite outgrowth *in vitro* (Bellosta et al., 1995; Nathan et al., 1994; Teter et al., 2002). However, while both the apoE-/- and apoE4 mice had an increase in the percentage of reinnervated endplates between 2 and 3 weeks post nerve crush,

reinnervation of NMJs in the apoE3 mice failed to progress despite an increase in regenerating axons (see Fig. 4.12). One possible explanation for this NMJ specific phenotype is that apoE3 alters the process of synaptic pruning that follows reinnervation at the NMJ. This would mean that endplates in apoE3 mice could be left in a poly-innervated state for longer than those in apoE-/- or apoE4 mice, which would mean that they would not be counted as being fully reinnervated, and thus lead to a lower percentage of reinnervated endplates in the apoE3 mice. This hypothesis is supported by a previous study by White and colleagues showing that apoE genotype can modulate synaptic plasticity *in vivo* (White et al., 2001), and is worthy of future study.

The reduced regenerative capacity of peripheral nerves in the apoE4 mice provides a possible explanation for several human cohort studies that have reported associations between the apoE4 genotype and poor prognosis in a number of PNS diseases. Both diabetic and HIV-associated neuropathies have been reported to have a higher frequency in individuals possessing the apoE4 allele (Bedlack et al., 2003; Corder et al., 1998; Tsuzuki et al., 1998). A number of human cohort studies have examined a potential relationship between apoE genotype and motor neuron disease, with conflicting results (Al-Chalabi et al, 1996; Bachus et al, 1997; Drory et al, 2001; Li et al, 2004b; Moulard et al, 1996; Mui et al, 1995; Siddique et al, 1998; Smith et al, 1996). Motor neuron regeneration is known to play an important role in motor neuron diseases such as ALS: as some motor neurons degenerate other, compensatory motor neurons sprout new branches in an attempt to reinnervate vacated endplates and thus

prolong muscle function (Schaefer et al., 2005). The finding that apoE4 impairs axonal regeneration and reinnervation therefore suggests that apoE genotype could impact on disease progression, as neurons in apoE4 patients would have reduced capacity for axonal sprouting and reinnervation. This could provide an explanation for those studies reporting an association between apoE-genotype and disease progression (Al-Chalabi et al, 1996; Drory et al, 2001; Li et al, 2004; Moulard et al, 1996). Clinically, the knowledge of an individual's apoE genotype could therefore provide insights into the likely success of regeneration following peripheral nerve trauma or disease, and lead to a more accurate, patient-specific, prognosis.

The proteomic experiments revealed widespread changes in the proteome of the peripheral nerves of apoE4 mice, both before and after nerve injury. In uninjured nerves apoE4 mice had altered expression levels of a range of myosin isoforms, and of proteins associated with regulation of the blood-nerve barrier. As these changes were found in normal, healthy, uninjured nerves it is possible to conclude that they were occurring as a direct result of the apoE genotype, rather than as a result of altered nerve regeneration. The three weeks post injury time point was chosen in order to analyse the protein expression levels of apoE3 and apoE4 nerves during the course of regeneration. At this time point changed expression levels of both myosin and actin proteins were found in the apoE4 nerves compared to the apoE3 nerves.

Actin is a major component of the cytoskeleton, and has been shown to be up-regulated following nerve injury. Its role as a modulator of cell morphology and outgrowth of neurons is well established (Arnold, 2009; Letourneau, 2009; McQuarrie and Lund, 2009; Tetzlaff et al., 1988). However, more recent work has shown that myosin is also involved in the regeneration process in nerves, and that interactions between myosin and actin proteins in neurons are necessary for successful nerve regeneration. Although myosin is more commonly thought of in connection with its role in muscle contraction many myosin isoforms have been found to be present in both the axonal and synaptic compartments of neurons (Bearer et al., 1993; Brown and Bridgeman, 2004; Vega-Riveroll et a., 2005). Myosin has been shown to drive neurite outgrowth *in vitro* (Wylie et al., 1998) and to have a role in regulating axonal path finding during development (Ma et al., 2006; Zhu et al., 2007). Similar to apoE, myosin Va is up-regulated in a time dependant manner at the site of injury (Calliari et al., 2002), and is essential for the transport of neurofilaments in neurons (Alami et al., 2009; Rao et al., 2002; Schaefer et al 2008). Given the importance of actin / myosin pathways in nerve regeneration the widespread changes in expression levels of these proteins in apoE4 peripheral nerves may contribute to the reduced regenerative capacity seen in the apoE4 mice. Further work is now needed to investigate the roles that specific myosin and actin proteins are playing in the apoE genotype-dependent regeneration of peripheral nerves.

In addition to the changes in the myosin / actin pathways, the proteomics experiments also revealed expression level changes in proteins associated with

haematological regulation in the apoE4 peripheral nerves, several of which are important in maintaining the integrity of the blood-brain barrier (BBB) and blood-nerve barrier (BNB). Previous studies using apoE-/- mice have shown that loss of apoE impairs both the BBB and the BNB (Fullerton et al., 2001; Methia et al., 2001). These studies both used Evan's blue dye to measure the levels of extravasation, and showed that in the absence of apoE the BBB and BNB become more leaky. More recently Nishitsuji and colleagues have investigated the effects of the apoE3 and apoE4 isoforms on the properties of the BBB *in vitro* (Nishitsuji et al. 2011). They showed that the function of the tight junctions between endothelial cells is impaired in cultures from apoE4 mice compared to wild-type or apoE3, leading to a greater permeability of the BBB in apoE4 (Nishitsuji et al. 2011). In my proteomics experiments Orosomucoid I, a protein which has been shown to modulate the permeability of the BBB (Yuan et al., 2010), was found to be up-regulated in both uninjured and regenerating apoE4 nerves. Another protein found to be up-regulated in apoE4 nerves was fibrinogen, which is known to leak into the CNS immediately following BBB disruption, a play a role in mediating neuronal damage (Schachtrup et al., 2010). Changes in expression levels of these proteins in the apoE4 mice provide potential molecular mechanisms through which the apoE4 genotype may be modulating the haematological regulation of the nervous system. Although it is not possible to link this directly to the reduced capacity for regeneration in the apoE4 mice, Previtali and colleagues have previously reported that nerve regeneration is impaired in the presence of breaches of the BNB in human sural nerves (Previtali et al., 2008). Further work is now needed to discover if any of

the proteins found altered in the PNS also have modified expression levels in the CNS, and if they are affecting the integrity of the BBB in an apoE-genotype specific manner.

In summary I have shown that apoE genotype significantly modifies the regenerative capacity of the PNS *in vivo,* with the apoE4 genotype giving rise to attenuated regeneration and reinnervation following nerve injury. Comparative proteomics experiments revealed concomitant changes in the proteome of peripheral nerve in apoE4 mice, which are likely to affect the form and function of the PNS, and are worthy of future study.

Chapter 5 - ERCC1

5.1 Introduction

DNA contains the blueprint for the normal functioning of every organism. However, the fundamental problem with DNA is that it is not chemically inert, and damage to DNA can alter its coding properties or transcription (Martin, 2008). DNA damage has been linked to carcinogenesis, aging and a number of genetic disorders (de Boer and Hoeijmakers, 2000; Schumacher et al., 2008).

Alterations to the structure of DNA can occur spontaneously due to intrinsic instability of the chemical bonds within DNA, or be caused by endogenous metabolic products (de Boer and Hoeijmakers, 2000; Lindahl, 1993). Exogenous environmental factors, such as ultraviolet radiation or chemical compounds in cigarette smoke, can also cause DNA damage (Cleaver, 1968; Pfeifer et al., 2002). DNA damage occurs in many forms, such as single- and double-strand breaks, inter- and intrastrand crosslinks and base modifications (de Boer and Hoeijmakers, 2000).

Several DNA repair strategies have evolved to fix damage to DNA and prevent it from having detrimental consequences for the organism. Different repair pathways act on different forms of damage, although there is a lot of overlap and many proteins are involved in more than one pathway (Lindahl et al., 1997). The main DNA repair mechanisms are base excision repair (BER), nucleotide

excision repair (NER), mismatch repair (MMR), and recombinational repair (for review see Jeppesen et al., 2011). BER removes single incorrect or damaged bases from DNA by breaking the base-sugar bond holding them in place, and replacing them (for review see David et al., 2007). NER removes bulky DNA distorting lesions, most commonly caused by UV radiation (for review see Niedernhofer, 2008). MMR is responsible for maintaining the accuracy of DNA replication by targeting incorrect bases which arise from replication errors (for review see Hsieh and Yamane, 2008). Recombinational repair mends single and double strand cross breaks by homologous recombination (for review see Kuzminov, 1999).

Deficiencies in any of the DNA repair pathways lead to genomic instability and can have severe consequences (Jeppesen et al., 2011). Several hereditary DNA repair deficiency disorders are associated with an increased risk of cancer. The link between compromised DNA repair and cancer was first established in 1968 by James Cleaver, who noticed that fibroblasts from patients with xeroderma pigmentosum (XP), a hereditary disease characterised by extreme photosensitivity and skin cancer, had defects in DNA repair following UV exposure (Cleaver, 1968). This study also connected DNA repair and neurodegeneration, as approximately 30% of patients with XP have neurological symptoms including microcephaly, ataxia, loss of reflexes and neurodegeneration with peripheral neuropathy (Kraemer et al., 2007; Rass et al., 2007).

As post-mitotic, terminally differentiated cells, neurons are thought to be particularly vulnerable to accumulating DNA lesions throughout life (de Waard et al., 2010). The number of DNA repair deficiency disorders that are characterised by neurodegeneration and neuropathological changes highlights this vulnerability (Barzilai et al., 2008). Neurons are also highly metabolically active, generating large quantities of reactive oxygen species (ROS) with the capacity to damage DNA (Halliwell, 2006; McKinnon, 2009).

It is thought that different regions of the brain are differentially affected by DNA repair defects (Barzilai et al., 2008). The cerebellum is particularly susceptible: diseases such as ataxia telangiectasia and spinocerebellar ataxia with axonal neuropathy 1 are caused by mutations that affect the repair of single- and double-strand breaks, and profoundly affect the cerebellum (McKinnon, 2009). However, the effect of DNA damage in the PNS and the role or DNA damage repair in maintaining motor neurons is not fully understood (de Waard et al., 2010).

Here I have investigated the effect of failure to repair DNA damage at the NMJ (which is known to be an early pathological target in many diseases; Wishart et al., 2006), using a strain of mouse with a mutation in the ERCC1 gene. ERCC1 is primarily involved in the nucleotide excision repair pathway (NER), but also plays a role in repairing some double strand breaks and interstrand crosslinks (Ahmad et al., 2008; Bergstralh and Sekelsky, 2008; Gregg et al., 2011). ERCC1 functions as part of a heterodimer with xeroderma pigmentosum group F (XPF),

severing damaged DNA 5′ to lesions identified in the NER pathway (Niedernhofer, 2008; Wood,
2010). Mutations in either ERCC1 or XPF give rise to a variety of conditions characterised by tissue degeneration and accelerated aging (Gregg et al., 2011), including XP (Niedernhofer, 2008; Nouspikel, 2008).

The Ercc1$^{\Delta/-}$ mice used in this chapter lack one ERCC1 allele, and produce a truncated form of the protein with reduced activity from the other allele. The Ercc1^{-} and Ercc1$^{\Delta}$ alleles were first generated in 1997 by Weeda and colleagues (Weeda et al., 1997). Ercc1$^{\Delta/-}$ mice have a prolonged life span and less severe degenerative phenotype than Ercc1$^{-/-}$ mice, due to the low level of residual ERCC1-XPF activity (Gregg et al., 2011). However, compared to wild-type littermates the Ercc1$^{\Delta/-}$ mice have reduced body weight, a shortened life span of 24-30 weeks and develop progressive motor abnormalities including tremors and ataxia (de Waard et al., 2010; Gregg et al., 2011).

I have used Ercc1$^{\Delta/-}$ mice to investigate the consequences of deficient DNA repair at the NMJ, using immunohistochemistry and confocal microscopy to study NMJ morphology in Ercc1$^{\Delta/-}$ mice at different ages.

5.2 Materials and methods

5.2.1 Mice

Mice were maintained in breeding colonies in animal care facilities in The Erasmus Medical Center, The Netherlands. All genotyping and basic dissection was performed in this location, and tissue was then shipped to Edinburgh for further dissection and analysis. $Ercc1^{\Delta/-}$ mice were obtained by crossing $Ercc1^{-/+}$ with $Ercc1^{\Delta/+}$ mice of C57Bl/6J and FVB backgrounds to yield $Ercc1^{\Delta/-}$ mice with C57Bl6J/FVB hybrid background. Wild-type C57Bl/6J mice maintained in breeding colonies at the University of Edinburgh were used as controls.

5.2.2 NMJ Immunohistochemistry

See general materials and methods, section 2.3.

5.2.3 Microscopy

See general materials and methods, section 2.4.

5.2.4 Quantification of NMJs

See general materials and methods, section 2.5. A minimum of 100 randomly selected endplates were categorized as being fully innervated (i.e. normal: neurofilament staining from a single incoming axon overlying the entire endplate), partially innervated, vacant (no neurofilament overlying the endplate), or poly-innervated (more than one axon converging on an individual endplate).

5.2.5 Statistical analysis

See general materials and methods, section 2.6.

5.3 Results

5.3.1 NMJ pathology in Ercc1$^{\Delta/-}$ mice

Synapses are known to be early pathological targets in many diseases, and thus in diseases affecting lower motor neurons the NMJ is often vulnerable (Murray et al 2010). Motor neurons are thought to be affected by DNA damage in Ercc1$^{\Delta/-}$ mice (de Waard et al., 2010), so I therefore analysed the integrity of NMJs in the lumbrical muscles of these mice. Analysis was carried out at three time points – 4 weeks, 8 weeks and 16 weeks of age. Ercc1$^{\Delta/-}$ mice have previously been shown to develop clasping of hind-limbs when lifted by their tails and tremors between 4 and 8 weeks (de Waard et al., 2010). By 16 weeks mice have developed severe locomotor deficits. Ercc1$^{\Delta/-}$ mice have a life span of 24-30 weeks (de Waard et al., 2010).

Qualitative assessment of muscles from a 16 week-old Ercc1$^{\Delta/-}$ mouse revealed many abnormalities at the NMJ (Fig. 5.1). By this age endplates in wild-type mice are fully occupied by an overlying nerve terminal and innervated by a single incoming axon collateral (mono-innervated). In contrast in the Ercc1$^{\Delta/-}$ mouse I found partial and vacant endplates within the same field of view as normal fully occupied endplates (Fig. 5.1A). Other endplates in the Ercc1$^{\Delta/-}$ mouse were poly-innervated (Fig. 5.1B). This morphology is only seen in wild-type mice under two weeks of age, before developmental synapse elimination prunes all excess inputs back leaving NMJs in their adult mono-innervated state.

Analysis of the motor nerve terminals also revealed neurofilament accumulation, which does not occur at healthy NMJs (Fig. 5.1A). Incoming axons also showed abnormal neurofilament distribution, with some blebbing, and some very thin sections in the pre-terminal axon (Fig. 5.1D). One of the muscles examined had large amounts of abnormal and excessive axon branching across its entirety (Fig. 5.1C).

Quantifying NMJ morphology in lumbrical muscles from Ercc1$^{\Delta/-}$ mice compared to wild-type controls at 4 weeks, 8 weeks and 16 weeks of age confirmed that these mice had high levels of pathology at the NMJ, manifesting in a variety of ways, which increased with age. Across the three time points there was a progressive and significant reduction in the percentage of normal mono-innervated and fully occupied endplates in the Ercc1$^{\Delta/-}$ mice (Fig. 5.2A). This corresponded with a significant increase in the levels of partially occupied endplates at 8 and 16 weeks of age (Fig. 5.2B) and an increase the percentage of vacant endplates across the time points studied (Fig. 5.2C). Levels of poly-innervation were also significantly increased in the Ercc1$^{\Delta/-}$ mice (Fig. 5.3).

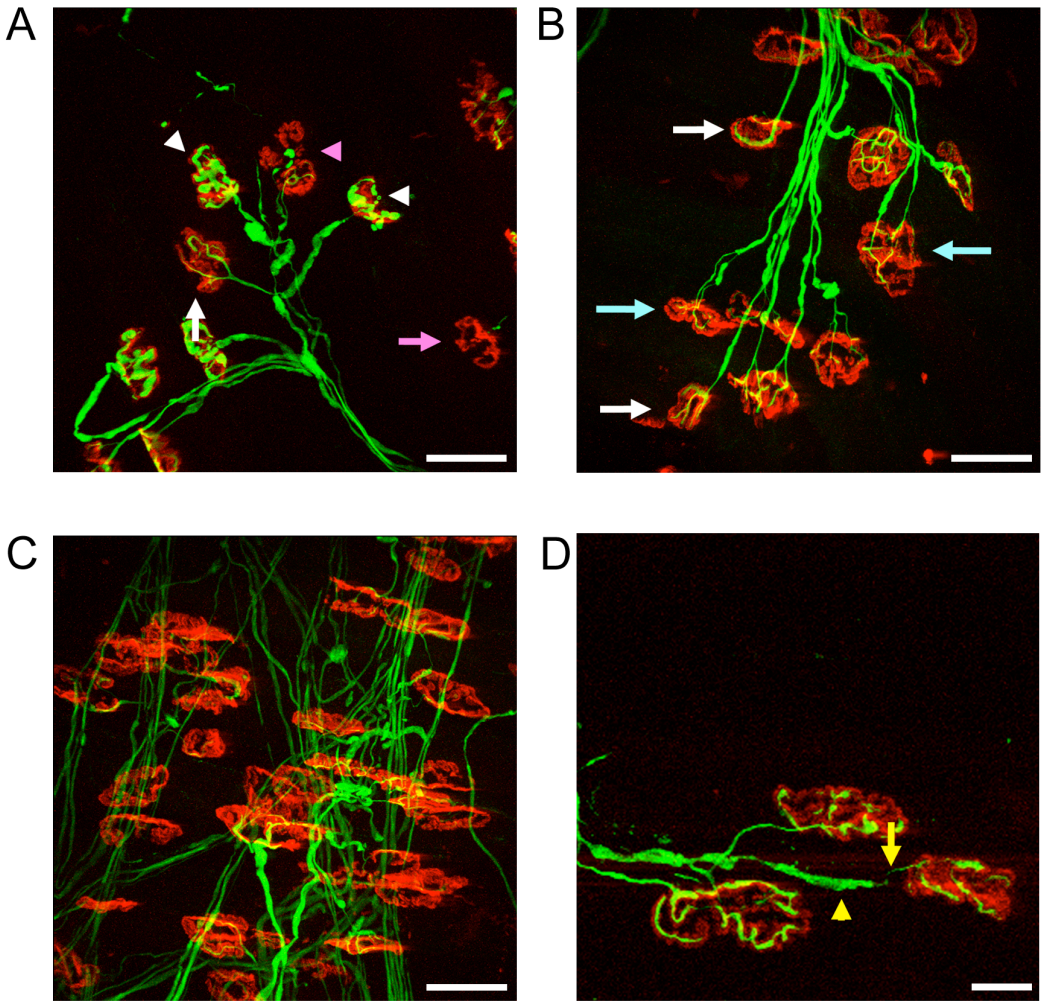

Figure 5.1 – NMJ abnormalities in 16 week-old Ercc1$^{\Delta/-}$ mice. Confocal micrographs of NMJs in the lumbrical muscles of Ercc1$^{\Delta/-}$ mice show a range of abnormalities. **A:** Whilst some endplates were still fully occupied and mono-innervated (i.e. normal; white arrow) others in the same field of view were vacant (pink arrow) or partially occupied with the overlying nerve terminal

appearing to retract (pink arrowhead). Other NMJs had large accumulations of neurofilament in their pre-terminal axons (white arrowhead). **B:** Confocal micrograph showing a range of mono-innervated and poly-innervated (i.e. more than one incoming axon collateral) NMJs. The white arrows indicate normal (i.e. mono-innervated) NMJs whereas the blue arrows show poly-innervated NMJs. **C:** Confocal micrograph showing large amounts of abnormal and excessive axon branching in an Ercc1$^{\Delta/-}$ lumbrical muscle. **D:** Confocal micrograph showing abnormal neurofilament distribution in distal axon branches in a lumbrical muscle from an Ercc1$^{\Delta/-}$ mouse. The incoming axon is very thin (yellow arrow), but also contains regions of neurofilament accumulation (blue arrow). Scale bars = 40μm (A, B and C) and 20μm (D).

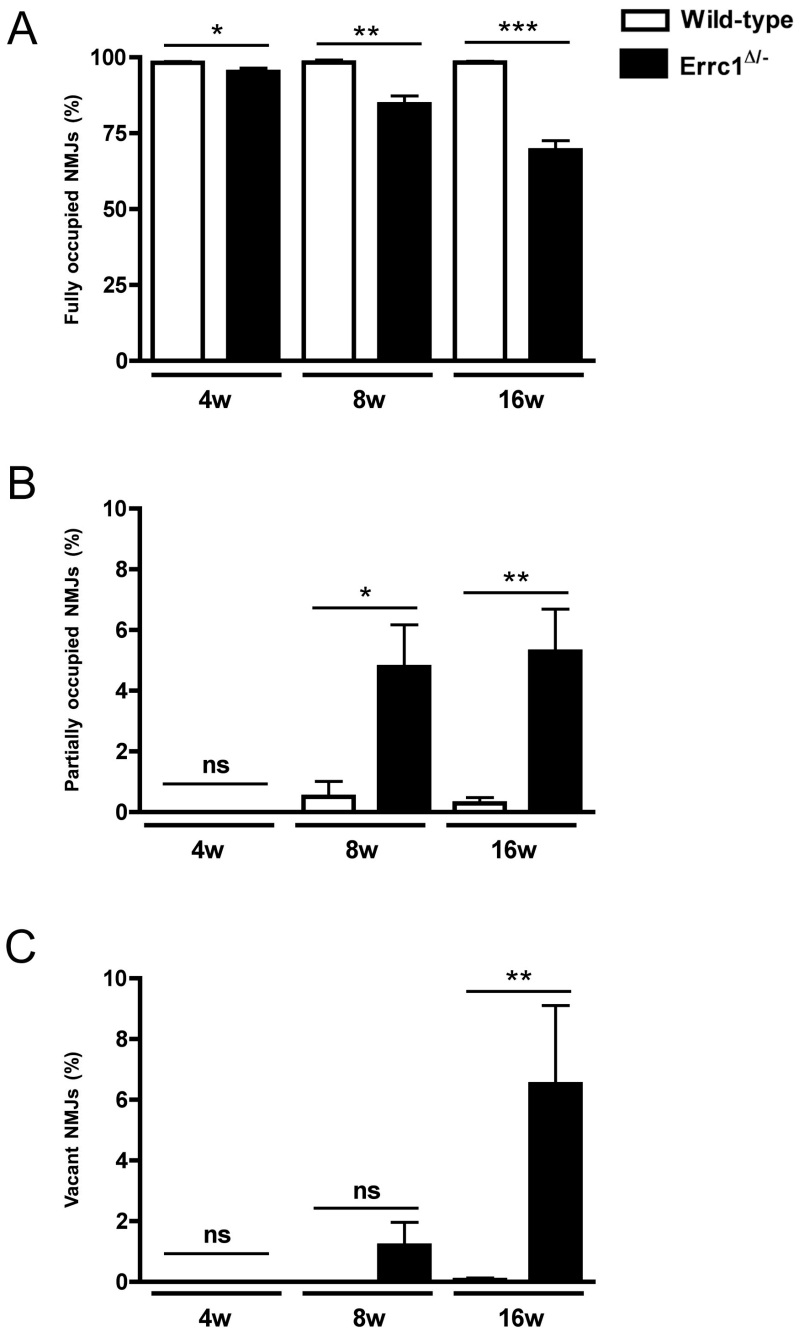

Figure 5.2 - Quantification of NMJ abnormalities in Ercc1$^{\Delta/-}$ mice compared to wild-type controls at 4, 8 and 16 weeks of age. A: Bar chart (mean±SEM)

showing significant reduction in the percentage of fully occupied endplates in lumbrical muscles of Ercc1$^{\Delta/-}$ mice at 4, 8 and 16-weeks of age (4 weeks $P<0.05$, 8 weeks $P<0.01$, 16 weeks $P<0.001$; Kruskal-Wallis test with Dunn's post-hoc test). **B:** Bar chart (mean±SEM) showing significant increase in the percentage of partially occupied endplates in lumbrical muscles of Ercc1$^{\Delta/-}$ mice at 8 and 16-weeks of age (4 weeks $P>0.05$, 8 weeks $P<0.05$, 16 weeks $P<0.01$; Kruskal-Wallis test with Dunn's post-hoc test). **C:** Bar chart (mean±SEM) showing increase in the percentage of vacant endplates in lumbrical muscles of Ercc1$^{\Delta/-}$ mice (4 weeks and 8 weeks $P>0.05$, 16 weeks $P<0.01$; Kruskal-Wallis test with Dunn's post-hoc test; 4 weeks wild-type N=25 Ercc1$^{\Delta/-}$ N=16, 8 weeks wild-type N=6 Ercc1$^{\Delta/-}$ N=10 , 16 weeks wild-type N=12 Ercc1$^{\Delta/-}$ N=16).

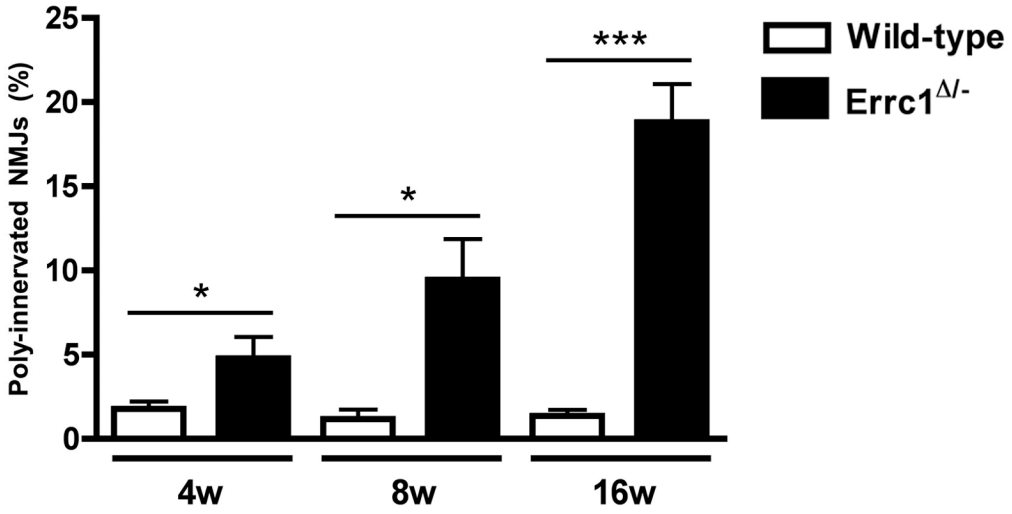

Figure 5.3 – Quantification of levels of poly-innervation in 4-16 week-old Ercc1$^{\Delta/-}$ mice compared to wild-type controls. Bar chart (mean±SEM) showing significantly increased levels of poly-innervation in the lumbrical muscles of Ercc1$^{\Delta/-}$ mice compared to wild-type controls at 4, 8 and 16-weeks of age (4 and 8 weeks $P<0.05$, 16 weeks $P<0.001$; Kruskal-Wallis test with Dunn's post-hoc test; 4 weeks wild-type N=25 Ercc1$^{\Delta/-}$ N=16 , 8 weeks wild-type N=6 Ercc1$^{\Delta/-}$ N=10 , 16 weeks wild-type N=12 Ercc1$^{\Delta/-}$ N=16).

5.4 Discussion

In this chapter I have shown that Ercc1$^{\Delta/-}$ mice develop age-dependant NMJ pathology in motor neurons, with morphological abnormalities such as neurofilament accumulation, abnormal and excessive axon branching and poly-innervation of some endplates.

Neurofilament accumulation is a common feature of neurodegenerative disease, and is seen in SMA, ALS, and Alzheimer's disease (Murray et al., 2008a; Rouleau et al., 1996; Sternberger et al., 1985). The major function of neurofilaments is to provide mechanical support to axons, and accumulations of neurofilament are thought to disrupt the cytoskeleton and impair axonal transport (de Waard et al., 2010; Zhang et al., 1997).

Poly-innervation of motor endplates is only seen in the healthy nervous system during development; in mice all endplates have usually reached the adult, mono-innervated state by two weeks of age (Keller-Peck et al., 2001). However, poly-innervation of adult endplates is seen in axons undergoing compensatory reinnervation following degeneration, for example in diseases such as ALS (Schaefer et al., 2005). The increase in the levels of poly-innervation in the Ercc1$^{\Delta/-}$ mice increases with age and coincides with increasing denervation of endplates, suggesting that some axons may be attempting to reinnervate vacated endplates, in an attempt to prolong muscle function.

The time course of neurodegeneration at the NMJ in the Ercc1$^{\Delta/-}$ mice correlates with the loss of motor neurons and an increase in motor abnormalities in these mice with age (de Waard et al., 2010). At 8 weeks of age Ercc1$^{\Delta/-}$ mice have tremors and show clasping of the hind limbs when lifted by the tail. By 16 weeks they have severe locomotor deficits and are unable to maintain balance (de Waard et al., 2010). This time point coincides with a 30% decrease in the number of fully innervated NMJs, which could account for the motor abnormalities these mice exhibit.

As ERCC1 is involved in several different DNA repair pathways (NER, double strand break repair and interstrand crosslink repair) it is not clear which pathway or combination of pathways and which type of DNA lesion causes the neurodegeneration in Ercc1$^{\Delta/-}$ mice. Studies have shown that patients specifically deficient in the NER pathway, such as people suffering from XP, develop neuronal degeneration, indicating that the NER pathway is sufficient to cause degeneration on its own (Kraemer et al., 2007). However, a strain of mice which are completely without a NER pathway, whilst developing several cancer phenotypes, have not been reported to show any evidence of neurodegeneration (Melis et al., 2008), suggesting that NER acting in conjunction with other repair pathways may be responsible for the NMJ pathology seen in Ercc1$^{\Delta/-}$ mice.

Build up of DNA damage due to deficiencies in DNA repair pathways has been linked to ALS (Bradley and Krasin, 1982; Coppedè et al., 2010), but at present there is no clear evidence that DNA repair genes are a causative factor in forms

of MND. One exception to this is the gene senataxin, mutations in which are linked to a rare autosomal dominant form of juvenile ALS (Chen et al., 2004). Senataxin is a DNA/RNA helicase, which has a role in the DNA damage response (specifically in double-strand repair), defending against oxidative stress (Suraweera et al., 2007). An early pathological event in ALS is the denervation of motor endplates (Fischer et al., 2004), as seen in the DNA repair deficient Ercc1$^{\Delta/-}$ mice. However, it is still unclear how DNA damage and motor neuron degeneration are linked.

The data presented in this chapter is compatible with the model that a build up of DNA damage affects motor neurons in Ercc1$^{\Delta/-}$ mice, and indicates that DNA repair pathways involving ERCC1 are necessary for the maintenance of a healthy neuromuscular system. Further work is now needed in order to determine the mechanisms underlying the link between DNA repair and neurons.

Chapter 6 – General Discussion

6.1 Overview of results

The overall aim of this thesis was to examine the influence that expression of three distinct genes and their respective protein products – YFP, APOE and ERCC1 – on the health and stability of the PNS. Here I have shown that experimental manipulation of all three of these genes resulted in distinct effects on the PNS *in vivo.*

YFP has been used as a reporter protein in the nervous system ever since the *thy1*-YFP mice were first generated in 2000 (Feng et al., 2000) and has previously reported to be inert (Feng et al., 2000; Ikawa et al., 1998; Lichtman and Sanes, 2003; Okabe et al., 1997). Here I have shown that YFP protein expressed in neurons is not inert, but causes an up-regulation of cell stress responses specifically in YFP-expressing cells, subtly alters the morphology of axons and NMJs in healthy adult mice, and has diverse and unpredictable effects on different types of motor neuron degeneration.

My studies on APOE have shown that alterations between the isoforms of apoE protein have consequences for both the regenerative capacity of the PNS *in vivo* and the proteome of peripheral nerves even in normal, healthy adult tissue. Presence of the human apoE4 isoform in mice selectively delays peripheral nerve regeneration and neuromuscular reinnervation, in the absence of any

effect on normal form or function, or on the rate of Wallerian degeneration following nerve crush injury. Proteomics experiments revealed alterations to the proteome of peripheral nerve in apoE4 mice, with changes in proteins associated with cellular outgrowth and regeneration, and integrity of the BNB.

Mutations to ERCC1 are known to affect DNA repair pathways. Here I have shown that a loss of Ercc1 affects the PNS, causing a range of abnormalities at the NMJ that increase with age, including loss of neuromuscular connectivity, poly-innervation and neurofilament accumulation.

6.2 Experimental manipulation of the PNS

The finding that YFP is not inert highlights an important requirement for researchers to be aware of how manipulating the PNS can have unpredictable effects on the system. Earlier studies considered the possibility that YFP could be affecting neurons, but the parameters checked (life span of *thy1*-YFP mice and gross morphology of neurons) were unaltered, leading to the labeling of YFP as inert (Feng et al., 2000).

Reporter proteins have been used both *in vivo* and *in vitro* for many years. Along with XFPs, other commonly used reporter proteins include β-galactosidase from *Escherichia coli* and firefly luciferase (Spergel et al., 2001). β-galactosidase has previously been reported to have toxic effects when expressed *in vitro* in primary cortical neurons, inducing apoptosis in these cells (Detrait et al., 2002). The effects of these two reporter proteins alone highlights the necessity of

performing appropriate controls in order to ensure that any responses recorded in a study are occurring as a result of experimental intervention, and not as a consequence of prior genetic manipulation of an organism.

6.3 Clinical implications

The finding that apoE genotype is a significant determinant of the success of nerve regeneration *in vivo* has implications for recovery from nerve injury in patients, and potentially for neurodegenerative diseases such as MND. Approximately 27% of the population is thought to carry at least one apoE4 allele (Utermann et al., 1980). It is possible that for apoE4 carriers nerve regeneration would be slower than in others without the apoE4 allele, and recovery following peripheral nerve injury or rate of decline in neurodegenerative disease would be correspondingly worse. Therefore knowing a patient's APOE genotype would allow clinicians to give a more accurate prognosis.

Similarly, the finding that mutations in genes contributing to DNA repair pathways (ERCC1) can lead to significant pathology of motor neurons suggests that further studies are now required to examine whether mutations in other genes contributing to DNA repair pathways play a significant role in human MND. The ever-increasing speed of development of genomics technologies is likely to assist in such screens.

By pinpointing specific genes affecting the PNS, such as APOE and ERCC1, the likelihood of one day being able to design patient-specific therapeutics to give the best possible chance of recovery becomes more possible.

6.4 Conclusion

The work described in this thesis highlights the effects that three separate genetic factors can have on the form and function of the PNS *in vivo.* As more genes affecting the PNS are identified and the molecular mechanisms underlying changes such as isoform specific regulation of the nervous system are unravelled, our knowledge of how the PNS functions will become clearer. Hopefully this study will be of benefit to future work on the genetic factors influencing the PNS in health and disease.

7 - References

Akaaboune, M., Villanova, M., Festoff, B.W., Verdiere-Sahuque, M. and Hantai, D. (1994) Apolipoprotein E expression at neuromuscular junctions in mouse, rat and human skeletal muscle. FEBS Lett. 351, 246-248.

Ahmad, A., Robinson, A.R., Duensing, A. van Drunen, E., Beverloo, H.B., Weisberg, D.B., Hasty, P., Hoeijmakers, J.H., and Niedernhofer, L.J. (2008) ERCC1-XPF endonuclease facilitates DNA double-strand break repair. Mol. Cell. Biol 28:5082–5092.

Agbulut, O., Coirault, C., Niederländer, N., Huet, A., Vicart, P., Hagège, A., Puceat, M., and Menasché, P. (2006) GFP expression in muscle cells impairs actin-myosin interactions: implications for cell therapy. Nat. Methods. 3(5):331.

Agbulut, O., Huet, A., Niederländer, N., Puceat, M., Menasché, P., and Coirault, C. (2007) Green fluorescent protein impairs actin-myosin interactions by binding to the actin-binding site of myosin. J. Biol. Chem. 6;282(14):10465-71.

Alami, N.H., Jung, P. and Brown, A. (2009) Myosin Va increases the efficiency of neurofilament transport by decreasing the duration of long-term pauses. J. Neurosci., 29, 6625–6634.

Alberts, M.J., Graffagnino, C., McClenny, C., DeLong, D., Strittmatter, W., Saunders, A.M., and Roses, AD. (1995) ApoE genotype and survival from intracerebral haemorrhage. Lancet 346, 575.

Al-Chalabi, A., Enayat, Z.E., Bakker, M.C., Sham, P.C., Ball, D.M., Shaw, C.E., Lloyd, C.M., Powell, J.F., and Leigh, P.N. (1996) Association of apolipoprotein E epsilon 4 allele with bulbar-onset motor neuron disease. Lancet 347, 159-160.

Allen, E., Ding, J., Wang, W., Pramanik, S., Chou, J., Yau, V., and Yang, Y. (2005) Gigaxonin-controlled degradation of MAP1B light chain is critical to neuronal survival. Nature. 438(7065):224-8.

Anderson, R., Barnes, J.C., Bliss, T.V., Cain, D.P., Cambon, K., Davies, H.A., Errington, M.L., Fellows, L.A., Gray, R.A., Hoh, T., Stewart, M., Large, C.H., and Higgins, G.A. (1998) Behavioural, physiological and morphological analysis of a line of apolipoprotein E knockout mouse. Neuroscience. 85(1):93-110.

Aoki, K., Uchihara, T., Sanjo, N., Nakamura, A., Ikeda, K., Tsuchiya, K. and Wakayama, Y. (2003) Increased expression of neuronal apolipoprotein E in human brain with cerebral infarction. Stroke. 34(4):875-80.

Arendt, T., Schindler, C., Brückner, M.K., Eschrich, K., Bigl, V. Zedlick, D., and Marcova, L. (1997) Plastic neuronal remodeling is impaired in patients with Alzheimer's disease carrying apolipoprotein epsilon 4 allele. J. Neurosci. 17,516-29.

Arnold, D.B. (2009) Actin and microtubule-based cytoskeletal cues direct polarized targeting of proteins in neurons. Sci. Signal. 2, 49.

Bachus, R., Bader, S., Gessner, R. and Ludolph, A.C. (1997) Lack of association of apolipoprotein E epsilon 4 allele with bulbar-onset motor neuron disease. Ann. Neurol. 41, 417.

Balice-Gordon, R.J., and Lichtman, J.W. (1990) In vivo visualization of the growth of pre- and postsynaptic elements of neuromuscular junctions in the mouse. J. Neurosci. 10(3):894-908.

Balice-Gordon, R.J. and Lichtman, J.W. (1994) Long-term synapse loss induced by focal blockade of postsynaptic receptors. Nature. 372(6506):519-24.

Barry, J.A., and Ribchester, R.R. (1995) Persistent polyneuronal innervation in partially denervated rat muscle after reinnervation and recovery from prolonged nerve conduction block. J. Neurosci. 15(10):6327-39.

Barzilai, A., Biton, S., and Shiloh, Y. (2008) The role of the DNA damage response in neuronal development, organization and maintenance. DNA Repair. 7(7):1010-27.

Basu, S.K., Brown, M.S., Ho, Y.K., Havel, R.J. and Goldstein, J.L. (1981) Mouse macrophages synthesize and secrete a protein resembling apolipoprotein E. Proc. Natl. Acad. Sci. USA. 78(12):7545-9.

Baudet, C., Pozas, E., Adameyko, I., Andersson, E., Ericson, J., and Ernfors, P. (2008) Retrograde signaling onto Ret during motor nerve terminal maturation. J. Neurosci. 28(4):963-75.

Bear, M.F., Connors, B.W., and Paradiso, M.A. (2001) Neurocience: Exploring the brain. 2nd Ed. Lippincott Williams and Williams.

Bearer, E.L., DeGiorgis, J.A., Bodner, R.A., Kao, A.W. and Reese, T.S. (1993) Evidence for myosin motors on organelles in squid axoplasm. Proc. Natl Acad. Sci. USA, 90, 11252–11256.

Bedlack, R.S., Strittmatter, W.J. and Morgenlander, J.C. (2000) Apolipoprotein E and neuromuscular disease: a critical review of the literature. Arch. Neurol. 57, 1561-1565.

Bedlack, R.S., Edelman, D., Gibbs, J.W., 3rd, Kelling, D., Strittmatter, W., Saunders, A.M., and Morgenlander, J. (2003) APOE genotype is a risk factor for neuropathy severity in diabetic patients. Neurology 60, 1022-1024.

Beirowski, B., Adalbert, R., Wagner, D., Grumme, D.S., Addicks, K., Ribchester, R.R., and Coleman, M.P. (2005) The progressive nature of Wallerian degeneration in wild-type and slow Wallerian degeneration (WldS) nerves. BMC Neurosci. 6:6.

Beirowski, B., Berek, L., Adalbert, R., Wagner, D., Grumme, D.S., Addicks, K., Ribchester, R.R., and Coleman, M.P. (2004) Quantitative and qualitative analysis of Wallerian degeneration using restricted axonal labelling in YFP-H mice. J. Neurosci. Methods. 134(1):23-35.

Belkas, J.S., Shoichet, M.S. and Midha, R. (2004) Peripheral nerve regeneration through guidance tubes. Neurol. Res. 26(2):151-60.

Bellosta, S., Nathan, B.P., Orth, M., Dong, L.M., Mahley, R.W. and Pitas, R.E. (1995) Stable expression and secretion of apolipoproteins E3 and E4 in mouse neuroblastoma cells produces differential effects on neurite outgrowth. J. Biol. Chem. 270, 27063-27071.

Bergstralh, D.T., and Sekelsky, J. (2008) Interstrand crosslink repair: can XPF-ERCC1 be let off the hook? Trends. Genet. 24(2):70-6.

Boillée, S., Vande Velde, C., and Cleveland, D.W. (2006) ALS: a disease of motor neurons and their nonneuronal neighbors. Neuron. 52(1):39-59.

Boyles, J.K., Pitas, R.E., Wilson, E., Mahley, R.W. and Taylor, J.M. (1985) Apolipoprotein E associated with astrocytic glia of the central nervous system and with nonmyelinating glia of the peripheral nervous system. J. Clin. Invest. 76:1501-13.

Boyles, J.K., Zoellner, C.D., Anderson, L.J., Kosik, L.M., Pitas, R.E., Weisgraber, K.H., Hui, D.Y., Mahley, R.W., Gebicke-Haerter, P.J., Ignatius, M.J. and Shooter, E.M. (1989) A role for apolipoprotein E, apolipoprotein A-I, and low density lipoprotein receptors in cholesterol transport during regeneration and remyelination of the rat sciatic nerve. Ji Clini Invest. 83:1015-31.

Bradley, W.G., and Krasin, F. (1982) A new hypothesis of the etiology of amyotrophic lateral sclerosis. The DNA hypothesis. Arch. Neurol. 39(11):677-80.

Bridge, K.E., Berg, N., Adalbert, R., Babetto, E., Dias, T., Spillantini, M.G., Ribchester, R.R. and Coleman, M.P. (2009) Late onset distal axonal swelling in YFP-H transgenic mice. Neurobiol. Aging. 2009 Feb;30(2):309-21. Epub 2007 Jul 19.

Brown, J., and Bridgman, P.C. (2003) Role of myosin II in axon outgrowth. J. Histochem. Cytochem. 51(4):421-8.

Brown, M.E. and Bridgman, P.C. (2004) Myosin function in nervous and sensory systems. J. Neurobiol. 58, 118-130.

Brown, M.C., Jansen, J.K., and Van Essen, D. (1976) Polyneuronal innervation of skeletal muscle in new-born rats and its elimination during maturation. J. Physiol. 261(2):387-422.

Caine, J., Sankovich, S., Antony, H., Waddington, L., Macreadie, P., Varghese, J., and Macreadie, I. (2007) Alzheimer's Abeta fused to green fluorescent protein induces growth stress and a heat shock response. FEMS Yeast. Res. 7(8):1230-6.

Cajal, S.R. (1888a) Estructura de los centros nerviosos de las aves. Rev. Trim. Histol. Norm. Patol. 1:1–10.

Cajal, S.R. (1888b) Sobre las fibras nerviosas de la capa molecular del cerebelo. Rev. Trim. Histol. Norm. Patol. 1:33–49.

Cajal, S.R. (1889) Conexión general de los elementos nerviosos. Med. Pract. 2:341–346.

Calliari, A., Sotelo-Silveira, J., Costa, M.C., Nogueira, J., Cameron, L.C., Kun, A., Benech, J. and Sotelo, J.R. (2002) Myosin Va is locally synthesized following nerve injury. Cell Motil. Cytoskeleton, 51, 169 – 176.

Chalfie ,M., Tu, Y., Euskirchen, G., Ward, W.W. and Prasher, D.C. (1994) Green fluorescent protein as a marker for gene expression. Science. 263(5148):802-5.

Chambers, D.M., Peters, J., and Abbott, C.M. (1998) The lethal mutation of the mouse wasted (wst) is a deletion that abolishes expression of a tissue-specific isoform of translation elongation factor 1alpha, encoded by the Eef1a2 gene. Proc. Natl. Acad. Sci. USA. 95(8):4463-8.

Chantler, P.D. and Wylie, S.R. (2003) Elucidation of the separate roles of myosins IIA and IIB during neurite outgrowth, adhesion and retraction. IEE Proc. Nanobiotechnol. 150, 111-125.

Charcot, J.M., and Joffroy, A. (1869). Deux cas d'atrophie musculaire progressive avec lesion de la substance grise et des faisceaux antero-lateraux de la moelle epiniere. Arch. Physiol. Neurol. Path. 2, 744–754.

Chaudhry, V., and Cornblath, D.R. (1992) Wallerian degeneration in human nerves: serial electrophysiological studies. Muscle. Nerve. 15:687-693.

Chen, Y.Z., Bennett, C.L., Huynh, H.M., Blair, I.P., Puls, I., Irobi, J., Dierick, I., Abel, A., Kennerson, M.L., Rabin, B.A., Nicholson, G.A., Auer-Grumbach, M., Wagner, K., De Jonghe, P., Griffin, J.W., Fischbeck, K.H., Timmerman, V., Cornblath, D.R., and Chance, P.F. (2004) DNA/RNA helicase gene mutations in a form of juvenile amyotrophic lateral sclerosis (ALS4). Am. J. Hum. Genet. 74(6):1128-35.

Chiesa, R., Piccardo, P., Dossena, S., Nowoslawski, L., Roth, K.A., Ghetti, B., and Harris, D.A. (2005) Bax deletion prevents neuronal loss but not neurological symptoms in a transgenic model of inherited prion disease. Proc. Natl. Acad. Sci. USA. 102(1):238-43.

Cifuentes-Diaz, C., Frugier, T., Tiziano, F.D., Lacène, E., Roblot, N., Joshi, V., Moreau, M.H., and Melki, J. (2001) Deletion of murine SMN exon 7 directed to skeletal muscle leads to severe muscular dystrophy. J. Cell. Biol. 152(5):1107-14.

Cleaver, J.E. (1968) Defective repair replication of DNA in xeroderma pigmentosum. Nature. 218(5142):652-6.

Cleveland, D.W., and Rothstein, J.D. (2001) From Charcot to Lou Gehrig: deciphering selective motor neuron death in ALS. Nat. Rev. Neurosci. 2:806–819.

Comley, L.H., Fuller, H.R., Wishart, T.M., Mutsaers, C.A., Thomson, D., Wright, A.K., Ribchester, R.R., Morris, G.E., Parson, S.H., Horsburgh, K., and

Gillingwater, T.H. (2011) ApoE isoform-specific regulation of regeneration in the peripheral nervous system. Hum Mol Genet. 20(12):2406-21.

Condeelis, J. (1995) Elongation factor 1 alpha, translation and the cytoskeleton. Trends. Biochem. Sci. 20(5):169-70.

Coppedè, F., Migheli, F., Lo Gerfo, A., Fabbrizi, M.R., Carlesi, C., Mancuso, M., Corti, S., Mezzina, N., del Bo, R., Comi, G.P., Siciliano, G., and Migliore, L. (2010) Association study between XRCC1 gene polymorphisms and sporadic amyotrophic lateral sclerosis. Amyotroph. Lateral. Scler. 11(1-2):122-4.

Corder, E.H., Saunders, A.M., Strittmatter, W.J., Schmechel, D.E., Gaskell, P.C., Small, G.W., Roses, A.D., Haines, J.L., and Pericak-Vance, M.A. (1993) Gene dose of apolipoprotein E type 4 allele and the risk of Alzheimer's disease in late onset families. Science. 261, 921-923.

Corder, E.H, Robertson, K., Lannfelt, L., Bogdanovic, N., Eggertsen, G., Wilkins, J., and Hall, C. (1998) HIV-infected subjects with the E4 allele for APOE have excess dementia and peripheral neuropathy. Nat. Med. 4:1182-4.

Corti, S., Locatelli, F., Donadoni, C., Guglieri, M., Papadimitriou, D., Strazzer, S., Del Bo, R., and Comi, G.P. (2004) Wild-type bone marrow cells ameliorate the phenotype of SOD1-G93A ALS mice and contribute to CNS, heart and skeletal muscle tissues. Brain. 127(Pt 11):2518-32.

Court, F.A., Gillingwater, T.H., Melrose, S., Sherman, D.L., Greenshields, K.N., Morton, A.J., Harris, J.B., Willison, H.J., and Ribchester, R.R. (2008) Identity, developmental restriction and reactivity of extralaminar cells capping mammalian neuromuscular junctions. J. Cell. Sci. 121(Pt 23):3901-11.

Cubitt, A.B., Heim, R., Adams, S.R., Boyd, A.E., Gross, L.A., and Tsien, R.Y. (1995) Understanding, improving and using green fluorescent proteins. Trends. Biochem. Sci. 20(11):448-55.

Chalfie, M., Tu, Y., Euskirchen, G., Ward, W.W., and Prasher, D.C. (1994) Green fluorescent protein as a marker for gene expression. Science. 263, 802– 805.

Clontech. (1996) Living Color GFP Application Notes. CLONTECH Lab, Palo Alto, CA.

Dale, H.H., and Feldberg, W. (1934) The chemical transmitter of vagus effects to the stomach. J. Physiol. 81(3):320-34.

David, S.S., O'Shea, V.L., and Kundu, S. (2007) Base-excision repair of oxidative DNA damage. Nature. 447(7147):941-50.

de Boer, J., and Hoeijmakers, J.H. (2000) Nucleotide excision repair and human syndromes. Carcinogenesis. 21(3):453-60.

De Carlos, J.A., and Borrell, J. (2007) A historical reflection of the contributions of Cajal and Golgi to the foundations of neuroscience. Brain. Res. Rev. 55(1):8-16.

Detrait, E.R., Bowers, W.J., Halterman, M.W., Giuliano, R.E., Bennice, L., Federoff, H.J., and Richfield, E.K. (2002) Reporter gene transfer induces apoptosis in primary cortical neurons. Mol. Ther. 5(6):723-30.

de Waard, M.C., van der Pluijm, I., Zuiderveen Borgesius, N., Comley, L.H., Haasdijk, E.D., Rijksen, Y., Ridwan, Y., Zondag, G., Hoeijmakers, J.H., Elgersma, Y., Gillingwater, T.H., and Jaarsma, D. (2010) Age-related motor neuron

degeneration in DNA repair-deficient Ercc1 mice. Acta Neuropathol. 120(4):461-75.

Dong, L.-M., Wilson, C., Wardell, M.R., Simmons, T., Mahley, R.W., Weisgraber, K.H., and Agard, D.A. (1994) Human apolipoprotein E. Role of arginine 61 in mediating the lipoprotein preferences of the E3 and E4 isoforms. J. Biol. Chem. 269:22358–65.

Drory, V.E., Birnbaum, M., Korczyn, A.D. and Chapman, J. (2001) Association of APOE epsilon4 allele with survival in amyotrophic lateral sclerosis. J. Neurol. Sci. 190, 17-20.

Elshourbagy, N.A., Liao, W.S., Mahley, R.W. and Taylor, J.M. (1985) Apolipoprotein E mRNA is abundant in the brain and adrenals, as well as in the liver, and is present in other peripheral tissues of rats and marmosets. Proc. Natl. Acad. Sci. 82(1):203-7.

Fawcett, J.W. and Keynes, R.J. (1990) Peripheral nerve regeneration. Annu. Rev. Neurosci. 13:43-60.

Feng, G., Mellor, R.H., Bernstein, M., Keller-Peck, C., Nguyen, Q.T., Wallace, M., Nerbonne, J.M., Lichtman, J.W., and Sanes, J.R. (2000) Imaging neuronal subsets in transgenic mice expressing multiple spectral variants of GFP. Neuron. 28(1):41-51.

Fox, M.A., Sanes, J.R., Borza, D.B., Eswarakumar, V.P., Fässler, R., Hudson, B.G., John, S.W., Ninomiya, Y., Pedchenko, V., Pfaff, S.L., Rheault, M.N., Sado, Y., Segal, Y., Werle, M.J., and Umemori, H. (2007) Distinct target-derived signals organize formation, maturation, and maintenance of motor nerve terminals. Cell. 129(1):179-93.

Fischer, L.R., Culver, D.G., Tennant, P., Davis, A.A., Wang, M., Castellano-Sanchez, A., Khan, J., Polak, M.A., and Glass, J.D. (2004) Amyotrophic lateral sclerosis is a distal axonopathy: evidence in mice and man. Exp. Neurol. 185(2):232-40.

Fullerton, S.M., Shirman, G.A., Strittmatter, W.J. and Matthew, W.D. (2001) Impairment of the blood–nerve and blood–brain barriers in apolipoprotein e knockout mice. Exp. Neurol., 169, 13–22.

Galvani, L. (1791) De viribus electricitatis in motu musculari commentarius (Commentary on the Force of Electricity on Muscular Motion). Accademia delle Scienze, Bologna.

Gaudet, A.D., Popovich, P.G., and Ramer, M.S. (2011) Wallerian degeneration: Gaining perspective on inflammatory events after peripheral nerve injury. J. Neuroinflammation. 8(1):110.

Gelman, B.B., Rifai, N., Goodrum, J.F., Bouldin, T.W. and Krigman, M.R. (1987) Apolipoprotein E is released by rat sciatic nerve during segmental demyelination and remyelination. J. Neuropathol. Exp. Neurol. 46, 644-652.

Genden, E.M., Watanabe, O., Mackinnon, S.E., Hunter, D.A. and Strasberg, S.R. (2002) Peripheral nerve regeneration in the apolipoprotein-E-deficient mouse. J. Reconstr. Microsurg. 18, 495-502.

Geranmayeh, F., Christian, L., Turkheimer, F.E., Gentleman, S.M. and O'Neill, K.S. (2005) A need to clarify the role of apolipoprotein E in peripheral nerve injury and repair. J. Peripher. Nerv. Syst. 10, 344-345.

Gerlach, J. (1871) Von den Ruckenmarke. In: Stricker S (ed) Handbuch der Lehre von den Geweben. Engelmann, Leipzig, pp 665–693.

Gillingwater, T.H. and Ribchester, R.R. (2001) Compartmental neurodegeneration and synaptic plasticity in the Wld(s) mutant mouse. J. Physiol. 534, 627-39.

Gillingwater, T.H., Ribchester, R.R. (2003) The relationship of neuromuscular synapse elimination to synaptic degeneration and pathology: insights from WldS and other mutant mice. J. Neurocytol. 32(5-8):863-81

Gillingwater, T.H., Thomson, D., Mack, T.G., Soffin, E.M., Mattison, R.J., Coleman, M.P. and Ribchester, R.R. (2002) Age-dependent synapse withdrawal at axotomised neuromuscular junctions in Wld(s) mutant and Ube4b/Nmnat transgenic mice. J. Physiol., 543, 739 – 755.

Golgi, C. (1873) Sulla struttura della sostanza grigia del cervelo. Gazzetta Medica Italiana. Lombardia 33, 244–246.

Greenbaum, L., Rothmann, C., Lavie, R., and Malik, Z. (2000) Green fluorescent protein photobleaching: a model for protein damage by endogenous and exogenous singlet oxygen. Biol. Chem. 381(12):1251-8.

Gordon, J.W., Chesa, P.G., Nishimura, H., Rettig, W.J., Maccari, J.E., Endo, T., Seravalli, E., Seki, T., and Silver, J. (1987) Regulation of Thy-1 gene expression in transgenic mice. Cell. 50(3):445-52.

Goto, H., Yang, B., Petersen, D., Pepper, K.A., Alfaro, P.A., Kohn, D.B., and Reynolds, C.P. (2003) Transduction of green fluorescent protein increased oxidative stress and enhanced sensitivity to cytotoxic drugs in neuroblastoma cell lines. Mol. Cancer. Ther. 2(9):911-7.

Gregg, S.Q., Robinson, A.R., and Niedernhofer, L.J. (2011) Physiological consequences of defects in ERCC1-XPF DNA repair endonuclease. DNA Repair (Amst). 10(7):781-91.

Griffin, J.W. and Thompson, W.J. (2008) Biology and pathology of nonmyelinating Schwann cells. Glia. 56(14):1518-31.

Guertin, A.D., Zhang, D.P., Mak, K.S., Alberta, J.A., and Kim, H.A. (2005) Microanatomy of axon/glial signaling during Wallerian degeneration. J. Neurosci. 25(13):3478-87.

Hall, S.M. (1986) The effect of inhibiting Schwann cell mitosis on the re-innervation of acellular autografts in the peripheral nervous system of the mouse. Neuropathol. Appl. Neurobiol. 12(4):401-14.

Halliwell, B. (2006) Oxidative stress and neurodegeneration: where are we now? J Neurochem. 97(6):1634-58.

Hardart, M.K., Burns, J.P., and Truog, R.D. (2002) Respiratory support in spinal muscular atrophy type I: a survey of physician practices and attitudes. Pediatrics. 110(2 Pt 1):e24.

Heim, R., Prasher, D.C., and Tsien, R.Y. (1994) Wavelength mutations and posttranslational autoxidation of green fluorescent protein. Proc. Natl. Acad. Sci. U S A. 20;91(26):12501-4.

Heim, R., and Tsien, R.Y. (1996) Engineering green fluorescent protein for improved brightness, longer wavelengths and fluorescence resonance energy transfer. Curr. Biol. 1;6(2):178-82.

Horsburgh, K., McCulloch, J., Nilsen, M., Roses, A.D. and Nicoll, J.A. (2000) Increased neuronal damage and apoE immunoreactivity in human apolipoprotein E, E4 isoform-specific, transgenic mice after global cerebral ischaemia. Eur. J. Neurosci. 12, 4309-4317.

Hsieh, P., and Yamane, K. (2008) DNA mismatch repair: molecular mechanism, cancer, and ageing. Mech. Ageing. Dev. 129(7-8):391-407.

Huang, W.Y., Aramburu, J., Douglas, P.S., and Izumo, S. (2000) Transgenic expression of green fluorescence protein can cause dilated cardiomyopathy. Nat. Med. 6(5):482-3.

Hughes, B.W., Kusner, L.L., and Kaminski, H.J. (2006) Molecular architecture of the neuromuscular junction. Muscle Nerve. 33(4):445-61.

Ignatius, M.J., Gebicke-Harter, P.J., Skene, J.H., Schilling, J.W., Weisgraber, K.H., Mahley, R.W. and Shooter, E.M. (1986) Expression of apolipoprotein E during nerve degeneration and regeneration. Proc. Natl. Acad. Sci. USA. 83, 1125-1129.

Ikawa, M., Kominami, K., Yoshimura, Y., Tanaka, K., Nishimune, Y. and Okabe, M. (1995) A rapid and non-invasive selection of transgenic embryos before implantation using green fluorescent protein (GFP). FEBS Lett. 13;375(1-2):125-8.

Ikawa, M., Yamada, S., Nakanishi, T., and Okabe, M. (1998) 'Green mice' and their potential usage in biological research. FEBS Lett. 430(1-2):83-7.

Jeppesen, D.K., Bohr, V.A., and Stevnsner, T. (2011) DNA repair deficiency in neurodegeneration. Prog. Neurobiol. 94(2):166-200.

Jha, A., Lammertse, D.P., Coll, J.R., Charlifue, S., Coughlin, C.T. et al. (2008) Apolipoprotein E epsilon4 allele and outcomes of traumatic spinal cord injury. J. Spinal. Cord. Med. 31(2):171-6.

Ji, Z.S., Pitas, R.E. and Mahley, R.W. (1998) Differential cellular accumulation/retention of apolipoprotein E mediated by cell surface heparan sulfate proteoglycans. Apolipoproteins E3 and E2 greater than e4. J. Biol. Chem. May 29;273(22):13452-60.

Keller-Peck, C.R., Walsh, M.K., Gan, W.B., Feng, G., Sanes, J.R., and Lichtman, J.W. (2001) Asynchronous synapse elimination in neonatal motor units: studies using GFP transgenic mice. Neuron. 31(3):381-94.

Kiang, J.G., and Tsokos, G.C. (1998) Heat shock protein 70 kDa: molecular biology, biochemistry, and physiology. Pharmacol. Ther. 80(2):183-201.

Korwek, K.M., Trotter, J.H., Ladu, M.J., Sullivan, P.M. and Weeber, E.J. (2009) ApoE isoform-dependent changes in hippocampal synaptic function. Mol. Neurodegener. 27,4:21.

Kraemer, K.H., Patronas, N.J., Schiffmann, R,. Brooks, B.P., Tamura, D., and DiGiovanna, J.J. (2007) Xeroderma pigmentosum, trichothiodystrophy and Cockayne syndrome: a complex genotype-phenotype relationship. Neuroscience. 145(4):1388-96.

Krejci, E., Thomine, S., Boschetti, N., Legay, C., Sketelj, J., and Massoulié, J. (1997) The mammalian gene of acetylcholinesterase-associated collagen. J Biol Chem. 272(36):22840-7.

Kühne, W. (1862) Uber dieperipherischen Endorgane der motorischen Nerven. Engelmann, Leipzig.

Kuzminov, A. (1999) Recombinational repair of DNA damage in Escherichia coli and bacteriophage lambda. Microbiol. Mol. Biol. Rev. 63(4):751-813.

Le, T.T., Pham, L.T., Butchbach, M.E., Zhang, H.L., Monani, U.R., Coovert, D.D., Gavrilina, T.O., Xing, L., Bassell, G.J., and Burghes, A.H. (2005) SMNDelta7, the major product of the centromeric survival motor neuron (SMN2) gene, extends survival in mice with spinal muscular atrophy and associates with full-length SMN. Hum. Mol. Genet. 14(6):845-57.

Letourneau, P.C. (2009) Actin in axons: stable scaffolds and dynamic filaments. Results. Probl. Cell. Differ. 48:65-90.

Li, Y.J., Hauser, M.A., Scott, W.K., Martin, E.R., Booze, M.W., et al. (2004a) Apolipoprotein E controls the risk and age at onset of Parkinson disease. Neurology. 62, 2005-2009.

Li, Y.J., Pericak-Vance, M.A., Haines, J.L., Siddique, N., McKenna-Yasek, D., Hung, W.Y., Sapp, P., Allen, C.I., Chen, W., Hosler, B., Saunders, A.M., Dellefave, L.M., Brown, R.H. and Siddique, T. (2004b) Apolipoprotein E is associated with age at onset of amyotrophic lateral sclerosis. Neurogenetics. 5, 209-213.

Lichtman, J.W., and Sanes, J.R. (2003) Watching the neuromuscular junction. J. Neurocytol. 32(5-8):767-75.

Lindahl, T. (1993) Instability and decay of the primary structure of DNA. Nature. 362(6422):709-15.

Lindahl, T., Karran, P., and Wood, R.D. (1997) DNA excision repair pathways. Curr. Opin. Genet. Dev. 7(2):158-69.

Liu, H.S., Jan, M.S., Chou, C.K., Chen, P.H., and Ke, N.J. (1999) Is green fluorescent protein toxic to the living cells? Biochem. Biophys. Res. Commun. 260(3):712-7.

Liyanage, Y., Hoch, W., Beeson, D. and Vincent, A. (2002) The agrin/muscle-specific kinase pathway: new targets for autoimmune and genetic disorders at the neuromuscular junction. Muscle Nerve. 25(1):4-16.

López-Muñoz, F., and Alamo, C. (2009) Historical evolution of the neurotransmission concept. J. Neural. Transm. 116(5):515-33.

Lupa, M.T., Gordon, H., and Hall, Z.W. (1990) A specific effect of muscle cells on the distribution of presynaptic proteins in neurites and its absence in a C2 muscle cell variant. Dev. Biol. 142(1):31-43.

Ma, X., Kawamoto, S., Uribe, J. and Adelstein, R.S. (2006) Function of the neuron-specific alternatively spliced isoforms of nonmuscle myosin II-B during mouse brain development. Mol. Biol. Cell, 17, 2138–2149.

Mahajan, N.P., Harrison-Shostak, D.C., Michaux, J., and Herman, B. (1999) Novel mutant green fluorescent protein protease substrates reveal the activation of specific caspases during apoptosis. Chem. Biol. 6(6):401-9.

Mahley, R.W. (1988) Apolipoprotein E: cholesterol transport protein with expanding role in cell biology. Science. 240(4852):622-30.

Mahley, R.W., Weisgraber, K.H., and Huang, Y. (2009) Apolipoprotein E: structure determines function, from atherosclerosis to Alzheimer's disease to AIDS. J. Lipid. Res. 50 Suppl:S183-8.

Malek, G., Johnson, L.V., Mace, BE, Saloupis, P., Schmechel, D.E. Rickman, D.W., Toth, C.A., Sullivan, P.M. and Bowes Rickman, C. (2005) Apolipoprotein E allele-dependent pathogenesis: a model for age-related retinal degeneration. Proc. Natl. Acad. Sci. USA. 102, 11900-5.

Martin, L.J. (2008) DNA damage and repair: relevance to mechanisms of neurodegeneration. J. Neuropathol. Exp. Neurol. 67(5):377-87.

Martin, L.J., Pan, Y., Price, A.C., Sterling, W., Copeland, N.G., Jenkins, N.A., Price, D.L., and Lee, M.K. (2006) Parkinson's disease alpha-synuclein transgenic mice develop neuronal mitochondrial degeneration and cell death. J. Neurosci. 26(1):41-50.

Matsumoto, G., Stojanovic, A., Holmberg, C.I., Kim, S., and Morimoto, R.I.. (2005) Structural properties and neuronal toxicity of amyotrophic lateral sclerosis-associated Cu/Zn superoxide dismutase 1 aggregates. J. Cell. Biol. 171(1):75-85.

McColl, B.W., McGregor, A.L., Wong, A., Harris, J.D., Amalfitano, A., Magnoni, S., Baker, A.H., Dickson, G. and Horsburgh, K. (2007) APOE epsilon3 gene transfer attenuates brain damage after experimental stroke. J. Cereb. Blood. Flow. Metab. 27, 477-487.

McKinnon, P.J. (2009) DNA repair deficiency and neurological disease. Nat. Rev. Neurosci. 10(2):100-12.

McQuarrie, I.G. (1986) Structural protein transport in elongating motor axons after sciatic nerve crush. Effect of a conditioning lesion. Neurochem. Pathol. 5(3):153-64.

McQuarrie, I.G. and Lund, L.M. (2009) Intra-axonal myosin and actin in nerve regeneration. Neurosurgery. 65(4 Suppl):A93-6.

Melis, J.P., Wijnhoven, S.W., Beems, R.B., Roodbergen, M., van den Berg, J., Moon, H., Friedberg, E., van der Horst, G.T., Hoeijmakers, J.H., Vijg, J. and van Steeg, H. (2008) Mouse models for xeroderma pigmentosum group A and group C show divergent cancer phenotypes. Cancer. Res. 68(5):1347-53.

Methia, N., Andre´, P., Hafezi-Moghadam, A., Economopoulos, M., Thomas, K.L. and Wagner, D.D. (2001) ApoE deficiency compromises the blood brain barrier especially after injury. Mol. Med., 7, 810–815.

Mi, W., Beirowski, B., Gillingwater, T.H., Adalbert, R., Wagner, D., Grumme, D., Osaka, H., Conforti, L., Arnhold, S., Addicks, K., Wada, K., Ribchester, R.R. and Coleman, M.P. (2005) The slow Wallerian degeneration gene, WldS, inhibits axonal spheroid pathology in gracile axonal dystrophy mice. Brain. 128: 405–416.

Miledi, R. and Slater, C.R. (1970) On the degeneration of rat neuromuscular junctions after nerve section. J. Physiol. 207, 507-28.

Millar, K., Nicoll, J.A., Thornhill, S., Murray, G.D. and Teasdale, G.M. (2003) Long term neuropsychological outcome after head injury: relation to APOE genotype. J Neurol Neurosurg Psychiatry. 74:1047-52.

Miller, F.D., Tetzlaff, W., Bisby, M.A., Fawcett, J.W. and Milner, R.J. (1989) Rapid induction of the major embryonic alpha-tubulin mRNA, T alpha 1, during nerve regeneration in adult rats. J. Neurosci. 9(4):1452-63.

Miura, M., Zhu, H., Rotello, R., Hartwieg, E.A. and Yuan, J. (1993) Induction of apoptosis in fibroblasts by IL-1 beta-converting enzyme, a mammalian homolog of the C. elegans cell death gene ced-3. Cell. 75(4):653-60.

Monani, U.R. (2005) Spinal muscular atrophy: a deficiency in a ubiquitous protein; a motor neuron-specific disease. Neuron. 48(6):885-96.

Morris, R. (1985) Thy-1 in developing nervous tissue. Dev. Neurosci. 7(3):133-60.

Moulard, B., Sefiani, A., Laamri, A., Malafosse, A. and Camu, W. (1996) Apolipoprotein E genotyping in sporadic amyotrophic lateral sclerosis: evidence for a major influence on the clinical presentation and prognosis. J. Neurol. Sci. 139, 34-37.

Mueller, B.K. (1999) Growth cone guidance: first steps towards a deeper understanding. Annu. Rev. Neurosci. 22:351-88.

Mui, S., Rebeck, G.W., McKenna-Yasek, D., Hyman, B.T. and Brown, R.H., Jr (1995) Apolipoprotein E epsilon 4 allele is not associated with earlier age at onset in amyotrophic lateral sclerosis. Ann. Neurol. 38, 460-463.

Müller, H.W., Gebicke-Härter, P.J., Hangen, D.H. and Shooter, E.M. (1985) A specific 37,000-dalton protein that accumulates in regenerating but not in nonregenerating mammalian nerves. Science. 228:499-501.

Murray, L.M., Comley, L.H., Thomson, D., Parkinson, N., Talbot, K. and Gillingwater, T.H. (2008a) Selective vulnerability of motor neurons and dissociation of pre- and post-synaptic pathology at the neuromuscular junction in mouse models of spinal muscular atrophy. Hum. Mol. Genet., 17,949 – 962.

Murray, L.M., Talbot, K. and Gillingwater, T.H. (2010) Neuromuscular synaptic vulnerability in motor neuron disease; amyotrophic lateral sclerosis and spinal muscular atrophy. Neuropathol. Appl. Neurobiol., 36, 133 – 156.

Murray, L.M., Thomson, D., Conklin, A., Wishart, T.M. and Gillingwater, T.H. (2008b) Loss of translation elongation factor (eEF1A2) expression in vivo differentiates between Wallerian degeneration and dying-back neuronal pathology. J. Anat., 213, 633 – 645.

Nathan, B.P., Bellosta, S., Sanan, D.A., Weisgraber, K.H., Mahley, R.W. and Pitas, R.E. (1994) Differential effects of apolipoproteins E3 and E4 on neuronal growth in vitro. Science. May 6;264(5160):850-2.

Nathan, B.P., Chang, K.C., Bellosta, S., Brisch, E., Ge, N., Mahley, R.W. and Pitas, R.E. (1995) The inhibitory effect of apolipoprotein E4 on neurite outgrowth is associated with microtubule depolymerization. J. Biol. Chem. Aug 25;270(34):19791-9.

Newbery, H.J., Gillingwater, T.H., Dharmasaroja, P., Peters, J., Wharton, S.B., Thomson, D., Ribchester, R.R., and Abbott, C.M. (2005) Progressive loss of motor neuron function in wasted mice: effects of a spontaneous null mutation in the gene for the eEF1 A2 translation factor. J. Neuropathol. Exp. Neurol. 64(4):295-303.

Niedernhofer, L.J. (2008) Nucleotide excision repair deficient mouse models and neurological disease. DNA Repair (Amst). 7(7):1180-9.

Nishimura, S., Nagai, S., Sata, M., Katoh, M., Yamashita, H., Saeki, Y., Nagai, R. and Sugiura, S. (2006) Expression of green fluorescent protein impairs the force-generating ability of isolated rat ventricular cardiomyocytes. Mol. Cell. Biochem. 286(1-2):59-65.

Nishitsuji, K., Hosono, T., Nakamura, T., Bu, G. and Michikawa, M. (2011) Apolipoprotein E regulates the integrity of tight junctions in an isoform-dependent manner in an in vitro blood-brain barrier model. J. Biol. Chem. 286(20):17536-42.

Nouspikel, T. (2008) Nucleotide excision repair and neurological diseases. DNA Repair (Amst). 7(7):1155-67.

Okabe, M., Ikawa, M., Kominami, K., Nakanishi, T. and Nishimune, Y. (1997) 'Green mice' as a source of ubiquitous green cells. FEBS Lett. 407(3):313-9.

Pan, J., Ruest, L.B., Xu, S., and Wang, E. (2004) Immuno-characterization of the switch of peptide elongation factors eEF1A-1/EF-1alpha and eEF1A-2/S1 in the central nervous system during mouse development. Brain. Res. Dev. Brain. Res. 149(1):1-8.

Pfeifer, G.P., Denissenko, M.F., Olivier, M., Tretyakova, N., Hecht, S.S., and Hainaut, P. (2002) Tobacco smoke carcinogens, DNA damage and p53 mutations in smoking-associated cancers. Oncogene. 21(48):7435-51.

Piedrahita, J. A., Zhang, S. H., Hagaman, J. R., Oliver, P. M. and Maeda, N. (1992) Generation of mice carrying a mutant apolipoprotein E gene inactivated by gene targeting in embryonic stem cells. Proc. Natl. Acad. Sci. USA 89, 4471–4475.

Pitas, R.E., Boyles, J.K., Lee, S.H., Foss, D. and Mahley, R.W. (1987) Astrocytes synthesize apolipoprotein E and metabolize apolipoprotein E-containing lipoproteins. Biochim. Biophys. Acta. Jan 13;917(1):148-61.

Popko, B., Goodrum, J.F., Bouldin, T.W., Zhang, S.H. and Maeda, N. (1993) Nerve regeneration occurs in the absence of apolipoprotein E in mice. J. Neurochem. 60, 1155-1158.

Prasher, D.C., Eckenrode, V.K., Ward, W.W., Prendergast, F.G., and Cormier, M.J. (1992) Primary structure of the Aequorea victoria green-fluorescent protein. Gene. 111(2):229-33.

Previtali, S.C., Malaguti, M.C., Riva, N., Scarlato, M., Dacci, P., Dina, G., Triolo, D., Porrello, E., Lorenzetti, I., Fazio, R. Comi, G., Bolino, A. and Quattrini, A. (2008) The extracellular matrix affects axonal regeneration in peripheral neuropathies. Neurology, 71, 322 – 331.

Purves, D., Augustine, G.J., Fitzpatrick, D., Hall, W.C., LaMantia, A-S., McNamara, J.O. and Williams, S.M. (2004) Neuroscience, 3rd Ed. Sinauer Associates Inc.

Rall, S.C.Jr., Weisgraber, K.H. and Mahley, R.W. (1982) Human apolipoprotein E. The complete amino acid sequence. J. Biol. Chem. 257:4171–78.

Ranvier, L.A. (1878) Le!onssur l'Histologie du Systeme Nerveux, vol.I.Paris: F.Savy.

Rao, M.V., Engle, L.J., Mohan, P.S., Yuan, A., Qiu, D., Cataldo, A., Hassinger, L., Jacobsen, S., Lee, V.M., Andreadis, A. Julien, J.P., Bridgman, P.C. and Nixon, R.A. (2002) Myosin Va binding to neurofilaments is essential for correct myosin Va distribution and transport and neurofilament density. J. Cell Biol., 159, 279 – 290.

Rass, U., Ahel, I., and West, S.C. (2007) Defective DNA repair and neurodegenerative disease. Cell. 130(6):991-1004.

Reddy, L.V., Koirala, S., Sugiura, Y., Herrera, A.A. and Ko, C.P. (2003) Glial cells maintain synaptic structure and function and promote development of the neuromuscular junction in vivo. Neuron. Oct 30;40(3):563-80.

Reist, N.E., Werle, M.J., and McMahan, U.J. (1992) Agrin released by motor neurons induces the aggregation of acetylcholine receptors at neuromuscular junctions. Neuron. 8(5):865-8.

Ribchester, R.R. and Taxt, T. (1983) Motor unit size and synaptic competition in rat lumbrical muscles reinnervated by active and inactive motor axons. J. Physiol. 344:89-111.

Roheim, P.S., Carey, M., Forte, T. and Vega, G.L. (1979) Apolipoproteins in human cerebrospinal fluid. Proc. Natl. Acad. Sci. USA Sep;76(9):4646-9.

Rosen, D.R., Siddique, T., Patterson, D., Figlewicz, D.A., Sapp, P., Hentati, A., Donaldson, D., Goto, J., O'Regan, J.P., Deng, H.X., et al. (1993). Mutations in Cu/Zn superoxide dismutase gene are associated with familial amyotrophic lateral sclerosis. Nature. 362, 59–62.

Rossi-Durand, C. (2006) Proprioception and myoclonus. Neurophysiol. Clin. 36(5-6):299-308.

Rothstein, J.D. (2009) Current hypotheses for the underlying biology of amyotrophic lateral sclerosis. Ann. Neurol. 65 Suppl 1:S3-9.

Rouleau, G.A., Clark, A.W., Rooke, K., Pramatarova, A., Krizus, A., Suchowersky, O., Julien, J.P., and Figlewicz, D. (1996) SOD1 mutation is associated with accumulation of neurofilaments in amyotrophic lateral sclerosis. Ann. Neurol. 39(1):128-31.

Sagot, Y., Dubois-Dauphin, M., Tan, S.A., de Bilbao, F., Aebischer, P., Martinou, J.C. and Kato, A.C. (1995) Bcl-2 overexpression prevents motoneuron cell body loss but not axonal degeneration in a mouse model of a neurodegenerative disease. J. Neurosci. 15(11):7727-33.

Salpeter, M.M. and Loring, R.H. (1985) Nicotinic acetylcholine receptors in vertebrate muscle: properties, distribution and neural control. Prog. Neurobiol. 25(4):297-325.

Sandrock, A.W. Jr., Dryer, S.E., Rosen, K.M., Gozani, S.N., Kramer, R., Theill, L.E. and Fischbach, G.D. (1997) Maintenance of acetylcholine receptor number by neuregulins at the neuromuscular junction in vivo. Science. 276(5312):599-603.

Sanes, J.R. and Lichtman, J.W. (1999) Development of the vertebrate neuromuscular junction. Annu. Rev. Neurosci. 22:389-442.

Saunders, A.M., Schmader, K., Breitner, J.C., Benson, M.D., Brown, W.T., Goldfarb, L., Goldgaber, D., Manwaring, M.G., Szymanski, M.H., McCown, N., et al. (1993a) Apolipoprotein E epsilon 4 allele distributions in late-onset Alzheimer's disease and in other amyloid-forming diseases. Lancet. 342, 710-711.

Saunders, A.M., Strittmatter, W.J., Schmechel, D., George-Hyslop, P.H., Pericak-Vance, M.A., Joo, S.H., Rosi, B.L., Gusella, J.F., Crapper-MacLachlan, D.R., Alberts, M.J., et al. (1993b) Association of apolipoprotein E allele epsilon 4 with late-onset familial and sporadic Alzheimer's disease. Neurology. 43, 1467-1472.

Schachtrup, C., Ryu, J.K., Helmrick, M.J., Vagena, E., Galanakis, D.K., Degen, J.L., Margolis, R.U. and Akassoglou, K. (2010) Fibrinogen triggers astrocyte scar

formation by promoting the availability of active TGF-beta after vascular damage. J. Neurosci., 30, 5843 – 5854.

Schaefer, A.M., Sanes, J.R., and Lichtman, J.W. (2005) A compensatory subpopulation of motor neurons in a mouse model of amyotrophic lateral sclerosis. J. Comp. Neurol. 490(3):209-19.

Schaefer, A.W., Schoonderwoert, V.T., Ji, L., Mederios, N., Danuser, G. and Forscher, P. (2008) Coordination of actin filament and microtubule dynamics during neurite outgrowth. Dev. Cell, 15, 146–162.

Schiefermeier, M., Kollegger, H., Madl, C., Polli, C., Oder, W., Kühn, H., Berr, F. and Ferenci, P. (2000a) The impact of apolipoprotein E genotypes on age at onset of symptoms and phenotypic expression in Wilson's disease. Brain. 123 Pt 3:585-90.

Schiefermeier, M., Kollegger, H., Madl, C., Schwarz, C., Holzer, M., Kofler, J. and Sterz, F. (2000b) Apolipoprotein E polymorphism: survival and neurological outcome after cardiopulmonary resuscitation. Stroke. 31(9):2068-73.

Schumacher, B., Garinis, G.A., and Hoeijmakers, J.H. (2008) Age to survive: DNA damage and aging. Trends. Genet. 24(2):77-85.

Sherrington, C.S. (1906) The integrative action of the nervous system. Yale University Press, New Haven.

Shimomura, O., Johnson, F.H., and Saiga, Y. (1962) Extraction, purification and properties of aequorin, a bioluminescent protein from the luminous hydromedusan, Aequorea. J. Cell. Comp. Physiol. 59, 223-39.

Shore, V.G. and Shore, B. (1973) Heterogeneity of human plasma very low density lipoproteins. Separation of species differing in protein components. Biochemistry. 12:502-507.

Siddique, T., Pericak-Vance, M.A., Caliendo, J., Hong, S.T., Hung, W.Y. Kaplan, J., McKenna-Yasek, D., Rimmler, J.B., Sapp, P., Saunders, A.M., Scott, W.K., Siddique, N., Haines, J.L. and Brown, R.H. (1998) Lack of association between apolipoprotein E genotype and sporadic amyotrophic lateral sclerosis. Neurogenetics. 1:213-6.

Skene, J.H. and Shooter, E.M. (1983) Denervated sheath cells secrete a new protein after nerve injury. Proc. Natl. Acad. Sci. USA. 80, 4169-4173.

Smith, R.G., Haverkamp, L.J., Case, S., Appel, V. and Appel, S.H.. (1996) Apolipoprotein E epsilon 4 in bulbar-onset motor neuron disease. Lancet. 348:334-5.

Snipes, G.J., McGuire, C.B., Norden, J.J. and Freeman, J.A. (1986) Nerve injury stimulates the secretion of apolipoprotein E by nonneuronal cells. Proc. Natl. Acad. Sci. USA. 83:1130-4.

Spergel, D.J., Krüth, U., Shimshek, D.R., Sprengel, R., and Seeburg, P.H. (2001) Using reporter genes to label selected neuronal populations in transgenic mice for gene promoter, anatomical, and physiological studies. Prog. Neurobiol. 63(6):673-86.

Sternberger, N.H., Sternberger, L.A., and Ulrich, J. (1985) Aberrant neurofilament phosphorylation in Alzheimer disease. Proc. Natl. Acad. Sci. USA. 82(12):4274-6.

Stevens, J.C., Chia, R., Hendriks, W.T., Bros-Facer, V., van Minnen, J., Martin, J.E., Jackson, G.S., Greensmith, L., Schiavo, G., and Fisher, E.M. (2010) Modification of superoxide dismutase 1 (SOD1) properties by a GFP tag--implications for research into amyotrophic lateral sclerosis (ALS). PLoS One. 5(3):e9541.

Stolinski, C. (1995) Structure and composition of the outer connective tissue sheaths of peripheral nerve. J. Anat. 186 (Pt 1):123-30.

Stoll, G. and Müller, H.W. (1986) Macrophages in the peripheral nervous system and astroglia in the central nervous system of rat commonly express apolipoprotein E during development but differ in their response to injury. Neurosci. Lett. 72(3):233-8.

Strebel, A., Harr, T., Bachmann, F., Wernli, M., and Erb, P. (2001) Green fluorescent protein as a novel tool to measure apoptosis and necrosis. Cytometry. 43(2):126-33.

Strittmatter, W.J., Saunders, A.M., Schmechel, D., Pericak-Vance, M., Enghild, J. Salvesen, G.S. and Roses, A.D. (1993) Apolipoprotein E: high-avidity binding to beta-amyloid and increased frequency of type 4 allele in late-onset familial Alzheimer disease. Proc. Natl. Acad. Sci. USA 90:1977–81.

Sunderland, S. (1965) The connective tissues of peripheral nerves. Brain. 88(4):841-54.

Sunderland, S. (1978) In nerves and nerve injuries. Edinburgh: Churchill Livingstone, 2nd Ed.

Suraweera, A., Becherel, O.J., Chen, P., Rundle, N., Woods, R., Nakamura, J., Gatei, M., Criscuolo, C., Filla, A., Chessa, L., Fusser, M., Epe, B., Gueven, N., and

Lavin, M.F. (2007) Senataxin, defective in ataxia oculomotor apraxia type 2, is involved in the defense against oxidative DNA damage. J. Cell. Biol. 177(6):969-79.

Takahashi, T., Nakajima, Y., Hirosawa, K., Nakajima, S., and Onodera, K. (1987) Structure and physiology of developing neuromuscular synapses in culture. J. Neurosci. 7(2):473-81.

Tansey, E.M. (2006) Henry Dale and the discovery of acetylcholine. C. R. Biol. 329(5-6):419-25.

Teasdale, G.M., Nicoll, J.A., Murray, G. and Fiddes, M. (1997) Association of apolipoprotein E polymorphism with outcome after head injury. Lancet. 350, 1069-1071.

Tesseur, I., Van Dorpe, J., Bruynseels, K., Bronfman, F., Sciot, R., Van Lommel. A. and Van Leuven. F. (2000) Prominent axonopathy and disruption of axonal transport in transgenic mice expressing human apolipoprotein E4 in neurons of brain and spinal cord. Am. J. Pathol. 157, 1495-510.

Teter, B., Xu, P.T., Gilbert, J.R., Roses, A.D., Galasko, D. and Cole, G.M. (2002) Defective neuronal sprouting by human apolipoprotein E4 is a gain-of-negative function. J. Neurosci. Res. 68, 331-336.

Tetzlaff, W., Bisby, M.A., and Kreutzberg, G.W. (1988) Changes in cytoskeletal proteins in the rat facial nucleus following axotomy. J. Neurosci. 8(9):3181-9.

Trapp, B.D., Hauer, P., and Lemke, G. (1988) Axonal regulation of myelin protein mRNA levels in actively myelinating Schwann cells. J. Neurosci. 8(9):3515-21.

Tsuzuki, S., Murano, T., Watanabe, H., Itoh, Y., Miyashita, Y. and Shirai K. (1998) The examination of apoE phenotypes in diabetic patients with peripheral neuropathy. Rinsho Byori 46, 829-833.

Utermann, G., Hees, M. and Steinmetz, A. (1977) Polymorphism of apolipoprotein E and occurrence of dysbetalipoproteinaemia in man. Nature. 269:604–7.

Utermann, G., Langenbeck, U., Beisiegel, U. and Weber, W. (1980) Genetics of the apolipoprotein E system in man. Am. J. Hum. Genet. 32:339–47.

Utermann, G., Steinmetz, A. and Weber, W. (1982) Genetic control of human apolipoprotein E polymorphism: comparison of one- and two-dimensional techniques of isoprotein analysis. Hum. Genet. 60(4):344-51.

Valentin, G.G. (1836) Uber den Verlauf und die letzten Enden der Nerven. Nova Acta Phys-Med Acad Leopoldina Breslau 18: 51–240.

Vega-Riveroll, L.J., Wylie, S.R., Loughna, P.T., Parson, S.H. and Chantler, P.D. (2005) Nonmuscle myosins IIA and IIB are present in adult motor nerve terminals. Neuroreport, 16, 1143–1146.

Vial, J. D. (1958). The early changes in the axoplasm during Wallerian degeneration. Journal of Biophysical and Biochemical Cytology 4, 551–555.

Virchow, R. (1855) Cellular-Pathologie. Virchow Archiv 8:3–39.

Waldeyer, H.W.G. (1891) Ueber einige neuere Forschungen im Gebiete der Anatomie des Centralnervensystems. Dtsc Med Wschr 17:1213–1218, 1244–1246, 1287–1289, 1331–1332, 1352–1356.

Waller, A. (1850). Experiments on the section of the glossopharyngeal and hypoglossal nerves of the frog, and observations of the alterations produced thereby in the structure of their primitive fibres. Philisophical Transactions of the Royal Society of London 140, 423–429.

Weeda, G., Donker, I., de Wit, J., Morreau, H., Janssens, R., Vissers, C.J., Nigg, A., van Steeg, H., Bootsma, D. and Hoeijmakers, J.H. (1997) Disruption of mouse ERCC1 results in a novel repair syndrome with growth failure, nuclear abnormalities and senescence. Curr. Biol. 7(6):427-39.

Weerasuriya, A. and Mizisin, A.P. (2011) The blood-nerve barrier: structure and functional significance. Methods. Mol. Biol. 686:149-73.

Weinberg, H.J. and Spencer, P.S. (1975) Studies on the control of myelinogenesis. I. Myelination of regenerating axons after entry into a foreign unmyelinated nerve. J. Neurocytol. 4(4):395-418.

Weisgraber, K. H., Rall, S.C.Jr. and Mahley, R.W. (1981) Human E apoprotein heterogeneity. Cysteine-arginine interchanges in the amino acid sequence of the apoE isoforms. J. Biol. Chem. 256: 9077–9083.

Wetterau, J.R., Aggerbeck, L.P., Rall, S.C.Jr. and Weisgraber, K.H. (1988) Human apolipoprotein E3 in aqueous solution. I. Evidence for two structural domains. J. Biol. Chem. 5;263(13):6240-8.

White, F., Nicoll, J.A., Roses, A.D., and Horsburgh, K. (2001) Impaired neuronal plasticity in transgenic mice expressing human apolipoprotein E4 compared to E3 in a model of entorhinal cortex lesion. Neurobiol. Dis. 8(4):611-25.

Winlow, W. and Usherwood, P.N. (1975) Ultrastructural studies of normal and degenerating mouse neuromuscular junctions. J. Neurocytol. 4(4):377-94.

Wirth, B. (2000) An update of the mutation spectrum of the survival motor neuron gene (SMN1) in autosomal recessive spinal muscular atrophy (SMA). Hum. Mutat. 15(3):228-37.

Wishart, T.M., Parson, S.H., and Gillingwater, T.H. (2006) Synaptic vulnerability in neurodegenerative disease. J. Neuropathol. Exp. Neurol. 65(8):733-9.

Wishart, T.M., Pemberton, H.N., James, S.R., McCabe, C.J. and Gillingwater, T.H. (2008) Modified cell cycle status in a mouse model of altered neuronal vulnerability (slow Wallerian degeneration; Wlds). Genome. Biol. 9: R101.

Wood, R.D. (2010) Mammalian nucleotide excision repair proteins and interstrand crosslink repair. Environ. Mol. Mutagen. 51(6):520-6.

Wood, S.J. and Slater, C.R. (1997) The contribution of postsynaptic folds to the safety factor for neuromuscular transmission in rat fast- and slow-twitch muscles. J. Physiol. 500 (Pt 1):165-76.

Wu, H., Xiong, W.C., and Mei, L. (2010) To build a synapse: signaling pathways in neuromuscular junction assembly. Development. 137(7):1017-33.

Wyatt, R.M. and Balice-Gordon, R.J. (2003) Activity-dependent elimination of neuromuscular synapses. J. Neurocytol. 32,777-94.

Wylie, S.R., Wu, P.J., Patel, H., and Chantler, P.D. (1998) A conventional myosin motor drives neurite outgrowth. Proc. Natl. Acad. Sci. USA. 95(22):12967-72.

Xu, C., Bailly-Maitre, B. and Reed, J.C. (2005) Endoplasmic reticulum stress: cell life and death decisions. J. Clin. Invest. 115: 2656–2664.

Xu, P.T., Gilbert, J.R., Qiu, H.L., Ervin, J., Rothrock-Christian, T.R., Hulette, C. and Schmechel, D.E. (1999) Specific regional transcription of apolipoprotein E in human brain neurons. Am. J. Pathol. 154(2):601-11.

Xu, P.T., Schmechel, D., Rothrock-Christian, T., Burkhart, D.S., Qiu, H.L., Popko, B., Sullivan, P., Maeda, N., Saunders, A.M., Roses, A.D. and Gilbert, J.R. (1996) Human apolipoprotein E2, E3, and E4 isoform-specific transgenic mice: human-like pattern of glial and neuronal immunoreactivity in central nervous system not observed in wild-type mice. Neurobiol. Dis. 3, 229-245.

Yuan, W., Li, G., Zeng, M. and Fu, B.M. (2010) Modulation of the blood–brain barrier permeability by plasma glycoprotein orosomucoid. Microvasc. Res. 80, 148 – 157.

Zannis, V.I., Just, P.W. and Breslow, J.L. (1981) Human apolipoprotein E isoprotein subclasses are genetically determined. Am. J. Hum. Genet. 33:11–24.

Zannis, V.I., Breslow, J.L., Utermann, G., Mahley, R.W., Weisgraber, K.H., Havel, R.J., Goldstein, J.L., Brown, M.S., Schonfeld, G., Hazzard, W.R. and Blum, C. (1982) Proposed nomenclature of apoE isoproteins, apoE genotypes, and phenotypes. J. Lipid. Res. 23:911–14.

Zannis, V.I., Nicolosi, R.J., Jensen, E., Breslow, J.L., and Hayes, K.C. (1995) Plasma and hepatic apoE isoproteins of nonhuman primates. Differences in apoE among humans, apes, and New and Old World monkeys. J Lipid Res. 26(12):1421-30.

Zareparsi, S., Kaye, J., Camicioli, R., Grimslid, H., Oken, B., Litt, M., Nutt, J., Bird, T., Schellenberg, G. and Payami, H. (1997) Modulation of the age at onset of Parkinson's disease by apolipoprotein E genotypes. Ann. Neurol. 42, 655-658.

Zhang, B., Tu, P., Abtahian, F., Trojanowski, J.Q., and Lee, V.M. (1997) Neurofilaments and orthograde transport are reduced in ventral root axons of transgenic mice that express human SOD1 with a G93A mutation. J. Cell. Biol. 139(5):1307-15.

Zhang, F., Hackett, N.R., Lam, G., Cheng, J., Pergolizzi, R., Luo, L., Shmelkov, S.V., Edelberg, J., Crystal, R.G., and Rafii, S. (2003) Green fluorescent protein selectively induces HSP70-mediated up-regulation of COX-2 expression in endothelial cells. Blood. 102(6):2115-21.

Zhang, F., and Zhu, H. (2006) Intracellular conformational alterations of mutant SOD1 and the implications for fALS-associated SOD1 mutant induced motor neuron cell death. Biochim. Biophys. Acta. 1760(3):404-14.

Zhong, N., and K. H. Weisgraber. (2009) Understanding the association of apolipoprotein E4 with Alzheimer's disease: clues from its structure. J. Biol. Chem. 284, 6027-31.

Zhu, X.J., Wang, C.Z., Dai, P.G., Xie, Y., Song, N.N., Liu, Y., Du, Q.S., Mei, L., Ding, Y.Q. and Xiong, W.C. (2007) Myosin X regulates netrin receptors and functions in axonal path-finding. Nat. Cell Biol., 9, 184 – 192.

8 - Appendices

Appendix 8.1 - iTRAQ proteomics methodology

All proteomics experiments were performed at the Keele University Mass Spectrometry and Proteomics Facility, Wolfson Centre for Inherited Neuromuscular Disease, Oswestry. The following proteomics methodology is from Comley et al., 2011;

"Reduction, alkylation and digestion steps were performed using the reagents and according to the recommendations in the iTRAQ labelling kit (Applied Biosystems). The extracts were diluted with 50mM TEAB so that the urea concentration was less than 1M, before the addition of trypsin and overnight incubation at 37°C. The digests were then dried down in a vacuum centrifuge and iTRAQ labelling was carried out according to the instructions in the iTRAQ labelling kit. The iTRAQ tags were assigned to samples as follows: 115-ApoE3 and 117-ApoE4. Each tag was incubated with 85μg of protein (as determined by a Bradford protein assay).

iTRAQ-labelled peptides were pooled and made up to a total volume of 2.4mls in SCX buffer A (10mM phosphate, pH3 in 20% acetonitrile (Romil, UK)). The pooled peptides (2.4mls) were then separated by strong cation-exchange chromatography (SCX) using a polysulfoethyl A column, 300A, 5uM (PolyLC))

at a flow rate of 400ul/minute. Following sample injection, the column was washed with SCX buffer A until the baseline returned. The gradient was run as follows: 0-50% SCX buffer B (10mM phosphate, 1M NaCl, pH3 in 20% acetonitrile) over 25 minutes followed by a ramp up from 50% to 100% SCX buffer B over 5 minutes. The column was then washed in 100% SCX buffer B for 5 minutes before equilibrating for 10 minutes with SCX buffer A. Fractions were collected (400ul) during the elution period and dried down completely in a vacuum centrifuge.

The iTRAQ tryptic peptide fractions were each resuspended in 30μl of RP buffer A (2% acetonitrile, 0.05% TFA in water (Sigma Chromasolv plus). Prior to mass spectrometry analysis, fractions were first separated by liquid chromatography (Dionex Ultimate 3000) on a Pepmap C18 column, 200μm x 15cm (LC Packings) at a flow rate of 3μl/minute. Fractions were injected by full-loop injection (20μl) and the order of loading was randomized to minimise effects from carry-over. The eluants used were: A. 0.05% TFA in 2% acetonitrile in water and B. 0.05% TFA in 90% acetonitrile in water. The gradient was run as follows: 10 minutes isocratic pre-run at 100% A, followed by a linear gradient from 0-30% B over 100 minutes, followed by another linear gradient from 30%-60% over 35minutes. The column was then washed in 100% B for a further 10 minutes, before a final equilibration step in 100% A for 10 minutes. During the elution gradient, sample was spotted at 10 second intervals using a Probot (LC Packings) with α-cyano-4-

hydroxycinnamic acid (CHCA) at 3mg/ml (70% MeCN, 0.1% TFA) at a flow rate of 1.2μl/min.

Both MS and MS/MS analysis was performed on the fractionated peptides using an Applied Biosystems 4800 MALDI TOF/TOF mass spectrometer. The mass spectrometer was operated under control of 4000 Series Explorer v3.5.2 software (Applied Biosystems). A total of 1000 shots per MS spectrum (no stop conditions) and 2500 shots per MS/MS spectrum (no stop conditions) were acquired. The following MS/MS acquisition settings were used: 2KV operating mode with CID on and precursor mass window resolution set to 300.00 (FWHM). Peak lists of MS and MS/MS spectra were generated using 4000 Series Explorer v3.5.2 software and the following parameters were used after selective labelling of monoisotopic mass peaks: MS peak lists: S/N threshold 10, Savitzky Golay smoothing (3 points across peak (FWHM)), no baseline correction, MS/MS peak lists: S/N threshold 14; smoothing algorithm: Savitzky Golay, smoothing (7 points across peak (FWHM)).

An automated database search was run using GPS Explorer v3.6 (Applied Biosystems). MASCOT was used as the search engine to search the NCBI non-redundant database (version 10/11/2009) using the following search parameters: precursor ion mass tolerance of 100ppm, MS/MS fragment ion mass tolerance of 0.3Da and iTRAQ fragment ion mass tolerance of 0.2Da. The enzyme was specified as trypsin with 1 missed cleavage permitted, oxidation of methionine residues were allowed as variable modifications and N-term

(iTRAQ), lysine (iTRAQ) and MMTS modification of cysteine residues were set as fixed modifications and the taxonomy was selected as Mus. The identification criterion was at least 2 unique peptides by MS/MS with the most stringent search settings in order to yield the most reliable data for iTRAQ quantification (peptide rank 1 and total ion score confidence intervals of at least 95%).

Peptides were reported as identified iTRAQ peptides only if they met the following criteria: iTRAQ ratio of greater than 0, all N-terminal and lysine residues were labelled and did not include tyrosine_iTRAQ modification. Quantification of the iTRAQ peptides was performed by applying the following formula: corrected cluster area of fragment / corrected cluster area of reference (i.e. 117 (ApoE4)/115 (ApoE3)). Following correction using kit-specific-iTRAQ correction factors, iTRAQ ratios were normalized to the median ratio using the following formula: iTRAQ Ratio = Ratio / (median iTRAQ Ratio of all found pairs). Both correction and normalization was performed using GPS Explorer software v3.6."

Appendix 8.2 – Publications

Mutsaers CA, Wishart TM, Lamont DJ, Riessland M, Schreml J, **Comley LH,** Murray LM, Parson SH, Lochmüller H, Wirth B, Talbot K, and Gillingwater TH. (2011) Reversible molecular pathology of skeletal muscle in spinal muscular atrophy. Hum Mol Genet. Epub ahead of print.

Comley LH, Fuller HR, Wishart TM, Mutsaers CA, Thomson D, Wright AK, Ribchester RR, Morris GE, Parson SH, Horsburgh K and Gillingwater TH. (2011) ApoE isoform-specific regulation of regeneration in the peripheral nervous system. Hum Mol Genet. 20(12):2406-21. Featured on the BBC News website with coverage in the Scotsman and Daily Express.

Comley LH, Wishart TM, Baxter B, Murray LM, Nimmo A, Thomson D, Parson SH and Gillingwater TH. (2011) Induction of cell stress in neurons from transgenic mice expressing yellow fluorescent protein: implications for neurodegeneration research. PLoS One. 6(3):e17639.

Murray LM, **Comley LH,** Gillingwater TH and Parson SH. (2011) The response of neuromuscular junctions to injury is developmentally regulated. FASEB J. 25(4):1306-13.

de Waard MC, van der Pluijm I, Zuiderveen Borgesius N, **Comley LH,** Haasdijk ED, Rijksen Y, Ridwan Y, Zondag G, Hoeijmakers JH, Elgersma Y, Gillingwater TH and Jaarsma D. (2010) Age-related motor neuron degeneration in DNA repair-deficient Ercc1 mice. Acta Neuropathol. 120(4):461-75.

Murray LM, **Comley LH,** Thomson D, Parkinson N, Talbot K and Gillingwater TH. (2008) Selective vulnerability of motor neurons and dissociation of pre- and post-synaptic pathology at the neuromuscular junction in mouse models of spinal muscular atrophy. Hum Mol Genet. 17(7):949-62.

Appendix 8.3 – Conference abstracts

2011 - ApoE, ApoE Receptors & Neurodegeneration Symposium: ApoE in the CNS and Periphery, Chicago, USA (Talk and poster)
"ApoE isoform-specific regulation of regeneration in the peripheral nervous system."

2011 – Edinburgh Neuroscience Day, UK (Poster)
"Induction of Cell Stress in Neurons from Transgenic Mice Expressing Yellow Fluorescent Protein: Implications for Neurodegeneration Research."

2010 – 7th FENS Forum of European Neuroscience, Amsterdam, The Netherlands (Poster)
"Apolipoprotein E4 selectively delays axonal regeneration and neuromuscular reinnervation in the peripheral nervous system."

2010 – Anatomical Society Winter Conference, Oxford, UK (Poster)
"APOE influences Wallerian degeneration and regeneration following nerve crush in the PNS."

2009 – 6th UK SMA Research Conference, Edinburgh, UK (Poster)
"Apolipoprotein E (APOE) genotype influences degenerative and regenerative events at the neuromuscular junction."

2009 - Edinburgh Neuroscience Day, UK (Poster)
"Apolipoprotein E (APOE) genotype influences degenerative and regenerative events at the neuromuscular junction."

2008 – 5th Annual Scottish neuroscience Group Meeting (Poster)
"Apolipoprotein E (APOE) genotype influences degenerative and regenerative events at the neuromuscular junction."

2008 – Anatomical Society Meeting, Nottingham, UK (Poster)
"Apolipoprotein E (APOE) genotype influences degenerative and regenerative events at the neuromuscular junction."

2008 – Edinburgh Neuroscience Day, UK (Poster)
"Apolipoprotein E (APOE) genotype influences degenerative and regenerative events at the neuromuscular junction."